Final Report for Period: 10/2007 - 09/2008
Submitted on: 01/30/2009
Principal Investigator: Fritz, Hermann M.
Award ID: 0421090
Organization: GA Tech Res Corp - GIT
Submitted By:

Title:
NEESR-SG: Physical modeling of 3D Tsunami Evolution Using a Landslide Tsunami Generator

Project Participants

Senior Personnel

Name: Fritz, Hermann
Worked for more than 160 Hours: Yes
Contribution to Project:

Name: Germanovich, Leonid
Worked for more than 160 Hours: Yes
Contribution to Project:

Name: Puzrin, Alexander
Worked for more than 160 Hours: Yes
Contribution to Project:

Post-doc

Graduate Student

Name: Kim, Sihyun
Worked for more than 160 Hours: Yes
Contribution to Project:
geotechnical graduate student under guidance of Prof. Germanovich and Prof. Puzrin. Sponsored by this award.

Name: Mohammed, Fahad
Worked for more than 160 Hours: Yes
Contribution to Project:
tsunami and fluid mechanics graduate student under the guidance of Dr. Fritz. Participated in the experiments in the Tsunami Wave Basin at OSU. Sponsored by this award.

Name: Yoo, Jeseon
Worked for more than 160 Hours: Yes
Contribution to Project:
coastal egnineering and fluid mechanics graduate student under the guidance of Dr. Fritz. Participated in the experiments in the Tsunami Wave Basin at OSU. Sponsored by this award.

Undergraduate Student

Name: Sokoloski, Robert
Worked for more than 160 Hours: Yes
Contribution to Project:
civil engineering undergraduate student under the guidance of Dr. Fritz. Participated in the design and construction of the novel landslide tsunami generator. Sponsored by this award.

Name: Grass, Chad

Worked for more than 160 Hours: Yes

Contribution to Project:

civil engineering undergraduate student under the guidance of Dr. Fritz. Participated in the design and construction of the novel landslide tsunami generator. Sponsored by this award.

Name: Bringman, Michael

Worked for more than 160 Hours: Yes

Contribution to Project:

civil engineering undergraduate student under the guidance of Dr. Fritz. Participated in the design and construction of the novel landslide tsunami generator. Sponsored by this award.

Technician, Programmer

Other Participant

Research Experience for Undergraduates

Organizational Partners

ETH Zurich

During the duration of this project Professor Alexander Puzrin became appointed as Head of the Institute for Geotechnical Engineering at the Department of Civil, Environmental and Geomatic Engineering at ETH Zurich. Graduate student Sihyun Kim spent some time at ETH with Professor Puzrin.

Norwegian Geotechnical Institute

The Norwegian Geotechnical Institute NGI invited Dr. Fritz as keynote speaker to the Geiranger Fjord in Western Norway. The Geiranger Fjord features a potential near future landslide tsunami due to the Aknes rockslide currently under monitoring. The Aknes Workshop covered the last week of August 2007. nGI covered the workshop travel expenses.

University of Oslo

The Univesrity of Oslo invited Dr. Fritz as speaker to the Department of Applied Mathematics in Oslo. The University of Oslo conducts block slide experiments related to the Geiranger Fjord, which features a potential near future landslide tsunami due to the Aknes rockslide currently under monitoring. Dr. Fritz visited the Department of Applied Mathematics in August 2007. The travel was paid for by the University of Oslo.

The University of Oslo is interested in possibly conducting experiments with Dr. Fritz's novel granular landslide tsunami generator either at OSU or by shipping the apparatus to the National Laboratory in Trondheim at SINTEF. A joint proposal to the Norwegian Research Council and NSF is currently targeted.

Other Collaborators or Contacts

Dr. Fritz was invited by University of Antilles Guyane at Point-a-Pitre, Guadeloupe (French Overseas Department in the Caribbean) to give three keynote presentations. One of them on landslide generated tsunamis. All expenses covered by the French (2008).

Dr. Fritz was invited to the SOPAC annual meeting on Tonga (SOPAC=Pacific Islands Applied Geoscience Commission) to give a keynote lecture on the landslide tsunami hazard in the Pacific Islands due to both subaerial landslide impacts and submarine landslide generated tsunamis as well as a second presentation on the 1 April Solomon Islands tsunami reconnaissance that highlighted many coastal landslides (2007).

Dr. Fritz was invited by University of Reunion Island (French Overseas Department in the South Indian Ocean) to give two keynote presentations. One of them on volcanic island collapse generated tsunamis. The presentation was in French. All expenses covered by the French foreign ministry (2006).

Informal contacts after the April 2007 Puerto Aysen landslide tsunami in Southern Chile with the Universidad de Valparaiso in Vina del Mar, Chile as well as with the Universidad de Chile in Santiago de Chile.

Hybrid modeling comparing landslide generated tsunami experiments with the iSale code are ongoing at present in 2D. The modeling with the iSale code is conducted by Dr. Weiss, Texas A&M and Dr. Wuennemann, Berlin, Germany.

Activities and Findings

Research and Education Activities:

Landslide Tsunami Generator (LTG) Design and Fabrication in Georgia, shipment to Oregon with Installation in the Tsunami Wave Basin (TWB) and Instrumentation with MTA, Video cameras above and below water, wave gauges, string pots, hydrophone, PIV:

The coupling between landslide motion and 3-dimensioinal tsunami wave propagation and runup is of critical importance given the local, strongly-directional source mechanism.
A unique landslide tsunami generator (LTG) was designed by the team at Georgia Tech and installed at the NEES Tsnuami Wave Basin (TWB) at OSU. The LTG simulated the impact of landslides that occur both above and below the water's surface. The LTG was constructed as 'an open box' that is mounted on a steel slide and filled with up to 1,350 kg of gravel. The box accelerates down the slide by means of four pneumatic pistons. The granular mass is accelerated inside the box and released while the sled is slowed down pneumatically. The box is 2.1 m by 1.2 m by 0.3 m with subdivisions to adjust initial slide length and thickness, and is placed on a slide that can vary in length. The box itself is able to travel approximately 2 m before the gravel is released down the 2H:1V slope at initial velocities up to 5 m/sec. Using cameras placed above and within the water, the researchers measured the shape, length, and thickness of the gravel masses while they were in motion. The granular landslide deposits were scanned with an acoustic multi-transducer array. Planar PIV was applied to the tsunami surface and revealed the fully 3D tsunami generation with the characteristic draw down of the shoreline in the back of the landslide and lateral collapse of the impact crater. Wave gauges were placed to measure the size and shape of the waves that were generated, including the lateral onshore runup.

Experiments:
Currently more than 60 successful runs have been completed and the main tsunamigenic parameters identified that serve as key benchmarks for numerical models.

Data Analysis:
The data analysis is finalized and several major publications are in last stages of preparation prior to submission.

Presentations:
-Fritz, H.M. ' Tsunami Generation by Earthquakes and Landslides', Georgia Institute of Technology, Geophysics (EAS), Atlanta, USA (01/23/2009). (Invited)
-Mohammed, F., H.M. Fritz (2008). Prediction of Tsunami Waves and Runup generated by granular Landslides, Eos Trans. AGU, 89(53), Fall Meet. Suppl., Abstract OS53B.
-Fritz, H.M. 'Granular Landslide generated Tsunami Experiments in the NEES 3D Tsunami Wave Basin', First International Caribbean Waves: Risk Evaluation of Natural Hazards in the Caribbean, Pointe-a-Pitre, Guadeloupe, French West Indies (12/09/2008). (invited)
-Fritz, H.M. 'Coastal Hazards Research based on recent events and experiments', Department of Civil Engineering, Hanyang University, Seoul, South Korea (08/29/2008). (Invited)
-Fritz, H.M. 'Coastal Hazards Research', Collaborative Research Experiences in Advanced Technology and Engineering (CREATE), NSF Research Experience for Undergraduates (REU), Georgia Institute of Technology, Savannah, Georgia (07/02/2008).
-Fritz, H.M. 'NEESR-SG: Physical modeling of 3D Tsunami Evolution Using a Landslide Tsunami Generator', Tsunami Wave Basin Tour, NSF: 6th NEES annual meeting, Corvallis, Oregon (06/20/2008).
-Fritz, H.M. ' Landslide Tsunami Generator Results', NSF: 6th NEES annual meeting, Portland, Oregon (06/19/2008).
-Fritz, H.M. 'Experimental Tsunami Research', NOAA Center for Tsunami Research (NCTR), Pacific Marine Environmental Laboratory (PMEL), National Oceanic and Atmospheric Administration (NOAA), Seattle, Washington (06/17/2008). (Invited)
- Mohammed, F., Fritz, H.M. (2008). 3D Granular Landslide Tsunami Experiments, Proc. 2008 Ocean Sciences Meeting, ASLO, 2-7 March 2008, Orlando, Florida.
-Fritz, H.M. 'Aspekte der Tsunami Forschung', Laboratory of Hydraulics, Hydrology and Glaciology (VAW), Swiss Federal Institute of Technology (ETH), Zurich, Switzerland (01/08/2007). (Invited)
-Fritz, H.M. 'Submarine landslide potential, including landslides in subduction zones and along canyon walls', 24th STAR (Science

Technology and Resources Network) Session, SOPAC (Pacific Islands Applied Geoscience Commission), Nuku'alofa, Tonga (11/27/2007). (Invited)
-Fritz, H.M. 'Investigaciones de tsunamis en el mundo y del maremoto del 15 Agosto en Pisco', Escuela Naval del Peru, Direccion de Hydrografia y Navegacion, Marina de Guerra, Lima, Peru (09/07/2007). (Invited)
-Fritz, H.M. 'Tsunami Research', Department of Mathematics, University of Oslo, Oslo, Norway (08/27/2007). (Invited)
-Fritz, H.M. '3D and 2D laboratory studies of granular landslide generated tsunami', Aknes landslide tsunami workshop, Norwegian Geotechnical Institute, Geiranger, Norway (08/31/2007). (Invited)
-Fritz, H.M. 'Landslide Tsunami Generator Experiments', NSF: 5th NEES annual meeting, Snowbird, Utah (06/20/2007).
-Fritz, H.M. 'Landslide tsunami experiments in the NEES tsunami wave basin', NSF: NEES Tsunami Modeling and Training Workshop, Corvallis, Oregon (07/27/2006). (Invited)
-Fritz, H.M. 'Physical Modeling of 3D Tsunami Evolution using a novel Pneumatic Landslide Tsunami Generator', NSF: 4th NEES annual meeting, Washington D.C. (06/21/2006). (Invited)
-Fritz, H.M. 'Modeling impact generated tsunami', The Tsunami Society, 3rd Tsunami Symposium, Honolulu, (05/25/2006). (Invited)

New Graduate Course Development and lectured first time Fall 2007 by Hermann Fritz at Georgia Tech:
CEE8813 'Coastal Hazards' a new graduate class was developed based primarily on coastal landslides, tsuanamis of landslide, volcanic and tectonic origins, hurricane strom surge and storm waves. The results from this project formed a key component of the course.

Findings:

Landslide generated tsunami waves were investigated in three-dimensional physical laboratory model based on the generalized Froude similarity. Landslides were successfully modeled with a deformable granular material. The developed pneumatic landslide generator allowed to control the slide impact characteristics. The herein presented results of the experimental study may be summarized as follows:
- The recorded wave profiles were extremely directional, unsteady, nonlinear, and located mostly in the intermediate water depth wave regime.
- Among the principal differences between a tectonic-generated tsunami and a landslide generated tsunami is that the latter has a strong directional component that can be devastating to the immediate area. Because it has a shorter wavelength, however, it dissipates quickly over a short distance. Landslide tsunamis exhibit a more dispersive and strongly directional propagation than tectonic tsunamis.
-The observed impulse waves were classified based on the slide Froude number F and the dimensionless slide parameters into four different wave types: weakly non-linear oscillatory wave, non-linear transition wave, solitary-like wave, and dissipative transient bore.
-The wave attenuation strongly depended upon the wave type and the wave characteristics. A representative draw down curve remains to be determined.
-The partition of the total wave height H between the crest and trough amplitudes strongly depended on the wave type. The maximum crest amplitudes at least matched and mostly exceeded the maximum trough amplitudes.
-The propagation velocity of the leading wave crest follows closely the theoretical approximations for a solitary wave. The second wave crest propagation velocity lagged by 20% on average.
-The macro-structure of the flow in the impact and wave generation area was deter?mined with particle image velocimetry (PIV).
-A flow separation criteria based on the slide Froude number F and the dimensionless slide parameters allowed to distinguish between separated and unseparated flow regimes in the impact and wave generation area. In the separated flow regime an impact crater forms.
-Besides the outward and backward collapsing a lateral collapsing of the impact crater was observed in many 3D cases, which was not observed previously in earlier 2D experiments.
-The maximum water displacement volume always exceeded the landslide volume.

Training and Development:

New Graduate Course CEE8813 'Coastal Hazards' Developed and lectured first time Fall 2007 by Hermann Fritz at Georgia Tech. The results have also been included in the Undegraduate CEE4200 'Hydraulic Engineering' course.

The undergraduate and graduate students gained invaluable hardware and software experiences in designing and automating the landslide tsunami generator (LTG), installation and operation of all the measurement systems including the data acquisition, recording and storage systems. Some of the softwares introduced are: Festo's Pneumatics Automation software FST. LaVision's Particle Image Velocimetry (PIV) software DaVis. Several Digital Image Processing and Analysis tools. Computational Fluid Dynamics (CFD) codes.
Last but not least: Operation of the Tsunami Wave Basin at Oregon State University (OSU) with all its subsystems.

Outreach Activities:

National TV-Documentary:
The History Channel (USA): 'Mega Disasters' series, The 1883 Krakatau Volcanic Explosion and Tsunami, (60'). The TV-documentary

encompassed the scale experiments of the Krakatau volcanic island collapse generated tsunami as part of the NEES landslide tsunami experiments in the tsunami wave basin at OSU, as well as various interviews of Hermann Fritz, among other international experts. (Co-Production: 12/2006, aired on National TV in 2007 on September 11, 12, 15, 21 and 22 and multiple replays).

TV-News
The experiment was also covered by different TV stations and newspapers who participated in the media day on 21st of December 2006. Following is the list of the participants that covered the landslide tsunami generation experiment.
? KGW-TV from Portland, Oregon.
? KATU-TV from Portland, Oregon.
? KEZI-TV from Eugene, Oregon.
? KVAL-TV from Eugene, Oregon.
? KMTR-TV from Eugene, Oregon.
? NSF Television and

Printed News Articles:
-Civil Engineering Magazine (ASCE flagship publication). Technology Highlight article 'Researchers Replicate Landslide-Generated Tsunamis' (February 2007)
-Gazette Times newspaper from Corvallis, Oregon (12/22/2006). Front-page lead article 'Landslide Tsunamis: Huge and Deadly' over 2 pages with photo.

K12-seminar presentation by Hermann Fritz:
'Civil Engineering and Coastal Hazards Research: Landslide generated tsunami experiments, the Indian Ocean Tsunami and Hurricane Katrina', Junior Achievement High School Students, Savannah, Georgia (02/02/2007)

NSF Highlight - literally:
The NEES Tsunami Research Facility hosts over 500 people at each of three open houses every year. The summer open house is held in conjunction with a science and engineering celebration in Corvallis Oregon. Goals included increasing public awareness of tsunamis and tsunami research, and encouraging science and engineering literacy. National Science Foundation George E. Brown Network for Earthquake Engineering Researcher (NEESR) Dr. Hermann Fritz was a guest speaker at the summer 2006 open house. Dr. Fritz's field research experience includes conducting field surveys along coastlines from Indonesia to Somalia in the aftermath of the 2004 Indian Ocean Tsunami.
He spoke to numerous groups of 25-40 people about tsunamis and tsunami research. This was a unique opportunity for visitors to interact with an active NEESR Principal Investigator. After the tours Fritz commented that '...it was important to explain how tsunamis are generated, how they propagate and what the Oregon coast could look like after a tsunami. Realistic scenarios were discussed without scaring people.' Tsunami awareness was raised by introducing tsunami precursors such as shoreline drawback and groundshaking as well as evacuation strategies. Educating the general public about tsunamis is important because experience gained from the recent Indian Ocean tsunami showed that educated and tsunami-aware coastal residents have a significantly higher chance of survival.

Journal Publications

Brett Hansen, "Researchers Replicate Landslide-Generated Tsunamis", Civil Engineering Magazine, p. 30, vol. 77(2), (2007). Published,

Fritz, H.M., "Lituya Bay Landslide Impact Generated Mega-Tsunami: 50th Anniversary", Pure Appl. Geophys., p. , vol. 166, (2009). Accepted, 10.1007/s00024-008-0435-4

Mohammed, F. and H.M. Fritz, "3D Granular Landslide Tsunami Experiments", Proceedings 2008 Ocean Sciences Meeting, ASLO, AGU, p. , vol. , (2008). Published,

Puzrin, AM; Germanovich, LN; Kim, S, "Catastrophic failure of submerged slopes in normally consolidated sediments", GEOTECHNIQUE, p. 631, vol. 54, (2004). Published,

Puzrin, AM; Germanovich, LN, "The growth of shear bands in the catastrophic failure of soils", PROCEEDINGS OF THE ROYAL SOCIETY A-MATHEMATICAL PHYSICAL AND ENGINEERING SCIENCES, p. 1199, vol. 461, (2005). Published, 10.1098/rspa.2004.137

Weiss, R., Fritz, H.M., Wuennemann, K., "Hybrid modeling of the mega-tsunami runup in Lituya Bay after half a century", Science, p. , vol. , (2009). Submitted,

Mohammed, F., H.M. Fritz, "Prediction of Tsunami Waves and Runup generated by granular Landslides", Eos Trans. AGU, 89(53), Fall Meet. Suppl., Abstract OS53B, p. , vol. , (2008). Published,

Puzrin, A.M., Saurer, E. and Germanovich,L.N., "Simplified dynamic solution of the shear band propagation in submerged landslides", Proc. of the International Symposium on Prediction and Simulation Methods for Geohazard Mitigation, 25-27 May, p. , vol. , (2009). Accepted,

Mohammed, F., H.M. Fritz, "Experiments on tsunamis generated by 3D granular landslides", Proceedings 4th International symposium on submarine mass movements, Austin, Texas., p. , vol. , (2009). Accepted,

Books or Other One-time Publications

Fritz, H.M., "Physical modeling of landslide generated tsunami.", (2006). Book, Published
Editor(s): A. Mercado-Irizarry and P.L.-F. Liu
Collection: Caribbean Tsunami Hazard
Bibliography: World Scientific, Singapore, 308-324.

Web/Internet Site

URL(s):

http://www.gtsav.gatech.edu/cee/groups/tsunami/

Description:

The site covers recent tsunami events and their timely field reconnaissance with observations on the front page.
The webpage shows all the tsunami related projects including this NEESR project.

Other Specific Products

Product Type:

TV Documentary

Product Description:

National TV-Documentary:
The History Channel (USA): 'Mega Disasters' series, The 1883 Krakatau Volcanic Explosion and Tsunami, (60'). The TV-documentary encompassed the scale experiments of the Krakatau volcanic island collapse generated tsunami as part of the NEES landslide tsunami experiments in the tsunami wave basin at OSU, as well as various interviews of Hermann Fritz, among other international experts. (Co-Production: 12/2006, aired on National TV in 2007 on September 11, 12, 15, 21 and 22 and multiple replays).

Sharing Information:

The TV-Documentary aired on National TV in 2007 on September 11, 12, 15, 21 and 22 and multiple replays within the Mega-Disasters Series on the History Channel

Contributions

Contributions within Discipline:

The project resulted in the design and construction of the landslide tsunami generator (LTG). The LTG represents a world wide unique laboratory apparatus to investigate tsunamis generated by granular landslides at large scale and in full three dimensions. The LTG can be deployed above water to study subaerial landslides impacting into the water body as well as within the water body to investigate partially submerged and submarine landslide generated tsunamis. The apparatus represents a key milestone in the discipline as it allows pneumatically controlled initial accelerations of granular landslides, which represents a major advancement over the classic non-deformable block slide experiments without controlled acceleration. The LTG compliments the tsunami wave basin (TWB) with its long wave paddle wave generator. The LTG was featured in the ASCE's flagship Civil Engineering Magazine, which is widely read by Civil Engineers both in research and practice.

The 60 experiments represent the largest data set for 3 dimensional granular landslide generated tsunamis. The data set is the key benchmark for the validation and advancement of numerical landslide and tsunami models. The subaerial landslide tsunami impact experiments revealed the formation of a large air cavity thereby displacing significanlty larger volumes of water than just the landslide volume itself. In three dimensions a new type of impact crater collapse was identified - the lateral collapse. This is a key finding as it directly drives the intitial tsunami generation. Further the shorter wave lengths of landslide generated tsunamis results in a more dispersive tsunami propagation, which reduces wave heights significantly faster than for tectonic earthquake generated tsunamis. The three-dimensional wave height distribution reveals the strong directional component of landslide generated tsunamis as well as the hill slope edge wave. The lateral edge wave runup poses the largest risk to coastal areas lateral and onshore of the offshore landslide motion.

Contributions to Other Disciplines:

The peaked onshore runup distribution with rapid decay is characteristic of landslide generated tsunamis. In the field the onshore edge wave runup of a landslide generated tsunami represents often the only way to distinguish between a tectonic and a landslide tsunami. This was documented in the field for the 17 July 2006 South Java tsunami generated by a tsunami earthquake, where only the peaked distribution allowed to point at a possible offshore submarine landslide source. Hence the project contributes to geophysics and in particular seismology, marine geology, and oceanography.

Contributions to Human Resource Development:

The specific characteristics of landslide generated tsunamis have implications also for tsunami evacuation and require specific tsunami education and awareness components.

Hermann Fritz lectured to more than 500 visitors at the DaVinci Weekend open house at the tsunami wave basin at Oregon State University. Being able to directly communicate to residents of a potentially at landslide tsunami risk coastline was important for both sides.

News articles in Civil Engineering Magazine and The Gazette-Times front page article increased the landslide tsunami awareness in the general public.

The History Channel (USA): 'Mega Disasters' series, The 1883 Krakatau Volcanic Explosion and Tsunami, (60'). The TV-documentary encompassed the scale experiments of the Krakatau volcanic island collapse generated tsunami as part of the NEES landslide tsunami experiments in the tsunami wave basin at OSU, as well as various interviews of Hermann Fritz, among other international experts. (Co-Production: 12/2006, aired on National TV in 2007 on September 11, 12, 15, 21 and 22, multiple replays since).
Further all major news TV stations in the Pacific-Northwest interviewed Hermann Fritz and lessons learned from the landslide tsunami experiments at the NEES facility were broadcasted with experiment footage at prime time.

K12-seminar presentations:
'Civil Engineering and Coastal Hazards Research: Landslide generated tsunami experiments, the Indian Ocean Tsunami and Hurricane Katrina', Junior Achievement High School Students, Savannah, Georgia (02/02/2007)

3 undergraduate students from GT were involved in the design and fabrication of the landslide tsunami generator (LTG). Numerous undergraduate, graudate and post-doc students participated in the operation of the landslide tsunami generator at the TWB at OSU. Two graduate students from Georgia Tech spent between one and two months at the NEES tsunami wave basin facility at Oregon State University running the experiments.

Contributions to Resources for Research and Education:

all the data of the more than 60 experiments was uploaded to NEES central and is available to the community.

the LTG landside tsunami generator is a unique tsunami generator that compliments the TWB main paddle long wave generator at the NEES facility.

A Coastal Hazards graduate class with a strong landslide tsunami component was developed by Hermann Fritz and taught the first time to graduate students at GT in Fall 2007.

Contributions Beyond Science and Engineering:

The various outreach, news and TV presentations have increased tsunami awareness and contributed to public safety through the education of the general public and coastal residents to tsunamis.
Several invited presentations in Asia (South Korea), Africa (Reunion Island), Europe (Norway, Geiranger Fjord), Peru, Caribbean

(Guadeloupe) and South Pacific (Solomon Islands, Tonga) were given to scientists, politicians, government emergency managers, and the general public of communities at risk to landslide generated tsunamis. These have directly impacted tsunami evacuation plans and increased public safety.

Conference Proceedings

Categories for which nothing is reported:

Any Conference

The landslide tsunami generator experiments were performed at the O. H. Hinsdale Wave Research Laboratory at the Oregon State University. The experiments were conducted in the Tsunami Wave Basin which is 48.8m long, 26.5m wide and 2.1m deep. The experiment primarily consists of studying tsunami waves generated by subaerial and submarine granular landslides. The landslides were created using a novel pneumatic landslide simulator which allows for controlled acceleration of the granular landslide material. This simulator is shown in figure 1. It consists of a sled which is driven by four pneumatic pistons which controls the acceleration of the granular landslide material.

Figure 1. The Landslide Tsunami Generator

Figure 2 shows the pneumatic scheme that governs and drives the pneumatic pistons which push the sled filled with the granular landslide material into the water, thus creating tsunami waves.

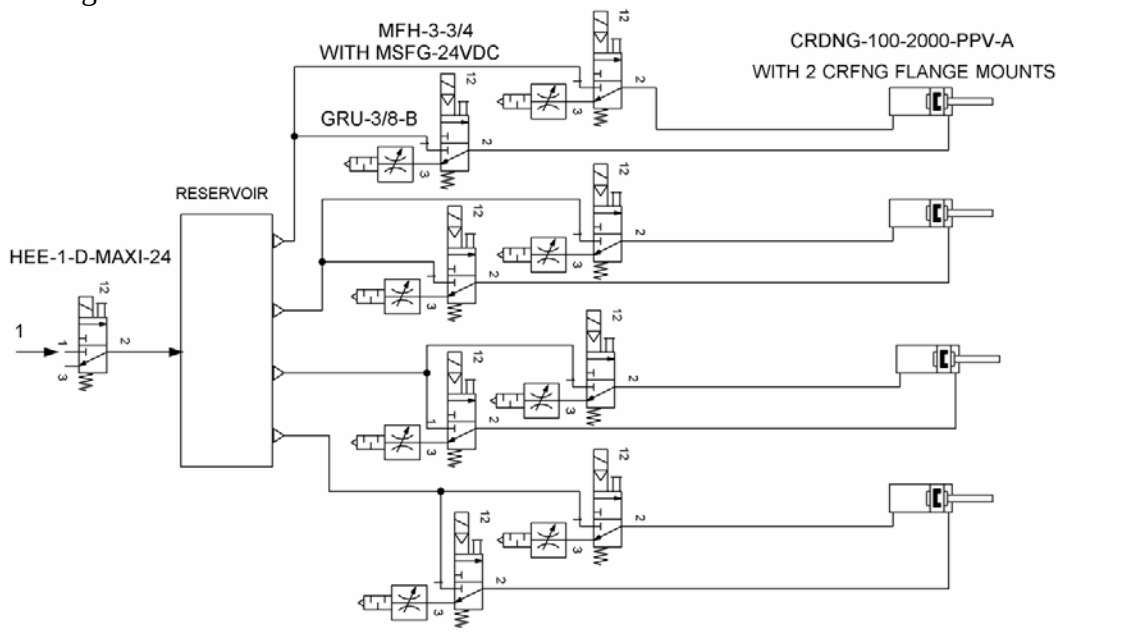

Figure 2. The pneumatic scheme governing the LTG

The landslide tsunami generation cycle is shown in the schematics presented in figure 3. The sled is loaded with gravel and is then pushed with a pneumatic piston into the water. Then the data acquisition system records the various landslide and wave measurements. After these measurements are stored for further analysis, the granular landslide material which gets deposited onto a flat steel plate at the bottom of the ramp is lifted and poured back into the sled to repeat the experiment with different conditions.

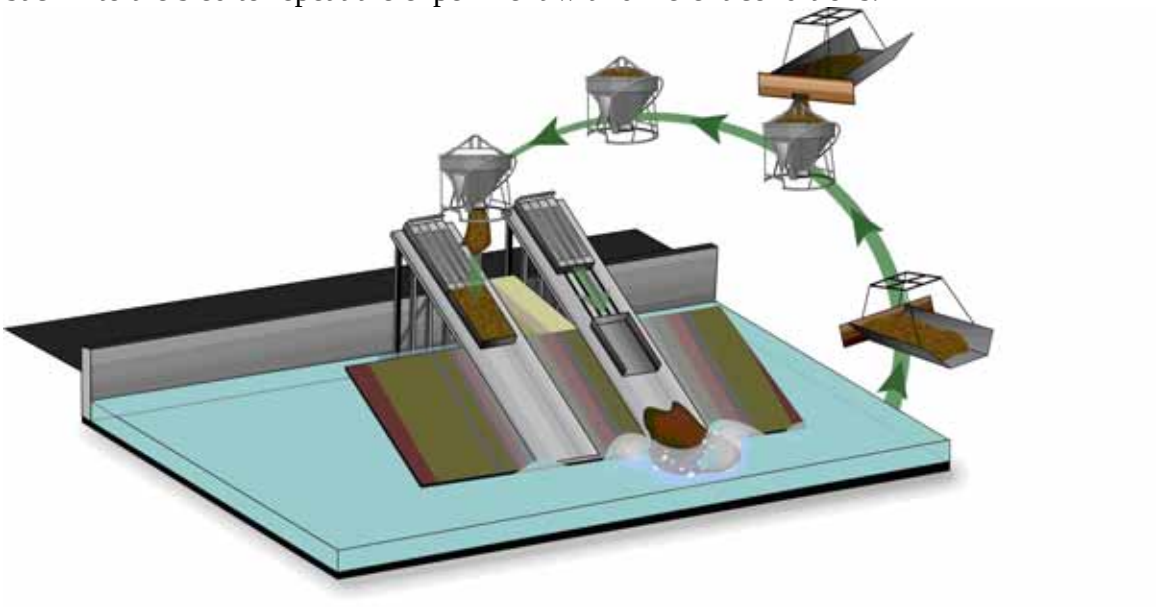

Figure 3. Landslide tsunami generation cycle.

The instrumentation includes several underwater and above cameras for measuring the landslide characteristics, a Multi Transducer Acoustic array (MTA) to map the bottom of the wave basin to measure the shape and volume of the deposited landslide material and resistance wave gages to measure the wave heights of the tsunami waves that were created by the landslides. The array of cameras provides valuable information on the slide characteristics, especially the transition in the slide velocity, thickness and shape as the slide moves from above the water surface into the water. The location of the cameras that measure these parameters is shown in figure 4.

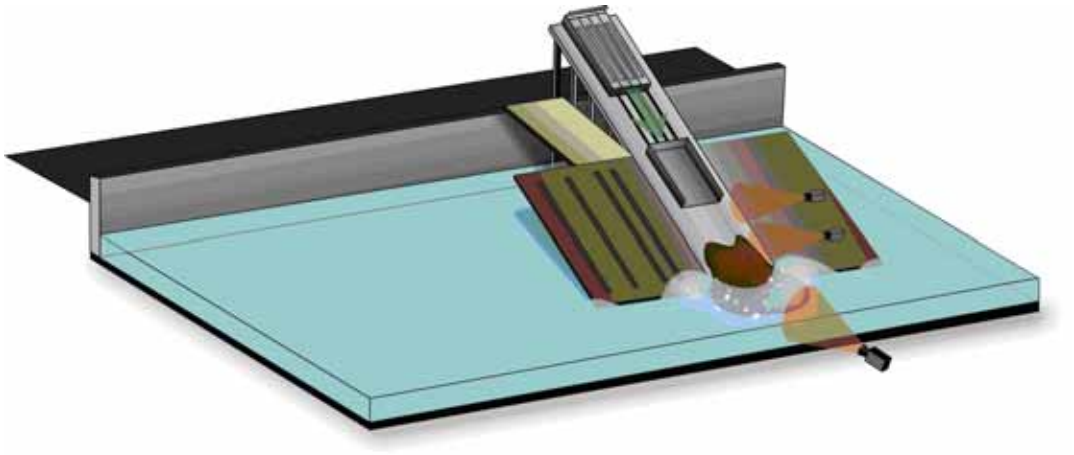

Figure 4. Camera locations to measure slide parameters.

An array of resistance wave gages is present in the wave basin to measure the tsunami wave height caused by the landslide. The plan view of the wave gage locations in the wave basin and the side view of the wave gages are shown in figure 5. The wave gage arrangement is determined to not only measure the linear dispersion of the generated tsunami waves, but also to measure the radial spread and decay of those waves. These measurements will enable us to determine the decay rate of the wave amplitudes in both radial as well as the angular direction. This will eventually help in developing empirical models that can predict arrival times and wave amplitudes when these tsunami waves impact on land.

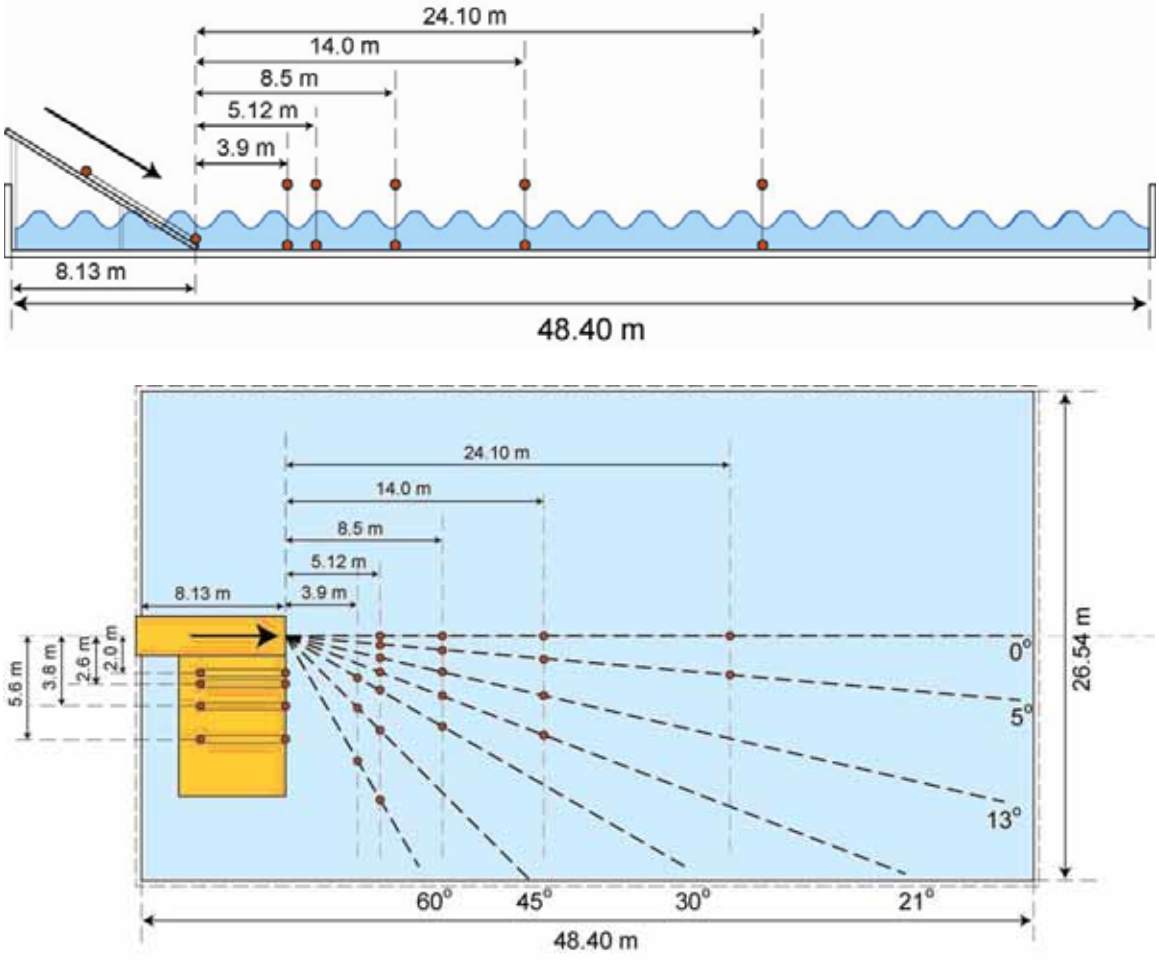

Figure 5. Wave gage arrangement in the wave basin to measure tsunami wave characteristics.

The calibration sequences for the video imagery measurements are shown in figures 6(a) and 6(b). The calibration boards were specifically made for the purpose of the camera array measurements in the wave basin. These calibrations will help in converting the data from the image pixel dimensions to the real world special dimensions.

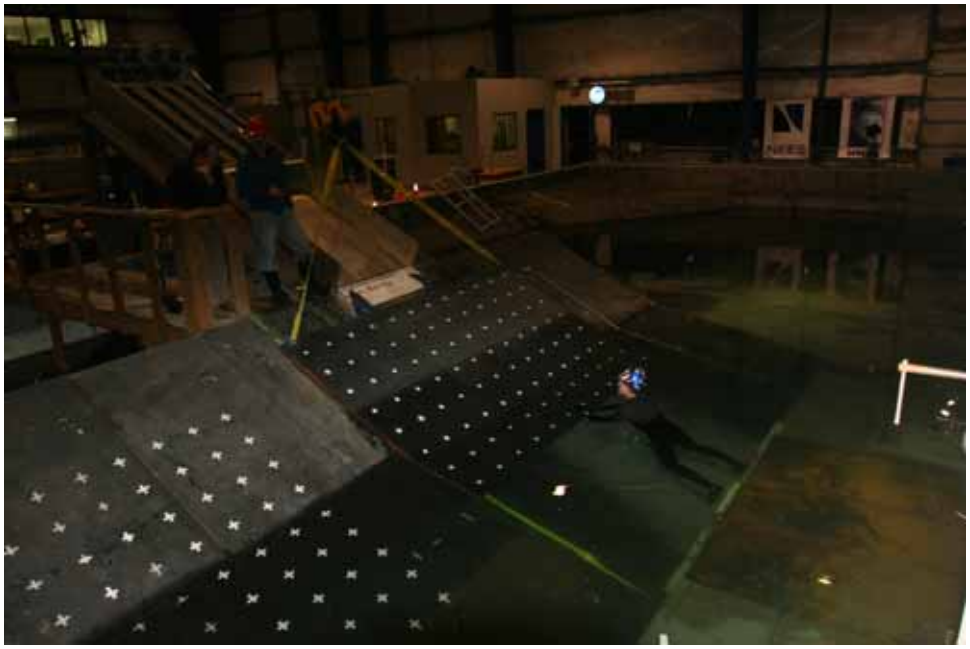

Figure 6(a). Video calibration to measure along slide data.

Figure 6(b). Video calibration to measure landslide characteristics.

Figure 7 shows the loading of the granular slide material into the sled which is then accelerated by the pneumatic pistons to simulate a landslide. Figure 8 shows the recovery of the slide material from underwater after all the measurements in the field are performed for a particular experimental trial.

Figure 7. Loading of the slide material in the box,

Figure 8. Recovery of the slide material after an experimental run.

Table 1 summarizes all the experimental trials that were performed to study the impulse wave characteristics caused by landslides and to explore the relationship between the characteristics of the landslide and the impulse wave that it creates. A total of 65 trials were conducted in varying water depths with different slide velocities and volumes. The first and the second column in the table indicate the trial number and the date on which the trial was conducted. The third column indicates the initial slide position and the location at the launch of the slide material from the box. For example, subaerial/subaerial indicates that initially the slide location is above the water surface and the slide material is also launched from the box above the water surface. Similarly, surface/submerged indicates that the initial position of the slide front is at the water surface and the slide material is launched underwater.

The fourth column indicates the water depth at which the slide was launched. The slide was launched at the water depths of 0.3m, 0.6m, 0.9m, 1.05m, 1.2m and 1.35m. These water depths help in studying the impulse wave characteristics from the deep water regime to the shallow water regime. The fifth column indicates the pressure with which the slide was launched into the water. Two different slide masses were launched to understand how slide volumes relate to the impulse waves created. This is shown in the sixth column and the slide masses were 1293kgs and 646kgs approximately.

The seventh column shows the maximum launch velocity of the box with the slide mass in m/s and the eight column shows the corresponding Froude number in terms of this launch velocity. The last two columns show the maximum wave amplitude and the runup amplitude that were measured by the wave gauge arrangement in the wave basin.

Table 1: Experimental trial characteristics

Trial #	Date	Initial Slide Position	Water Depth (m)	Pressure (bar)	Slide Mass (kg)	V_o (m/s)	Froude No.	Max Wave Amplitude (cm)	Max Runup Amplitude (cm)
1	11/16/06	Subaerial/ Subaerial	0.6	10.00	1292.73	4.00	1.65	-	-
2	11/17/06	Subaerial/ Subaerial	0.58	10.00	1292.73	4.00	1.68	-	-
3	11/20/06	Subaerial/ Subaerial	0.6	10.00	1292.73	4.00	1.65	4.69	7.87
4	11/21/06	Subaerial/ Subaerial	0.6	8.00	1292.73	3.00	1.24	-	-
5	11/21/06	Subaerial/ Subaerial	0.6	8.00	1292.73	3.00	1.24	5.18	9.34
6	11/22/06	Subaerial/ Subaerial	0.6	6.00	1292.73	2.80	1.15	3.25	6.27
7	11/22/06	Subaerial/ Subaerial	0.6	8.00	1292.73	3.00	1.24	3.73	7.46

8	11/22/06	Subaerial/ Subaerial	0.6	4.00	1292.73	2.35	0.97	2.37	4.09
9	11/22/06	Subaerial/ Subaerial	0.6	10.00	1292.73	4.00	1.65	4.54	8.98
10	11/29/06	Subaerial/ Subaerial	0.6	10.00	1292.73	4.00	1.65	4.58	7.97
11	11/29/06	Subaerial/ Subaerial	0.6	10.00	1292.73	4.00	1.65	4.62	7.86
12	11/29/06	Subaerial/ Subaerial	0.6	10.00	646.37	4.00	1.65	4.50	7.74
13	11/29/06	Subaerial/ Subaerial	0.6	8.00	646.37	3.00	1.24	3.93	5.52
14	11/30/06	Subaerial/ Subaerial	0.6	6.00	646.37	2.80	1.15	3.33	4.88
15	11/30/06	Subaerial/ Subaerial	0.6	4.00	646.37	2.35	0.97	2.60	3.38
16	11/30/06	Subaerial/ Subaerial	0.9	10.00	646.37	4.00	1.35	5.26	7.95
17	12/1/06	Subaerial/ Subaerial	0.9	8.00	646.37	3.00	1.01	4.11	7.43
18	12/1/06	Subaerial/ Subaerial	0.9	6.00	646.37	2.80	0.94	3.38	5.77
19	12/1/06	Subaerial/ Subaerial	0.9	4.00	646.37	2.35	0.79	2.61	4.25
20	12/1/06	Subaerial/ Subaerial	0.9	4.00	1292.73	2.35	0.79	2.22	3.95
21	12/1/06	Subaerial/ Subaerial	0.9	6.00	1292.73	2.80	0.94	3.17	6.40
22	12/1/06	Subaerial/ Subaerial	0.9	8.00	1292.73	3.00	1.01	3.86	8.11
23	12/1/06	Subaerial/ Subaerial	0.9	10.00	1292.73	4.00	1.35	5.85	10.29
24	12/5/06	Subaerial/ Surface	1.2	10.00	1292.73	4.00	1.17	12.71	13.33
25	12/5/06	Subaerial/ Surface	1.2	10.00	1292.73	4.00	1.17	11.12	14.57
26	12/5/06	Subaerial/ Surface	1.2	4.00	1292.73	2.35	0.68	2.78	4.92
27	12/6/06	Subaerial/ Surface	1.2	10.00	646.37	4.00	1.17	9.38	10.32
28	12/6/06	Subaerial/ Surface	1.2	8.00	646.37	3.00	0.87	5.77	10.20
29	12/6/06	Subaerial/ Surface	1.2	10.00	646.37	4.00	1.17	6.79	9.77
30	12/6/06	Subaerial/ Surface	1.2	6.00	646.37	2.80	0.82	4.23	7.46
31	12/6/06	Subaerial/ Surface	1.2	4.00	646.37	2.35	0.68	3.00	5.99
32	12/7/06	Subaerial/ Surface	1.2	10.00	646.37	4.00	1.17	10.24	9.71
33	12/7/06	Subaerial/ Surface	1.2	6.00	1292.73	2.80	0.82	4.63	8.88
34	12/7/06	Subaerial/ Surface	1.2	10.00	1292.73	4.00	1.17	11.78	12.63

35	12/7/06	Subaerial/ Surface	1.2	8.00	1292.73	3.00	0.87	7.22	11.10
36	12/8/06	Subaerial/ Surface	1.2	10.00	1292.73	4.00	1.17	11.78	12.75
37	12/12/06	Surface/ Submerged	1.2	10.00	1292.73	4.00	1.17	3.78	10.29
38	12/12/06	Surface/ Submerged	1.2	10.00	1292.73	4.00	1.17	5.77	8.38
39	12/13/06	Surface/ Submerged	1.2	10.00	1292.73	4.00	1.17	5.52	9.60
40	12/13/06	Surface/ Submerged	1.2	10.00	1292.73	4.00	1.17	5.54	7.52
41	12/13/06	Surface/ Submerged	1.2	10.00	1292.73	4.00	1.17	5.85	7.62
42	12/14/06	Surface/ Submerged	1.2	4.00	1292.73	2.35	0.68	3.58	6.88
43	12/14/06	Surface/ Submerged	1.2	6.00	1292.73	2.80	0.82	4.00	6.36
44	12/14/06	Surface/ Submerged	1.2	8.00	1292.73	3.00	0.87	4.00	6.36
45	12/14/06	Surface/ Submerged	1.35	10.00	1292.73	4.00	1.10	5.48	6.81
46	12/14/06	Surface/ Submerged	1.35	4.00	1292.73	2.35	0.65	3.32	5.79
47	12/15/06	Subaerial/ Surface	0.6	10.00	1292.73	4.00	1.65	7.60	18.74
48	12/18/06	Subaerial/ Surface	0.6	8.00	1292.73	3.00	1.24	5.91	13.84
49	12/18/06	Subaerial/ Surface	0.6	8.00	646.37	3.00	1.24	5.77	15.60
50	12/18/06	Subaerial/ Surface	0.6	10.00	646.37	4.00	1.65	7.82	16.26
51	12/18/06	Subaerial/ Surface	0.6	6.00	646.37	2.80	1.15	3.71	10.01
52	12/18/06	Subaerial/ Surface	0.6	4.00	646.37	2.35	0.97	2.65	7.73
53	12/19/06	Subaerial/ Surface	0.3	4.00	646.37	2.35	1.37	2.32	3.43
54	12/19/06	Subaerial/ Surface	0.3	6.00	646.37	2.80	1.63	2.92	4.95
55	12/19/06	Subaerial/ Surface	0.3	8.00	646.37	3.00	1.75	3.77	5.53
56	12/19/06	Subaerial/ Surface	0.3	10.00	646.37	4.00	2.33	5.65	7.60
57	12/19/06	Subaerial/ Surface	0.3	10.00	1292.73	4.00	2.33	7.06	9.57
58	12/20/06	Subaerial/ Surface	1.05	10.00	1292.73	4.00	1.25	7.10	11.71
59	12/20/06	Subaerial/ Surface	1.05	10.00	1292.73	4.00	1.25	7.48	14.47
60	12/20/06	Subaerial/ Surface	1.05	10.00	1292.73	4.00	1.25	6.04	12.93
61	12/20/06	Subaerial/ Surface	1.05	10.00	1292.73	4.00	1.25	5.77	12.68
62	12/21/06	Subaerial/	1.05	10.00	1292.73	4.00	1.25	4.79	11.48

		Surface							
63	12/21/06	Subaerial/ Surface	1.05	10.00	1292.73	4.00	1.25	8.07	13.17
64	12/21/06	Subaerial/ Surface	1.05	10.00	1292.73	4.00	1.25	7.42	14.44
65	12/21/06	Subaerial/ Surface	1.05	10.00	1292.73	4.00	1.25	8.69	13.80

The following set of figures shows the measured wave form along radial directions from the point of impact. Figure 9 shows the wave forms measured by four wave gauges directly in front of the impact location, along the 0^o radial line. The first wave gauge was located at a distance of 5.12m away from the point of impact. Similarly, the second, third and the fourth gauges were located at the distances of 8.5m, 14.0m and 24.1m respectively from the point of impact. These wave forms show the gradual decay of the impulse wave as it travels away from the point of impact.

Similar to figure 9, figure 10 also shows the wave forms from three wave gauges along the 30^o radial direction. These wave gauges are located at the distances of 4.5m, 5.912m and 9.8m. Figure 11 shows the runup wave forms measured along a slope beside the slide. These wave gauges are located at distances of 2m, 2.6m, 3.8m and 5.6m. This set of data helps us in understanding the runup characteristics of the local impulse waves created by the landslides. These are generally higher than the measured waves away from the impact, as can be seen in figures 9, 10 and 11.

Figures 9, 10 and 11 shows the wave profile measured for the experimental trial 11, dated November 29, 2006. This trial corresponds to the pneumatic firing pressure of 10 bar, which gives the maximum slide impact velocity and at a water depth of 60cm for full mass of sled loading. Figures 12, 13 and 14 show the wave profile measured at the wave gages along the center line, the radial line at 30^o and the runup along the slope for the experimental trial 8 dated November 22, 2006. This trial corresponds to a pneumatic firing pressure of 4 bar which gives the lowest slide impact velocity at the water depth of 60cm for full mass sled loading.

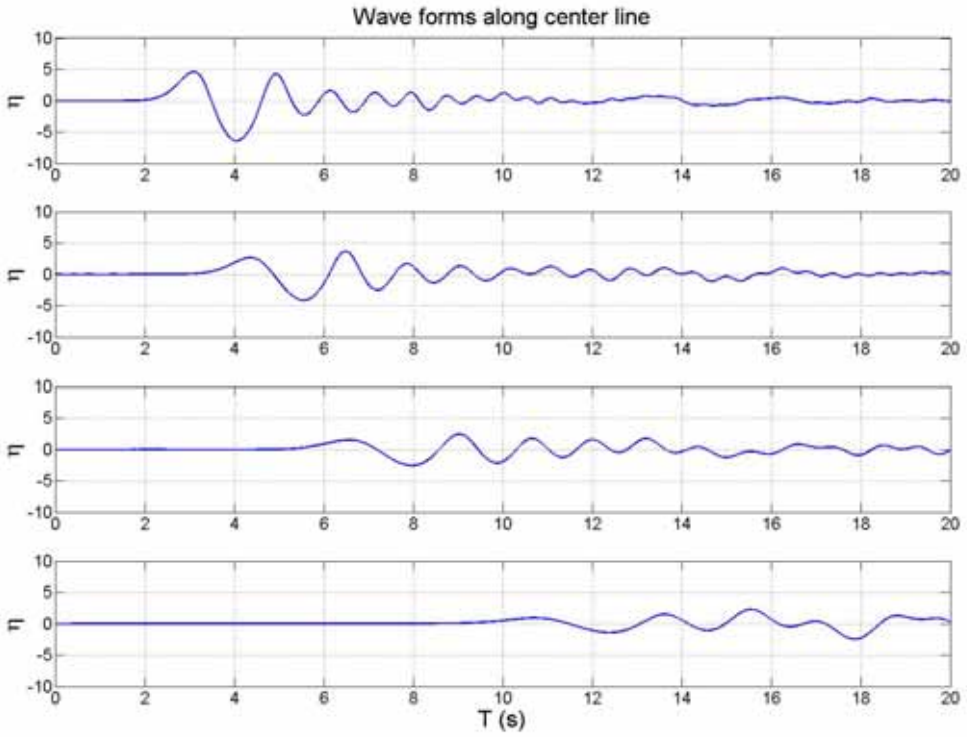

Figure 9. Centerline wave form for trial 11, 11/29/06

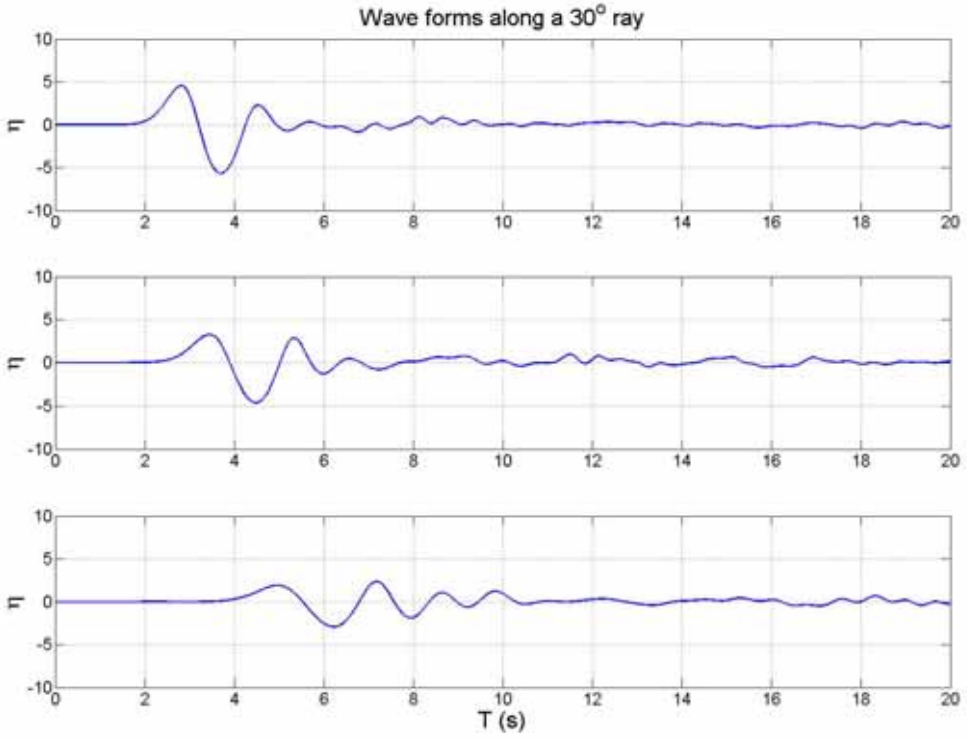

Figure 10. Wave form along 30° ray for trial 11, 11/29/06

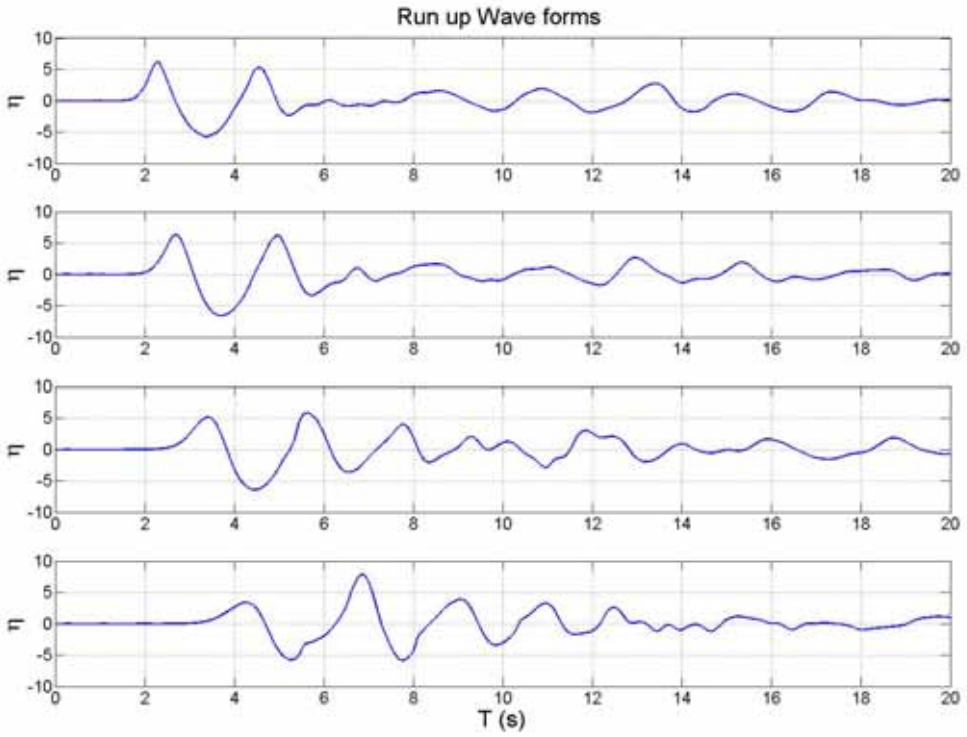

Figure 11. Runup wave form for trial 11, 11/29/06

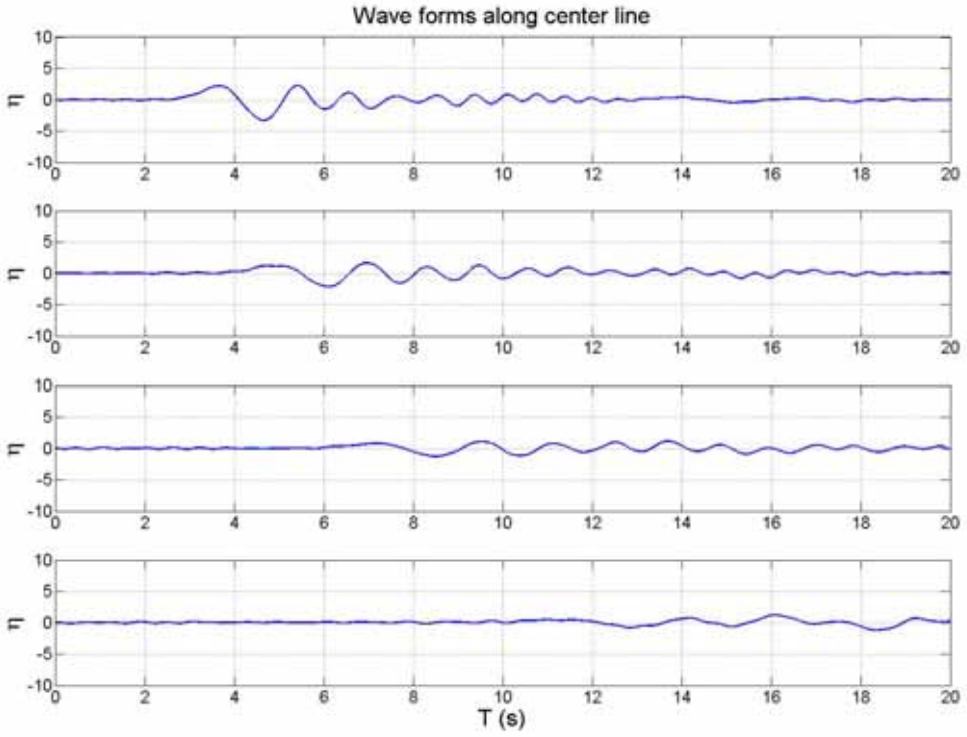

Figure 12. Centerline wave form for trial 8, 11/22/06

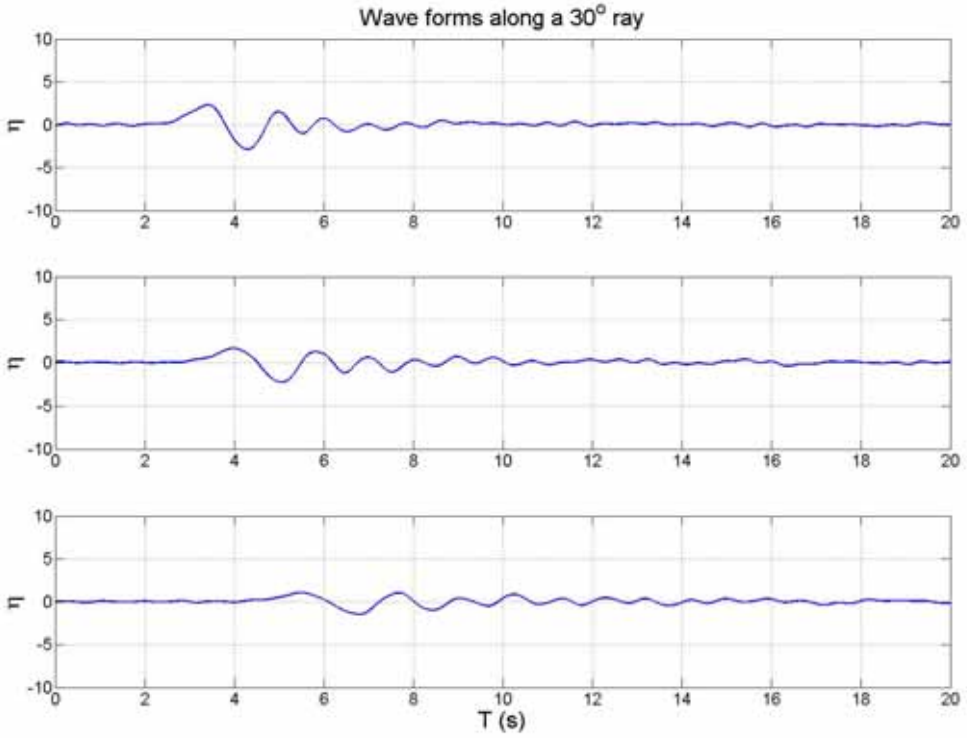

Figure 13. Wave form along 30^{o} ray for trial 8, 11/22/06

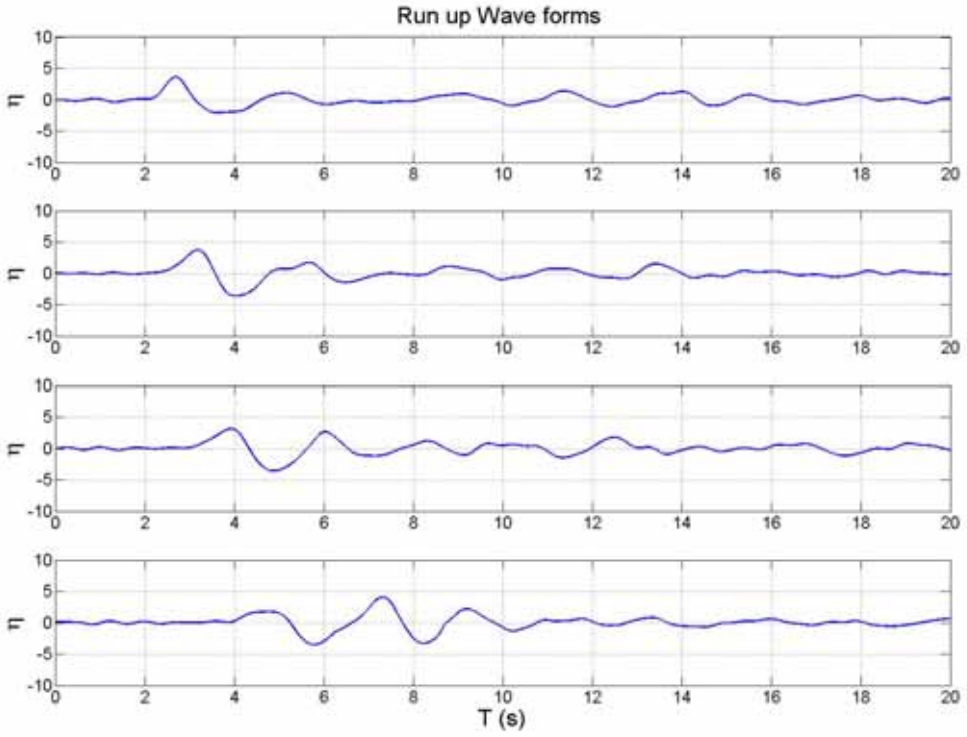

Figure 14. Runup wave form for trial 8, 11/22/06

The measured wave forms provide valuable information on the generated tsunami wave characteristics. It is important to understand and learn the rate and distance with which the impulse wave decays. In figures 15, 16 and 17, the wave amplitude decay is shown in both the radial distance as well as in the angular direction. These figures were obtained from the wave data of trial 11, dated 11/29/06. The maximum wave amplitude was obtained at each wave gauge in the experiment. Then these maximum wave amplitudes were plotted against the radial distance from the point of impact and the angular direction around the point of impact. The angles vary from 0^o, which is the ray pointing in the direction of the slide propagation or the centerline of the wave basin, to 90^o which is the direction of the runup wave propagation along the slope of the slide.

In figure 17, the different curves represent the waves measured along sections parallel to the slope runup direction. The highest curves are for the gauges which are at a horizontal distance of 3.9m from the point of impact. The subsequent decreasing curves are obtained from measurements made at sections which are 5.12m, 8.5m, 14m and 24.1m away from the point of impact.

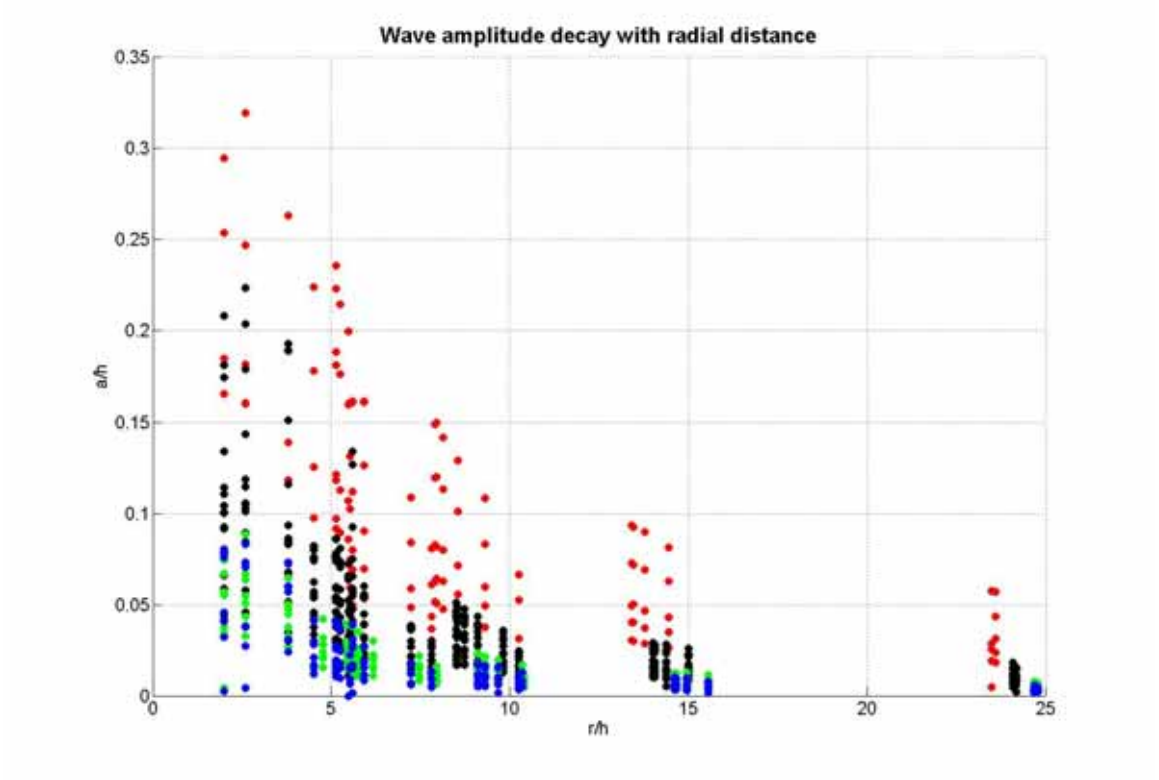

Figure 15: Wave amplitude decay with radial distance

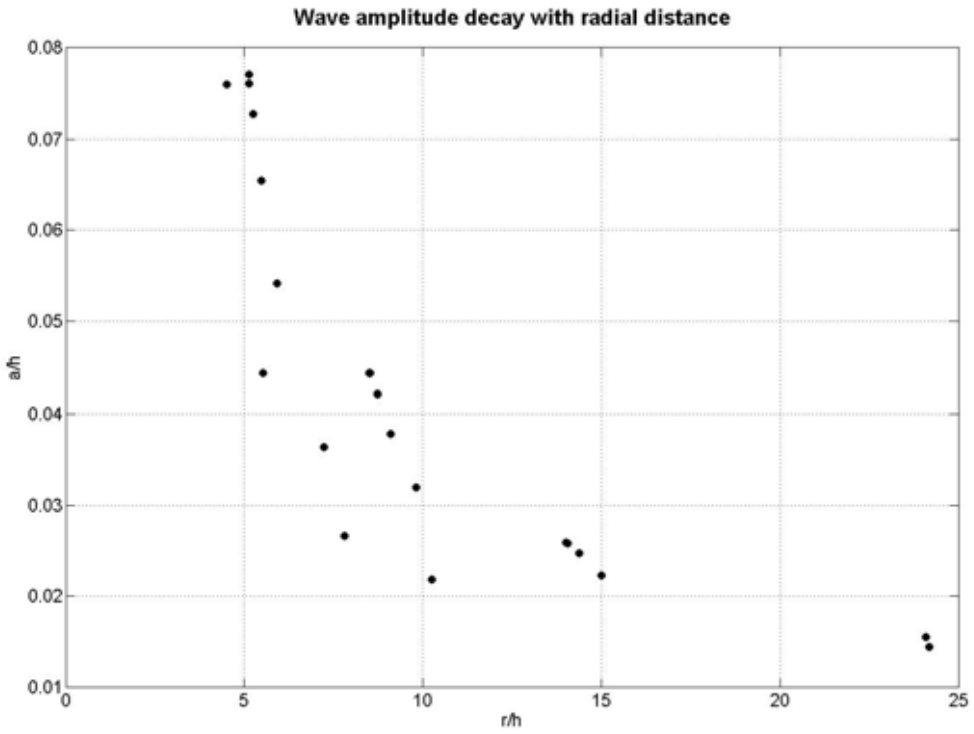

Figure 16. Wave amplitude decay with radial distance for trial 11, 11/29/06

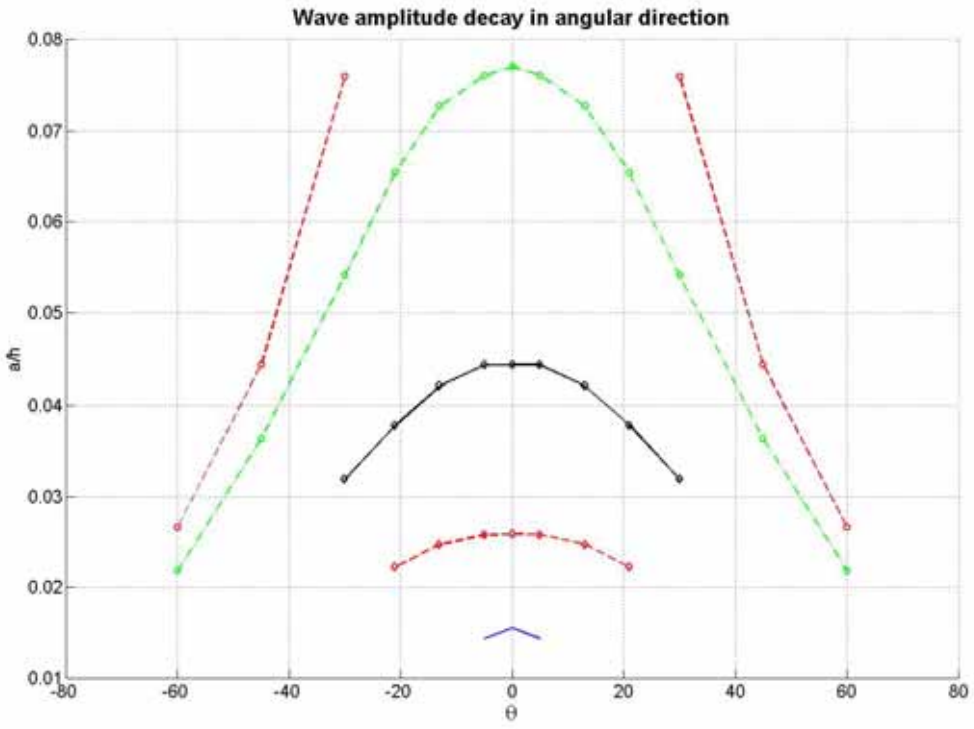

Figure 17. Wave amplitude decay with in the angular direction for trial 11, 11/29/06

The first crest wave amplitude that is measured at all the wave gages in the wave basin is shown in figure 18. The surface envelop of the amplitude is shown in the field. The wave amplitude is non-dimensionalized by the water depth. The long shore and the onshore distances are also non-dimensionalized using the water depth. This envelop shows the attenuation of the wave amplitude with the distance away from the landslide source.

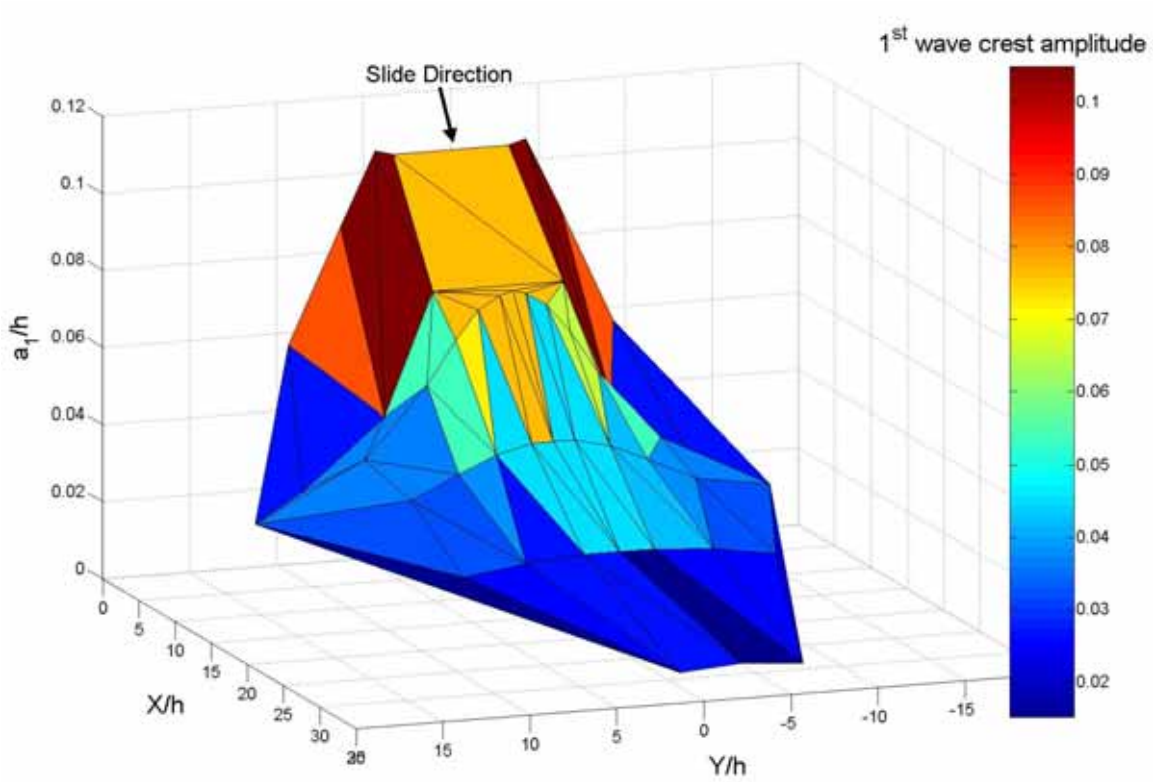

Figure 18. First wave crest amplitude surface measured at all the wave gages fro trial 11, 11/29/06

The maximum wave amplitude of the generated wave is assumed to decay with radial distance away from the landslide source according to the relation given by equation 1.

$$a = \frac{k}{r^n} \quad \textbf{(1)}$$

a is the maximum amplitude measured at the wavegage, and ***r*** is the radial distance of that wavegage from the landslide source. The factor ***k*** depends on the angular direction θ away from the landslide source and the landslide parameters that generate the tsunami wave such as the slide impact velocity, the slide thickness and the slide width at the impact location. The maximum measured amplitude at each wave gage for all the experimental trials, irrespective of the trial condition is plotted against the radial distance. Then a regression analysis gives us the factors ***k***, which is constant for a particular experimental trial and ***n*** which is constant for a particular water depth case. This indicates that the spatial decay rate of the maximum amplitude of the tsunami wave depends on the generated wave characteristics and the source characteristics. Figure 19 shows the amplitude decay with the spatial distance in terms of the above evaluated parameters.

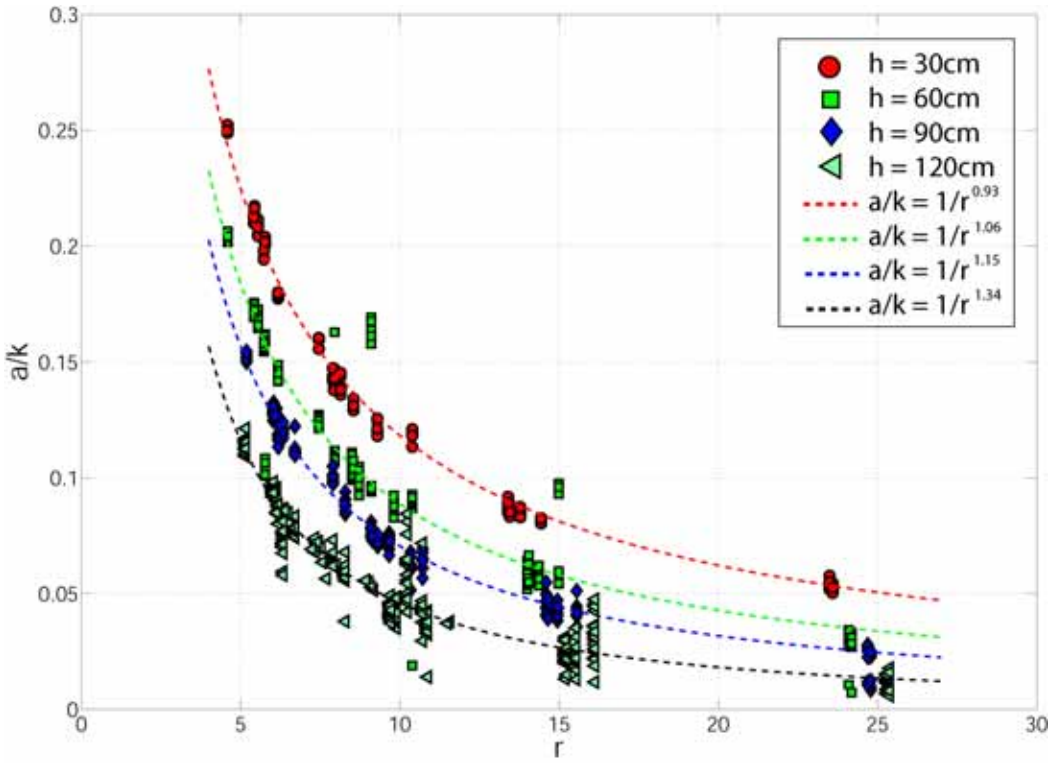

Figure 19. Wave amplitude decay with radial distance

The measured wave profile also provides data to measure the speed with which the wave propagates in the direction away from the landslide. This information is used to predict the travel time and the arrival time of the generated tsunami waves and helps in developing better tsunami forecasting systems. For tsunami waves generated by landslides, the first few waves from the generated wave train are usually the most destructive in nature. The zero-upcrossing method is used to identify the first three waves in the generated wave train in these experiments. Then by measuring the time taken for these three waves to travel from one wave gage to another in one particular direction, the celerity of these waves are estimated. Since the distance between the wave gages are known, the celerity of the waves are calculated by dividing the distance the wave travels between the wave gages with the time taken by these waves to travel that particular distance. Thus the wave celerity c_1, c_2 and c_3 are estimated for the crest and trough for the first three waves. Figure 20 shows the plot of the wave celerity versus the respective crest and trough amplitude for the first three waves for all the experimental trials. The wave celerity is non-dimensionalized using the shallow water wave speed $\sqrt{gh}$ and the crest and trough amplitude is non-dimensionalized with the water depth. The dashed line indicates the theoretical limit of the wave speed for the Stokes wave. The first wave speed corresponds to the Stokes wave speed, while the second and third wave speed is significantly lower. This is due to the strong dispersive nature of the landslide generated tsunami waves.

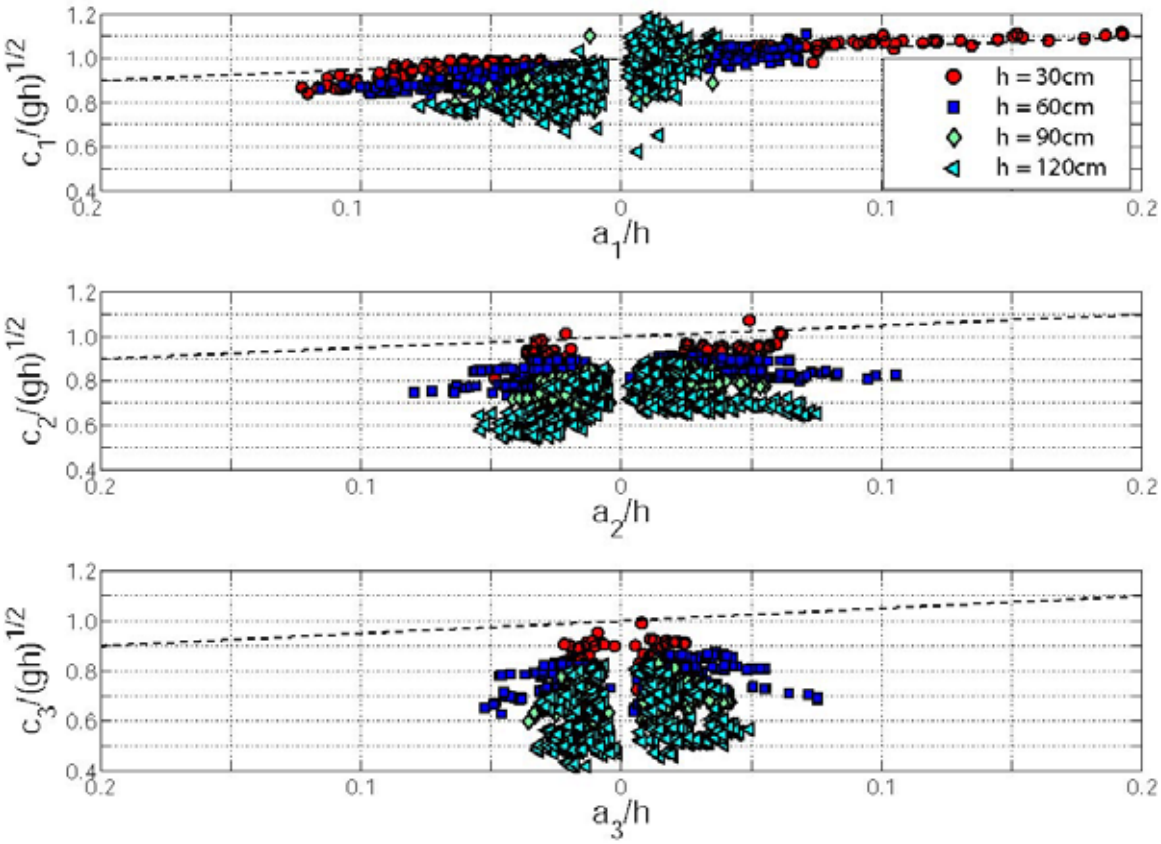

Figure 20. Wave celerity versus wave amplitude

The time period for the first three waves is measured from the measured wave profiles by subtracting the successive upcrossing points. The difference between the first and the zero upcrossing points gives the time period of the first wave. Subsequently the time period of the second and the third wave is also evaluated. Figures 21, 22 and 23 show the measured time period of the first three waves versus the radial distance. The plots show the variation in the time period as the wave travels radially away from the landslide source and transits from the non linear wave to linear wave regime. The time period is non-dimensionalized by $\sqrt{h/g}$ and the radial distance is non-dimensionalized by the water depth. A regression analysis for the entire dataset yields the time period dependency on the radial distance of the first three waves as given by equation 3.

$$T\sqrt{(g/h)} = 3.46(r/h)^{0.4}$$
$$T\sqrt{(g/h)} = 2.30(r/h)^{0.34} \quad \textbf{(3)}$$
$$T\sqrt{(g/h)} = 2.01(r/h)^{0.31}$$

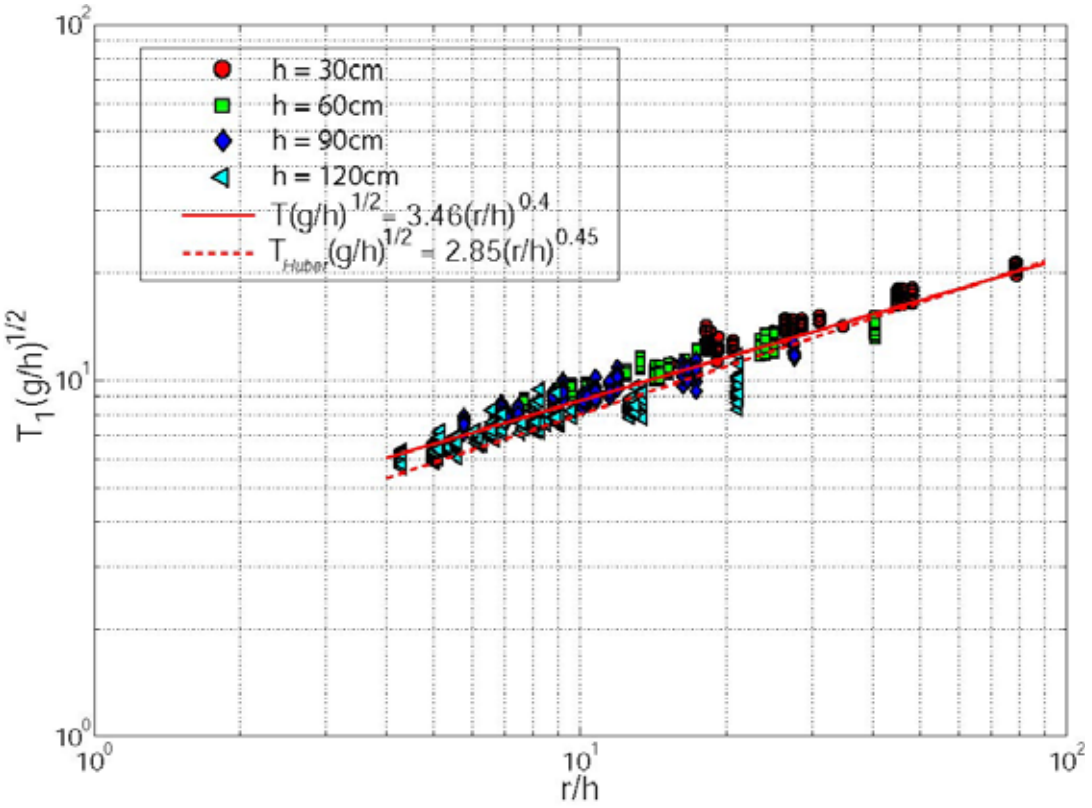

Figure 21. First wave time period T_1 versus distance travelled by the wave r

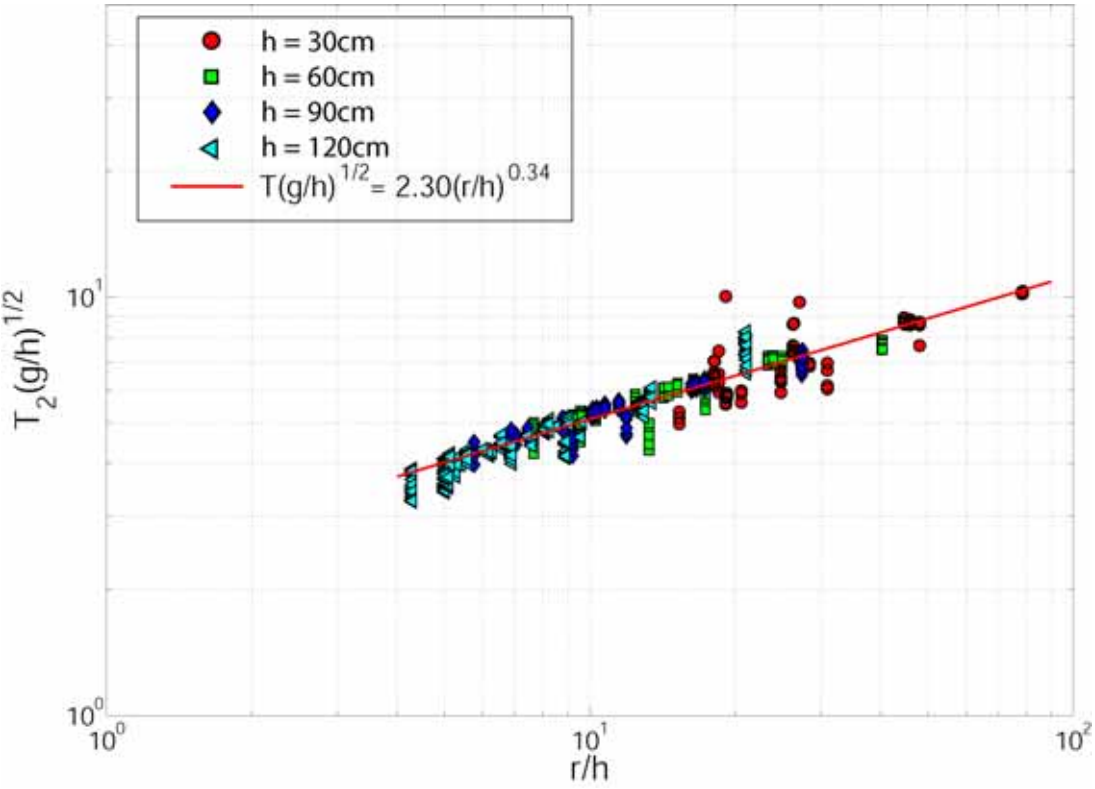

Figure 22. Second wave time period T_2 versus distance travelled by the wave r

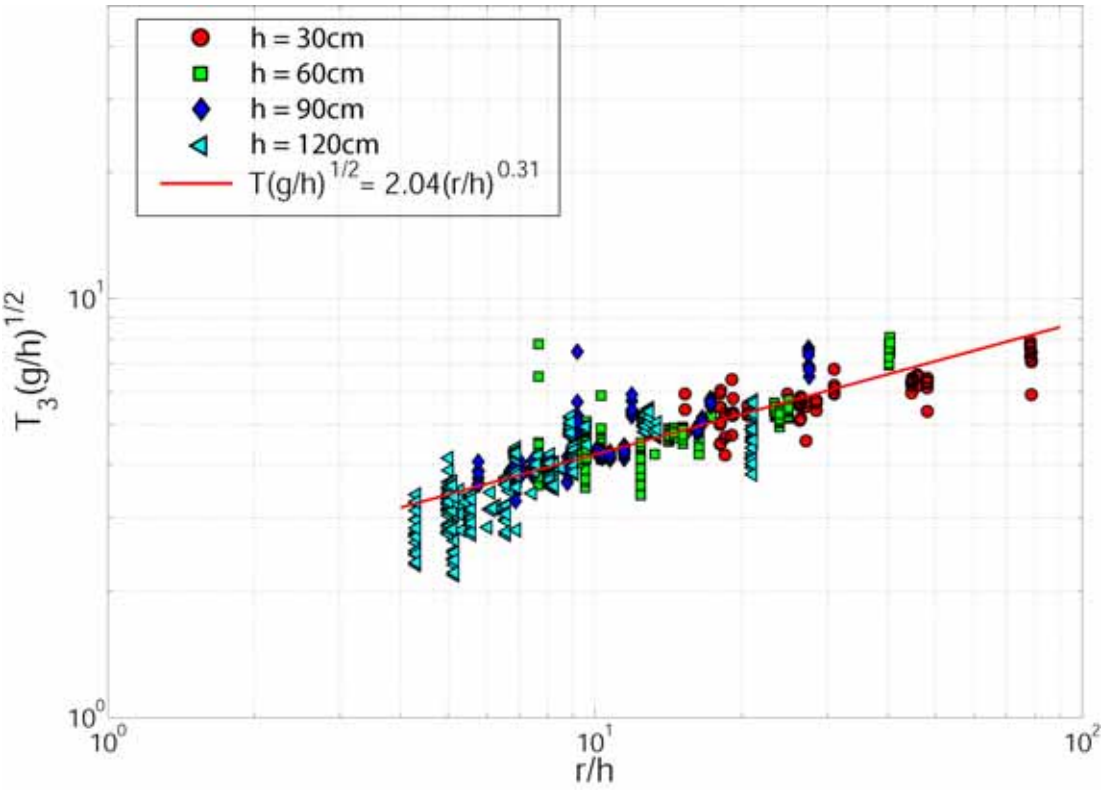

Figure 23. Third wave time period T_3 versus distance travelled by the wave r

The wave lengths of the first three waves are calculated next. The celerity of the wave is approximated as the mean celerity of the wave crest and trough. Then the wave celerity multiplied by the measured time period gives the wave length of the wave. Figure 24 shows the wave length of the first three waves as functions of the radial distance away from the landslide source. The wave length and the radial distance are non-dimensionalized by the water depth.

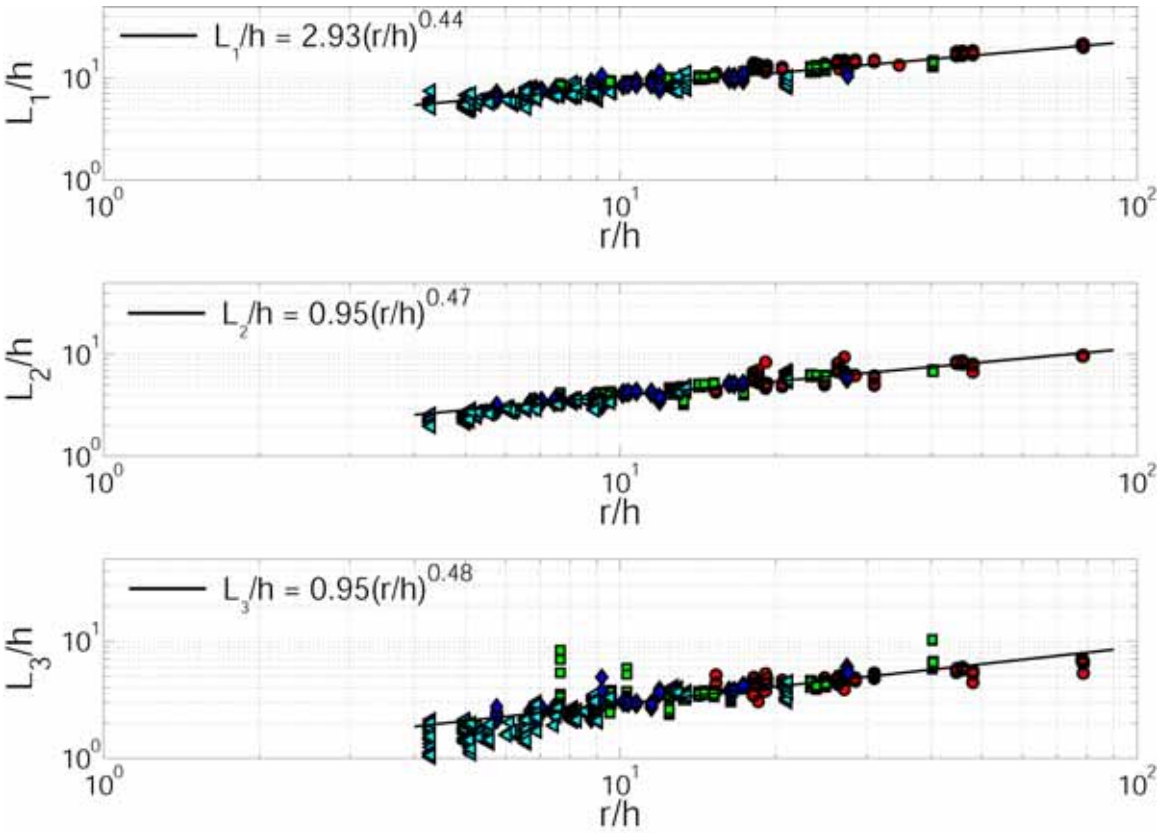

Figure 24. Wave lengths L_1, L_2 and L_3 of the first three generated waves versus distance r travelled by the wave

A regression analysis of the calculated wave length data for all the experimental trials yield the dependence of the wave length with the distance the wave travels. These functions are given by equation 3.

$$\frac{L_1}{h} = 2.93\left(\frac{r}{h}\right)^{0.44}$$
$$\frac{L_2}{h} = 0.95\left(\frac{r}{h}\right)^{0.47} \quad \textbf{(3)}$$
$$\frac{L_3}{h} = 0.95\left(\frac{r}{h}\right)^{0.47}$$

These obtained functions show that the compared to the first wavelength, the second and the third wavelength display similar behavior as the generated tsunami propagates away from the landslide source.

An array of underwater and above water cameras is present to record the experiment during each trial. These cameras continuously record the landslides from the inception of the slide motion, impact at the water surface and deposit at the bottom of the wave basin. The different camera positions help to visualize the landslide behavior and the tsunami generation process from different angles. These help to extract all the relevant data across all the dimensions. The different locations of the cameras shown are shown in figure 4. The top camera provides an overall view on the experiment and shows the landslide dynamics and the wave generation aspects clearly. The view from this camera is shown in figure 25.

Figure 25. Top camera view of the experiment area

The above water side angle camera is placed on the slide slope above the water surface. It covers the extent of area on the slope form the release of the slide from the sled to the splash zone location near the water surface where it impacts the water surface and generates the tsunami wave. The view from this camera is shown in figure 26. This view enables us to extract the slide front velocity above the water surface as the slide moves to impact the water surface. It also provides us information on the maximum thickness of the landslide above the water surface on the slide slope. This information combined with the slide width data provide an approximate rate of the mass flow as the slide flows down the slope and impacts the water surface.

Figure 26. Above water side view of the experiment area

Figure 27 shows the view of the experiment as seen from the underwater side view camera.

Figure 27. Underwater side view of the experiment area

The recordings from the underwater side camera yield information on the slide front velocity underwater and the slide thickness after the slide impacts the water surface and goes down the slope to deposit at the bottom of the wave basin. A camera placed in front of the slide slope provides a view which directly looks out at the toe of the slide slope. The view from this camera is shown in figure 28. The recordings from this camera yield data on the width of the slide underwater and the final deposited shape of the slide at the end of the experimental trial.

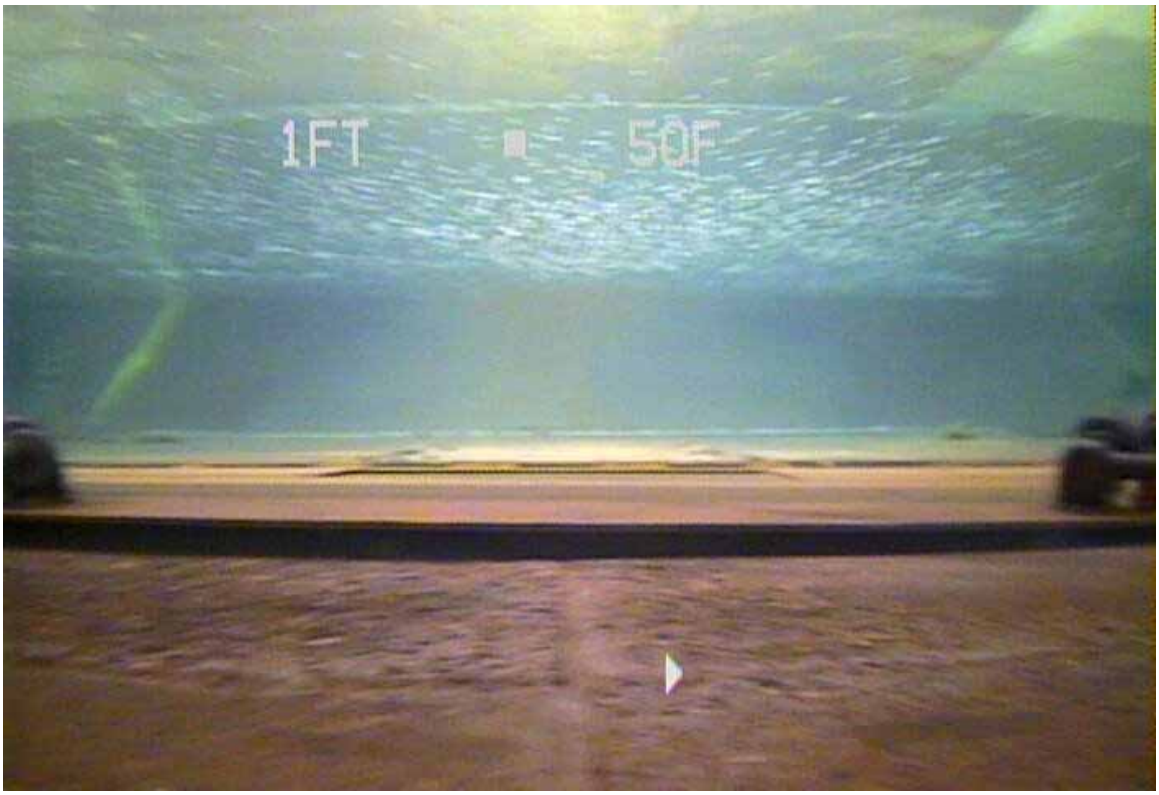

Figure 28. Underwater front camera view of the experiment area

A camera is placed above water such that the viewing plane of the camera is the plane of the slide slope. The view of this camera is shown in figure 29. This view helps us in extracting information related to the runup wave or the edge wave along the slide slope. Information such as the speed of the wave, time period, the wave length and wave amplitude can be obtained and corroborated by the data obtained from the runup wave gages.

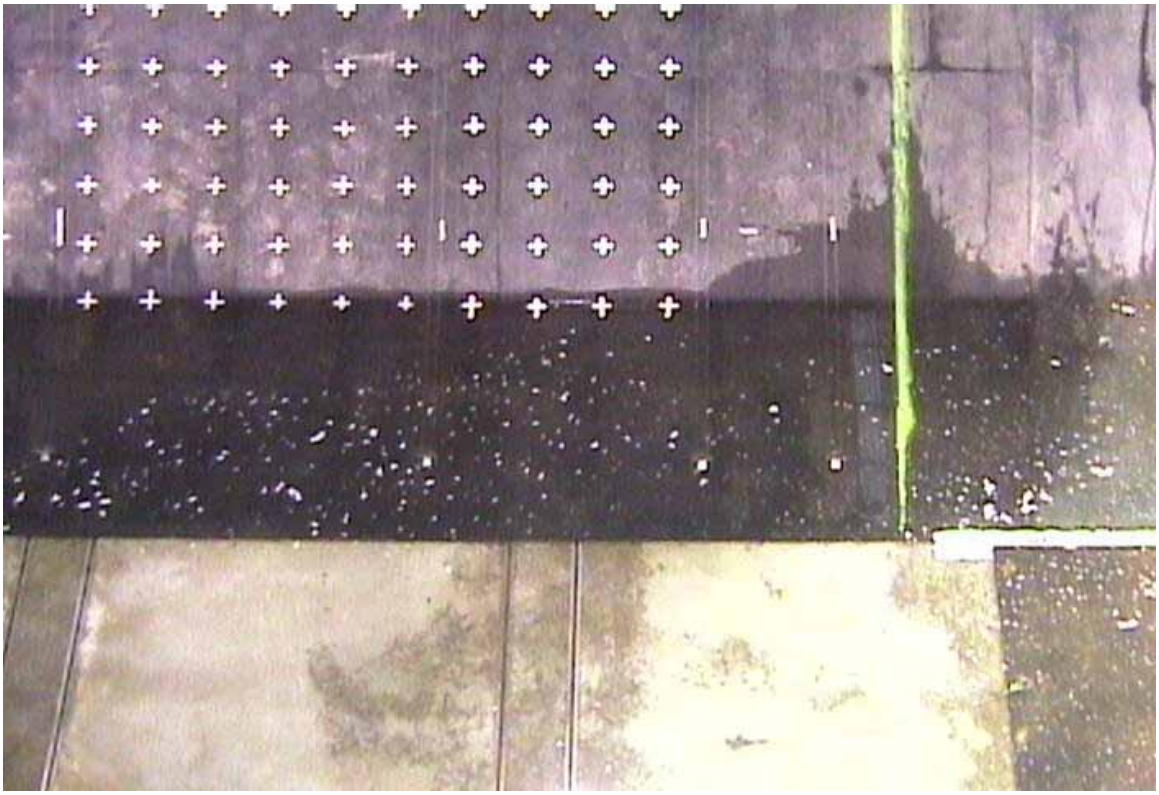

Figure 29. Above water view of the runup wave area

In the next set of figures, a sequence of images which illustrate the landslide tsunami generation is shown from the different views provided by the different cameras. All the images shown belong to the experiment trial which was conducted at a water depth of 60cm for a full sled mass loading and the maximum firing pressure. This corresponds to trial 11 dated November 29, 2006. Figure 30 shows the landslide tsunami generation sequence as recorded by the top camera.

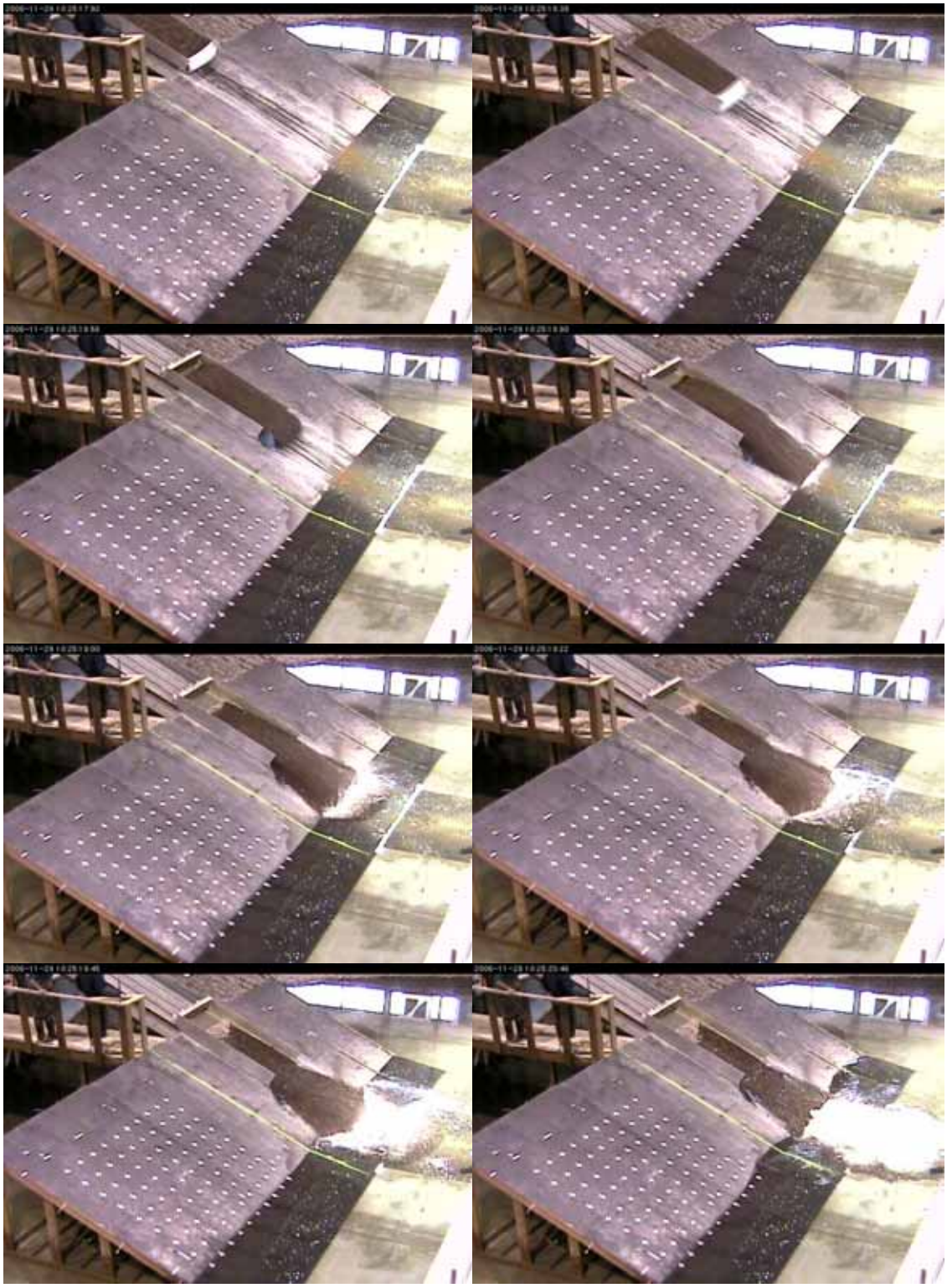

Figure 30. LTG experiment seen form the top camera

Figure 31 shows the same landslide tsunami generation process as seen from the above water side camera.

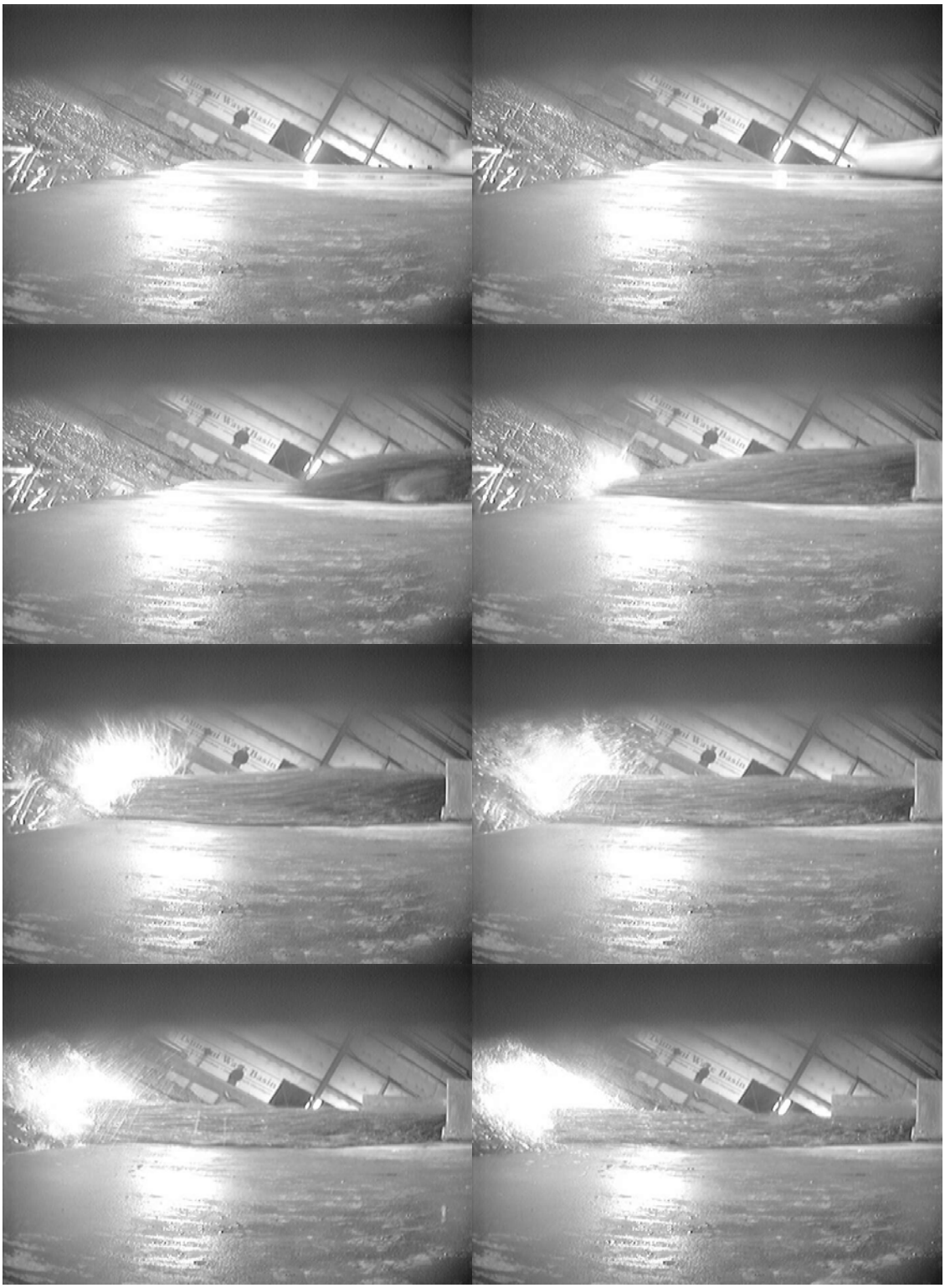

Figure 31. LTG experiment send from the above water side camera

Figure 32 shows the same landslide tsunami generation process as seen from the underwater side camera.

Figure 32. LTG experiment send from the underwater side camera

Figure 33 shows the same experimental trial as seen from the underwater front camera.

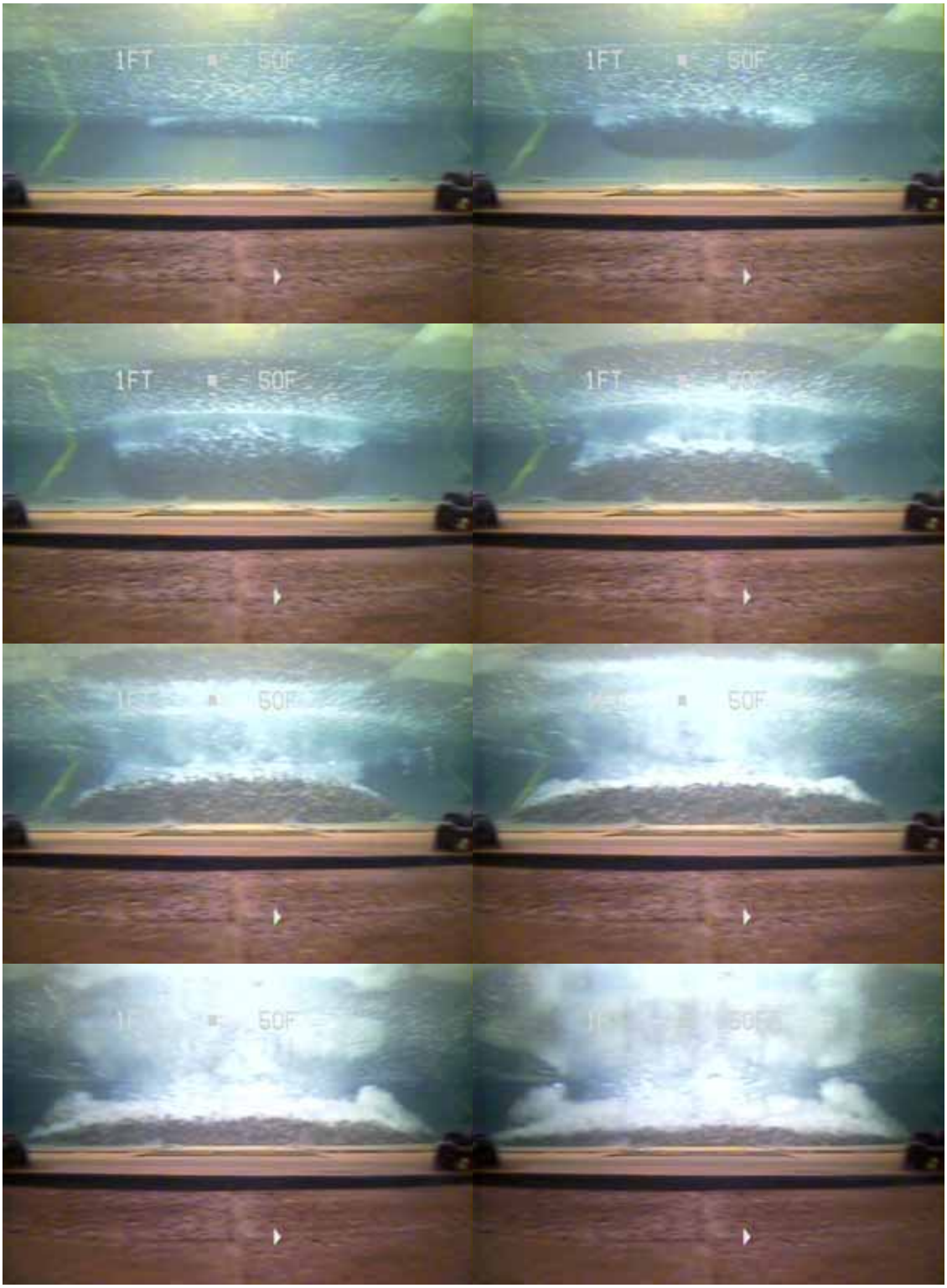

Figure 33. LTG experiment send from the underwater side camera

Figure 34 shows the generated runup water as seen from the above water runup camera.

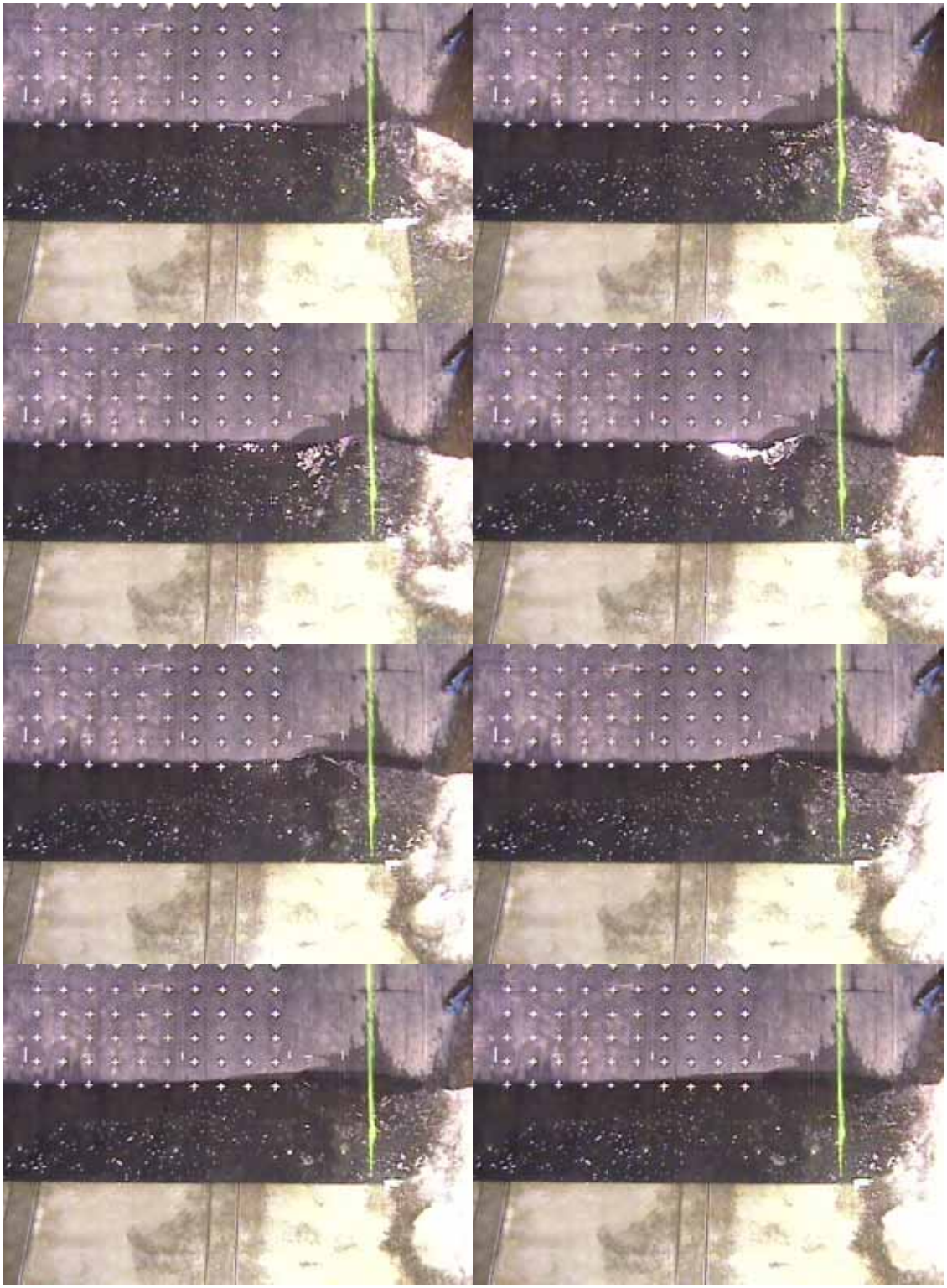

Figure 34. Runup wave as seen by the above water runup camera

Apart from the above cameras, a high resolution Particle Image Velocimetry (PIV) camera was also present to measure the velocity characteristics of the landslide and the water surface during the tsunami generation process. These cameras also yield images which are used to extract the slide width information above the water surface, on the slide slope as the landslide impacts the water surface and generates the tsunami wave. This set of images with the slide edge is shown in figure 35.

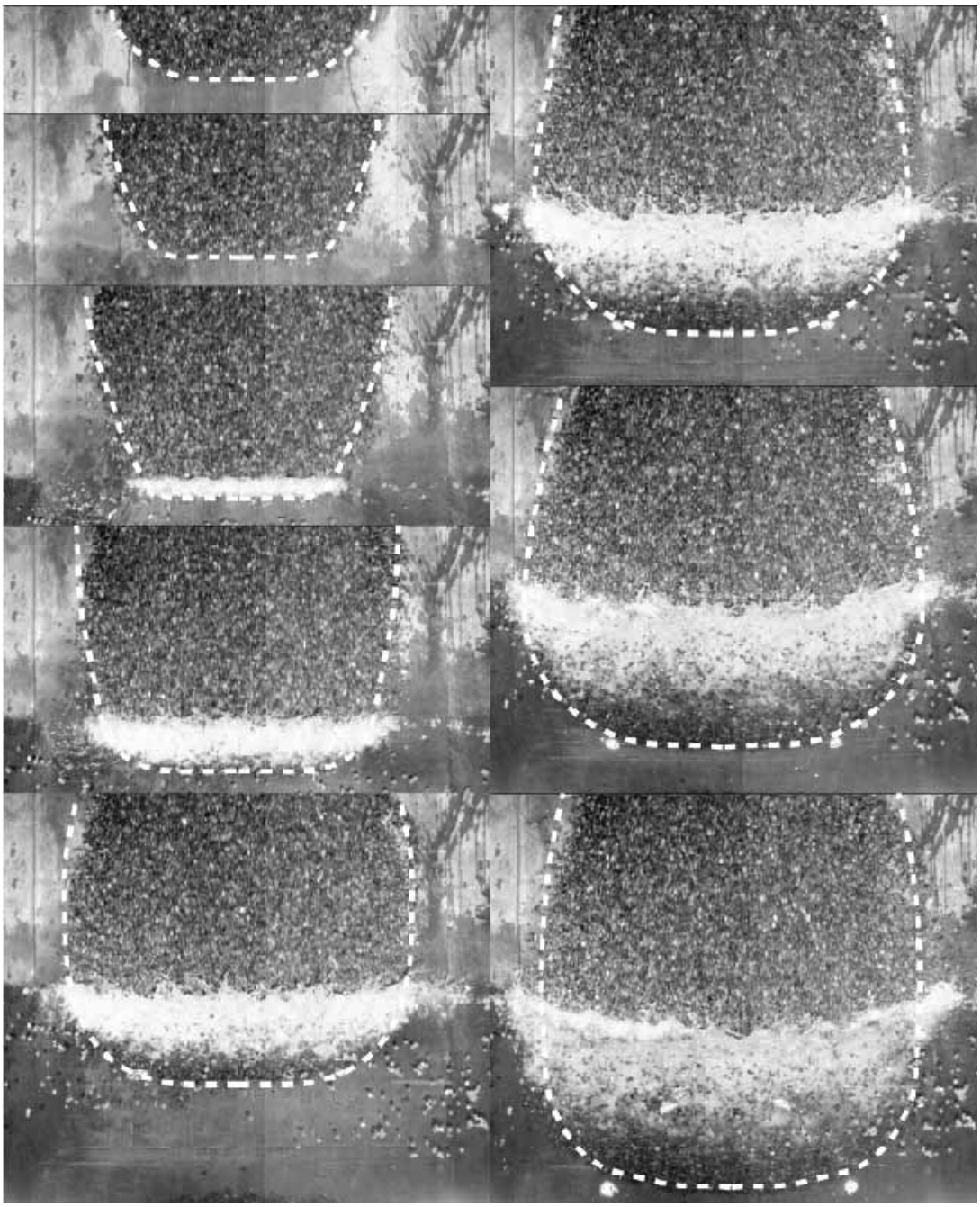

Figure 35. PIV camera images of the slide above the water surface for trial 11, 11/29/06

From the set of images shown in figure 35, a row of pixels at the water surface is extracted and placed in a time stack to obtain a new image. This image is shown in figure 36. In the time stack shown, the x axis corresponds to the width in pixel which is converted by the known calibration factors into the real world scale. The y axis represents the time scale, with time increasing as we go down in the time stack image.

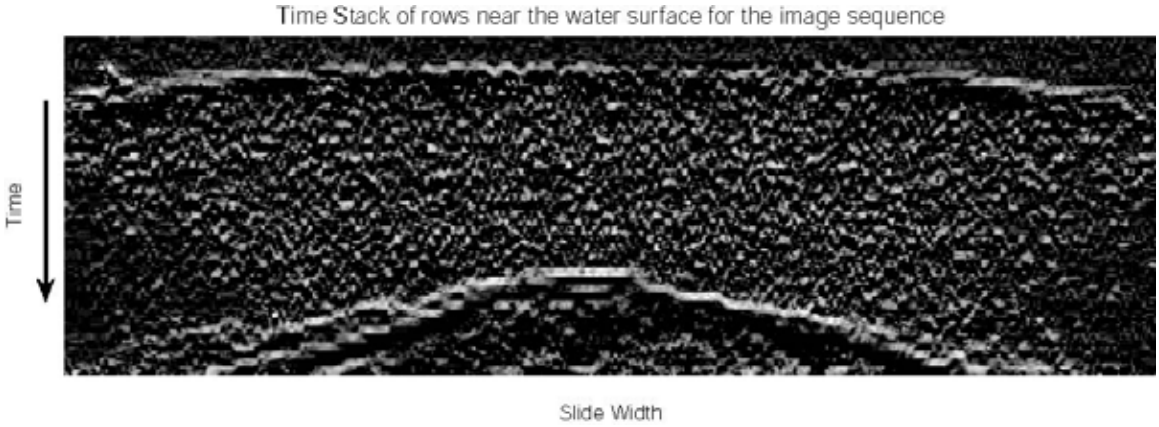

Figure 36. Time Stack of a row at water surface for width extraction for trial 11, 11/29/06

By thresholding the image shown in figure 36, it is converted into a binary black and white image. Then various morphological operations are performed on the binary image to clear the noise in the image and identify the bulk area in the middle corresponding to the granular slide material. Then the edge of this area is extracted which when translated to the original image gives us the slide width. Figure 37 shows the same time stack image after the edge is extracted.

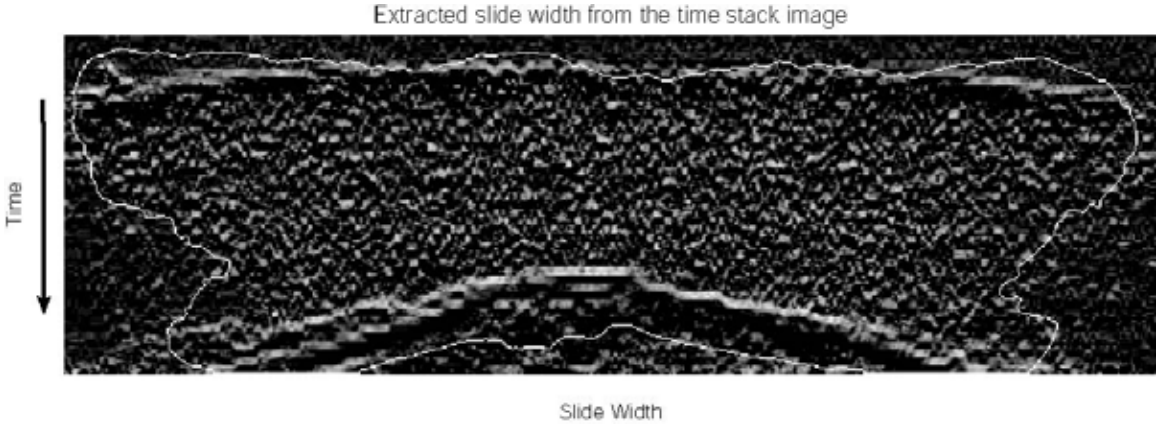

Figure 37. Extracted edge of the time stack image for trial 11, 11/29/06

After the edges are extracted in all the images across all the rows, we get the entire data set corresponding to the width information of the slide at any location above the water surface and at any time. Figure 38 shows the sample slide width versus time at the water surface. The initial slide width in the sled is 1.2m. At the water surface, this width reaches to a maximum of 2.5m. In the figure shown, $t = 0$ corresponds to the time when the landslide impacts the water surface.

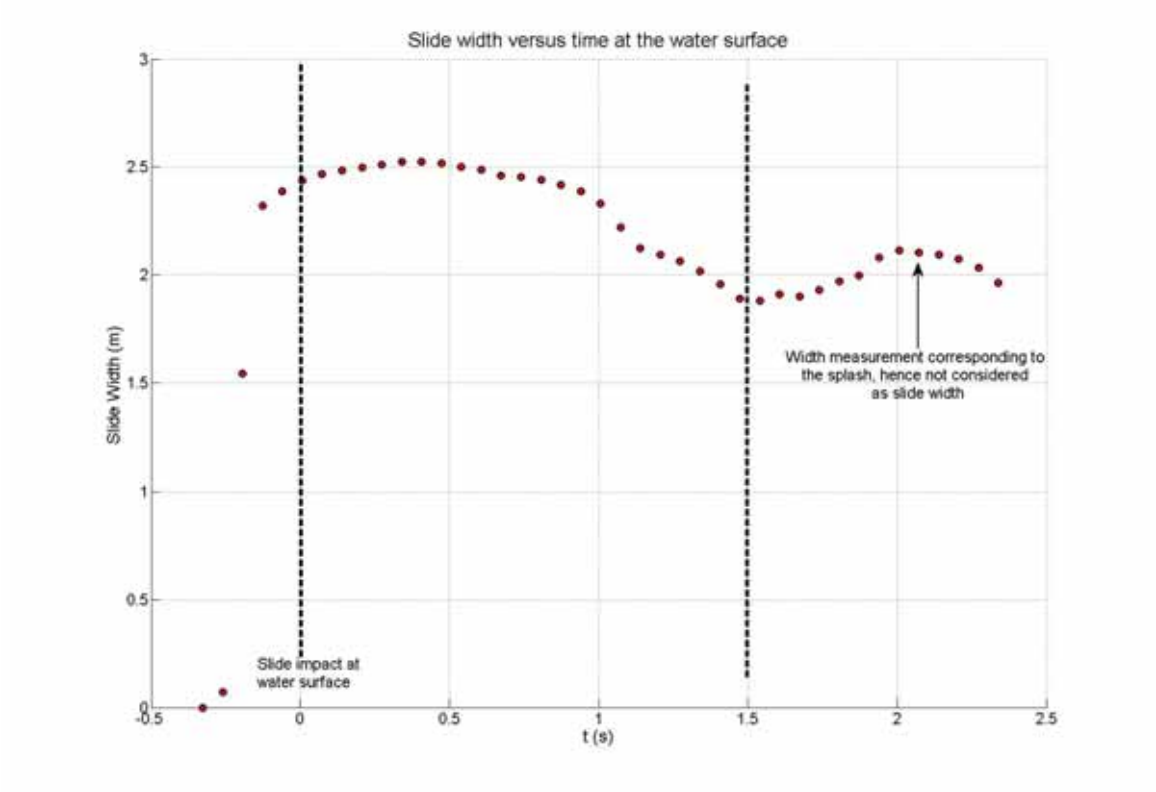

Figure 38. Slide width versus time at the water surface for trial 11, 11/29/06

The images from the underwater side camera are used to measure the slide characteristics such as slide front velocity, volume and maximum thickness of the slide from the moment of impact till the slide comes to rest. An edge extraction is shown in figure 39 for the experimental trial 11 dated 11/29/06.

The sequential images are shown in figure 39 as a stacked array. The image sequences are separated by about 0.1-0.4 seconds. The frame rate of recording was not constant and hence had a variable time difference between the image sequences. The edges were obtained by subtracting each image from the sequence from the stationary image before the slide was launched to obtain a gray scale image.

Then using a series of image smoothing, gradient transformations and distance transformation operations, areas are identified in the image which denote rapid gradients in the image intensities. These areas correspond to the edges in the image and thus the slide edges were identified. This slide data is then used to calculate the slide front velocity underwater and the changes in the slide thickness as it comes to rest on the bottom of the basin.

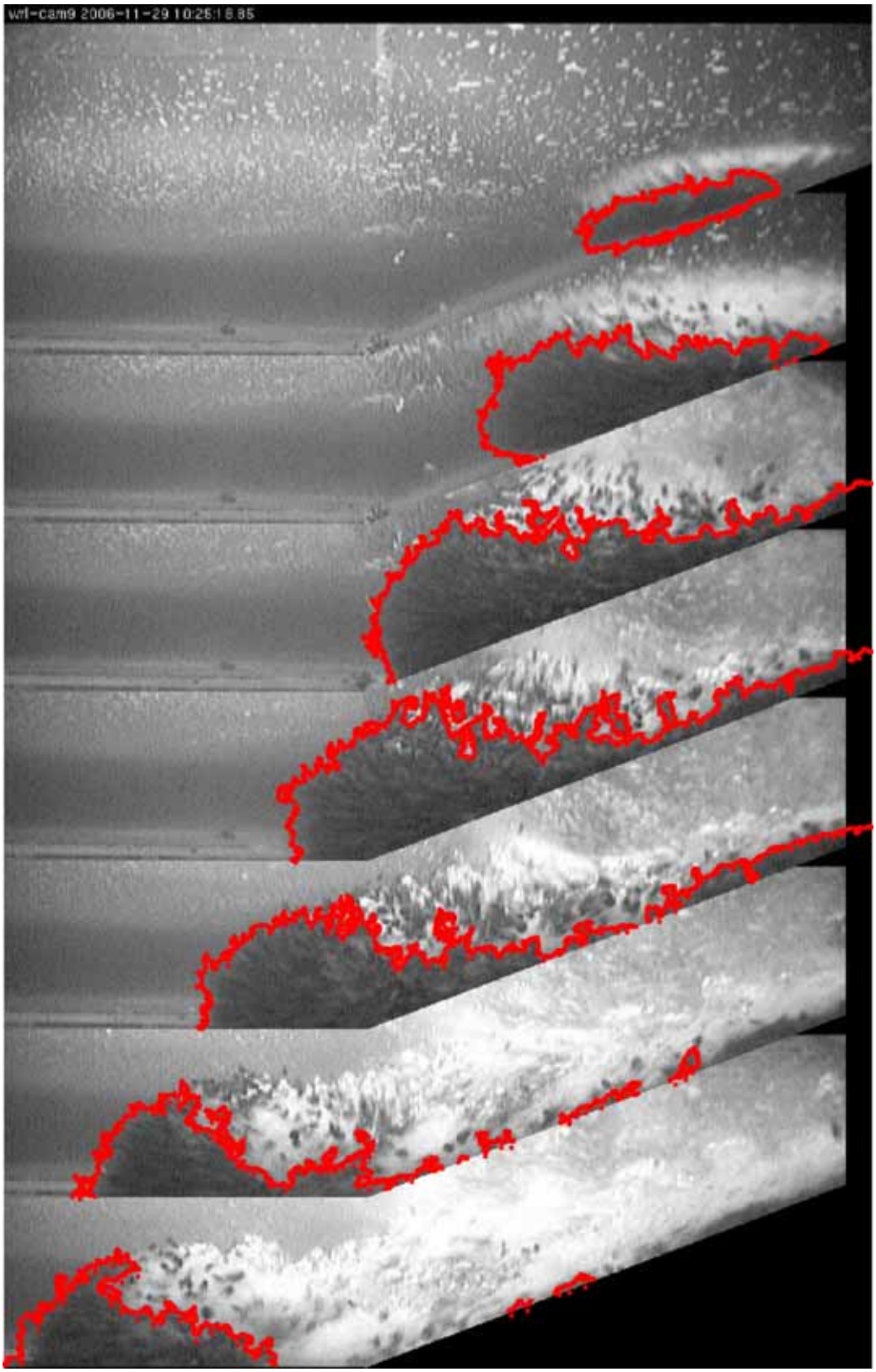

Figure 39. Slide edge extracted in the underwater side camera images for trial 11, 11/29/06

A Particle Image Velocimetry setup was used to capture the water surface images during the impact of the slide at the water surface. This system is used to obtain the slide velocities at the time of impact and the water surface velocities at that time. An example of the computation of surface velocity vectors is shown in figure 40. The sequence consists of 8 images which are separated by 0.33 seconds. This sequence was obtained for the experimental trial 11 dated 11/29/06.

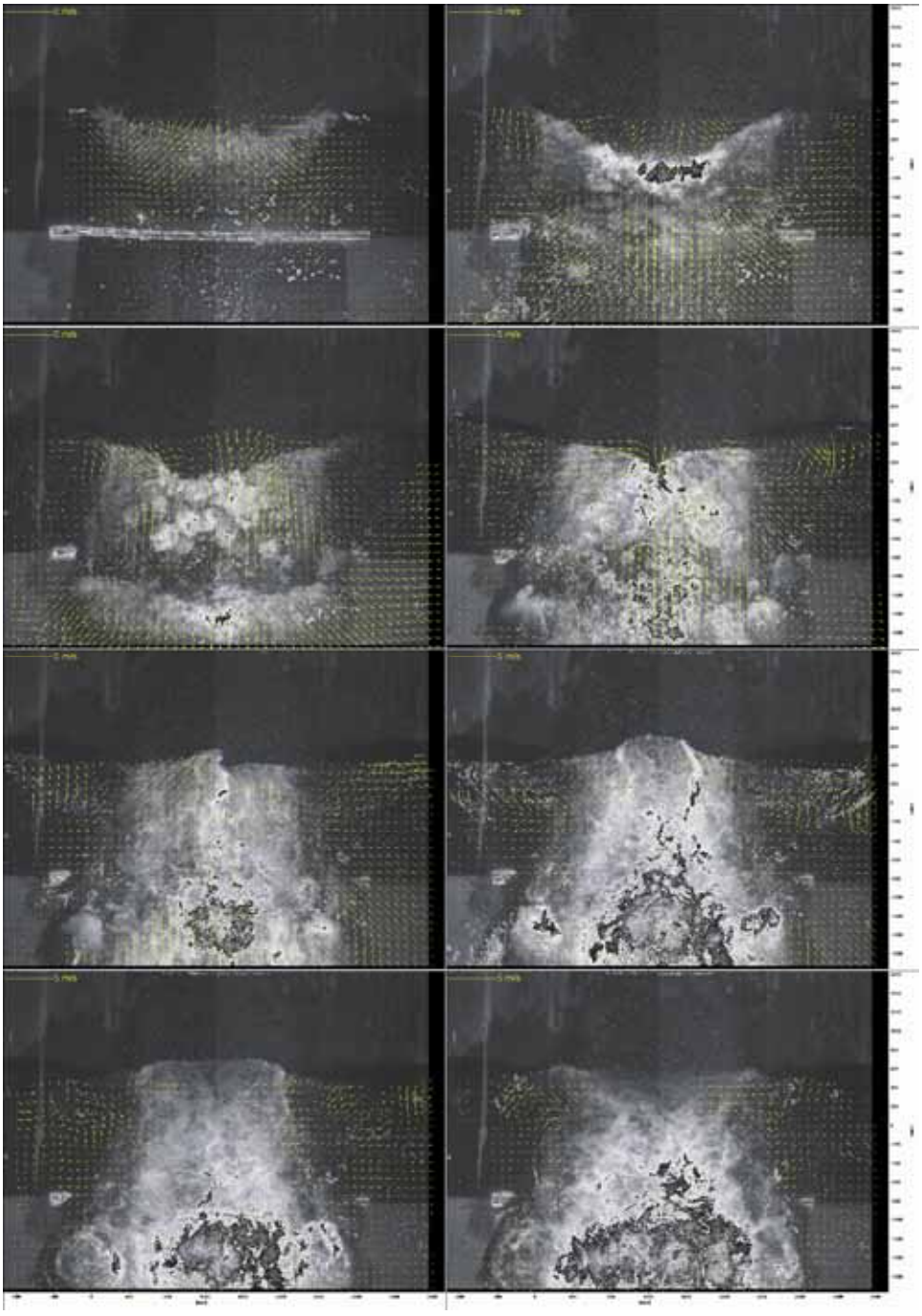

Figure 40. Velocity vectors obtained on the water surface during the landslide tsunami generation for trial 11, 11/29/06

Figure 41 shows the velocity vectors obtained after the PIV processing on both the landslide surface and the water surface. The landslide surface velocity data along with the maximum thickness and the width data will provide information on the mass flow rate and thus the mass flux for the landslide. The velocity vectors computed on the water surface provides an insight into the kinematics of the wave generation process and help in better understanding the dynamics of the landslide generated tsunami waves.

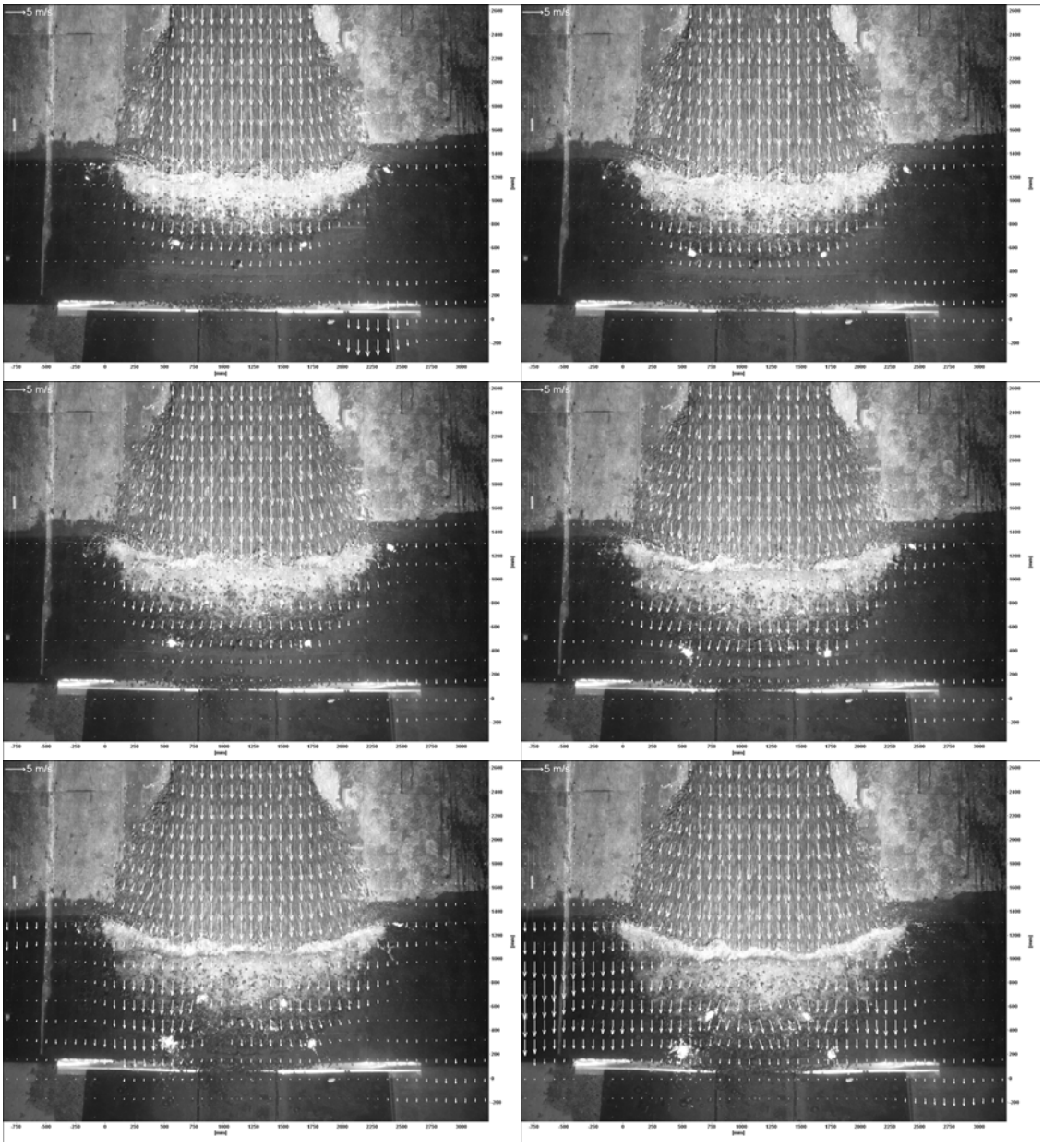

Figure 41. PIV vector sequences on the slide surface and the water surface

The above camera data yields information on the slide front velocity. This information is extremely important as it provides us with the knowledge of the energy transfer between the slide material and the generated wave during the wave generation process. Slide impact velocity is one of the important parameters that govern the characteristics of the generated tsunami waves. Figure 42 shows the slide front velocity obtained from the stringpot data from the sled and the image sequences obtained from the PIV camera. The location where the slide impacts the surface is also shown in the figure. The acceleration of the landslide is also calculated.

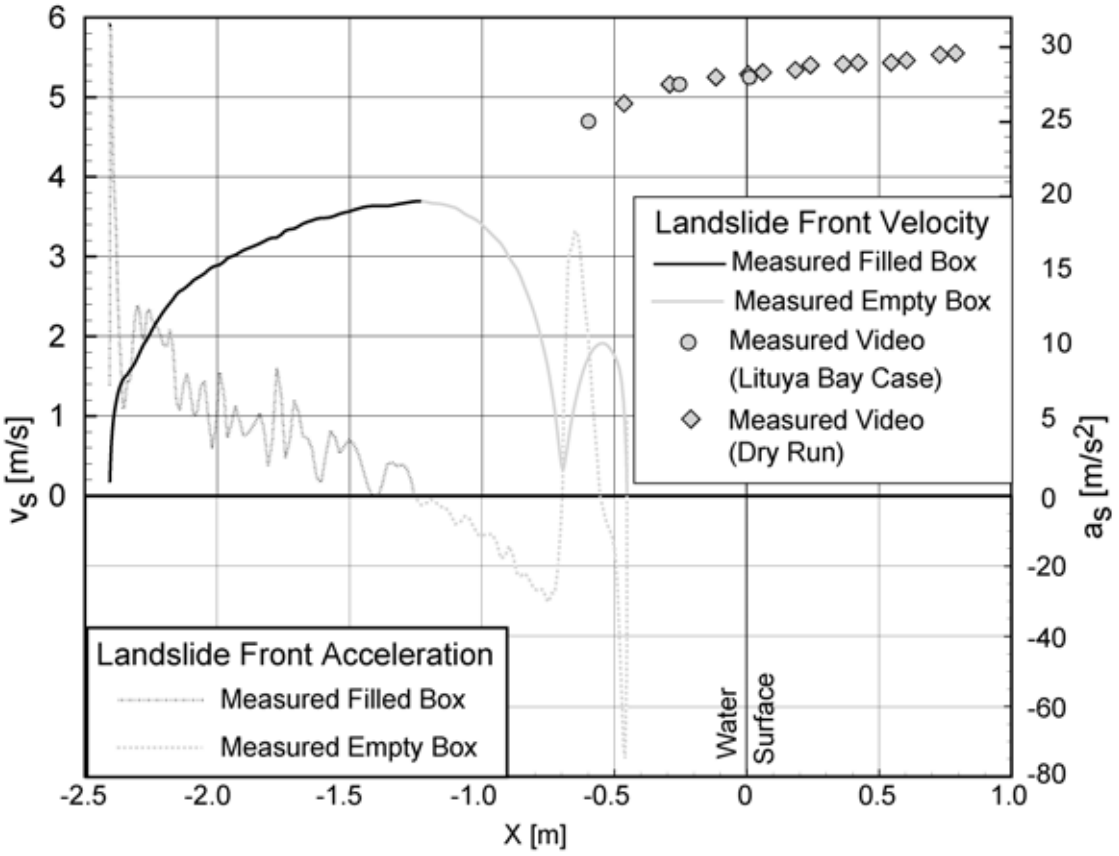

Figure 42. Slide front velocity above the water surface

The Multi Transducer Acoustic Array is used to map the bottom of the wave basin after each experimental trial to survey the deposited landslide. This data provides us information on how the granular landslide material deposits on the sea bed and on the shape and volume of the deposited slide. The MTA is mounted on a bridge which runs across the wave basin. This bridge is then slowly dragged in the on shore direction towards the landslide source. The survey data is constantly recorded by the DAQ system as the MTA slowly moves across the deposited slide. The raw MTA data is shown in figure 43 for trial 11, dated November 29, 2006.

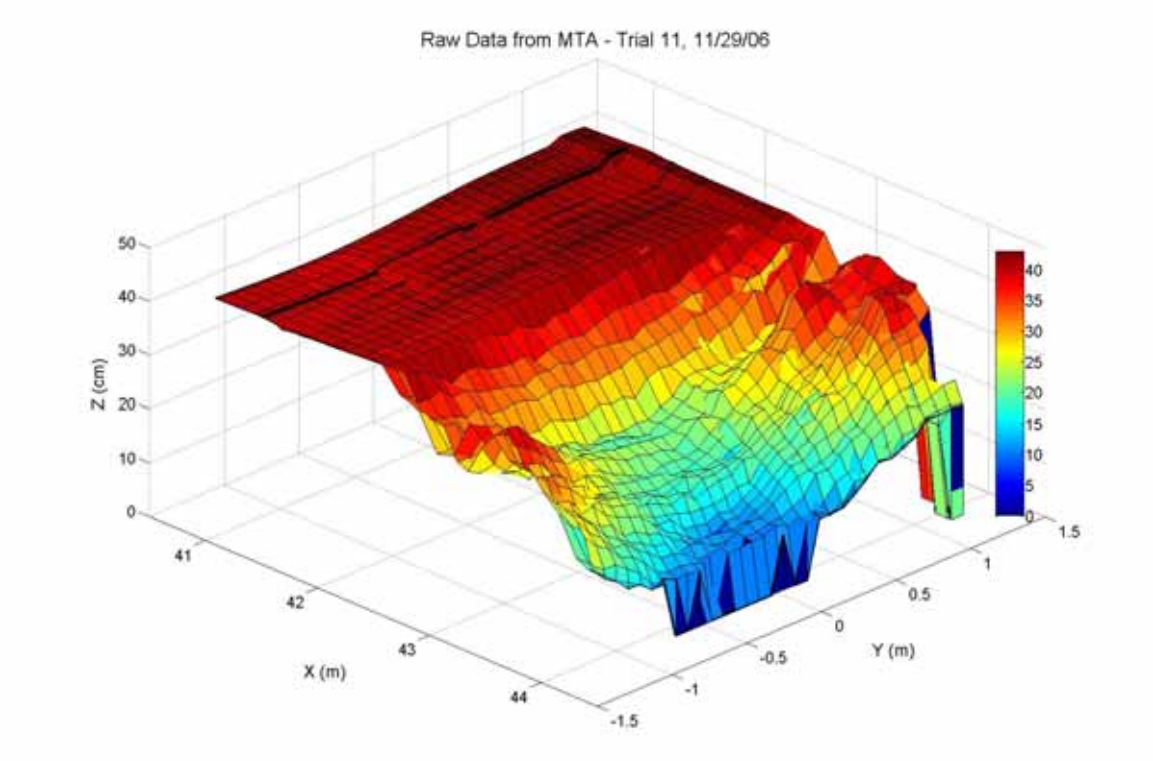

Figure 43. Raw MTA data for trial 11, 11/29/06

This raw data is then converted in to a coordinate system which conforms to the wave basin. In this coordinate system, the basin bottom is at zero level, the landslide impact location is the zero in the on shore direction and the centre of the landslide is the zero in the long shore direction. The converted data is shown in figure 44. This figure shows the top surface of the deposited landslide material on the bottom of the wave basin. The peaks in the data represent noise due to the echo reflected by the concrete bottom. This noisy data is then denoised to provide the error free data, which is shown in figure 45. This figure also shows the slope along which the landslide travels down and impacts the water surface to generate the tsunami waves and the bottom of the wave basin where the slide material deposits. We also obtain the smoothed data from this denoised data, which is shown in figure 46.

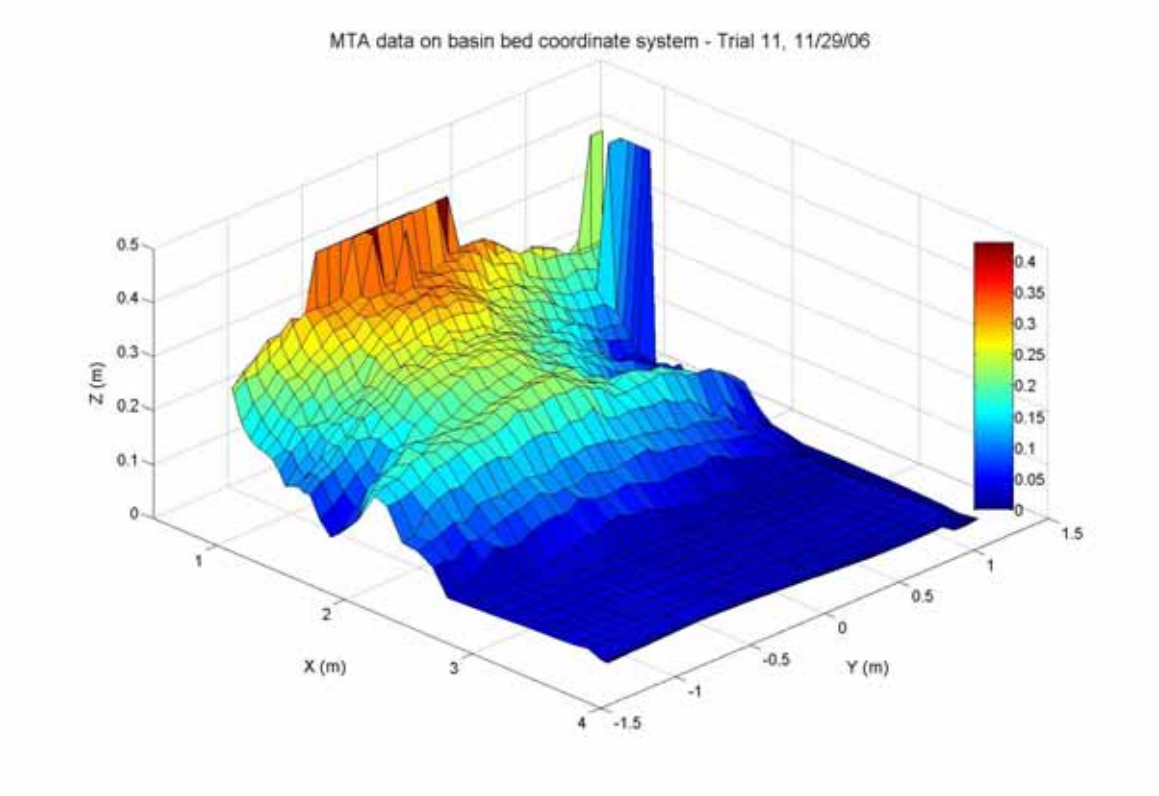

Figure 44. MTA data on the basin bed coordinate system for trial 11, 11/29/06

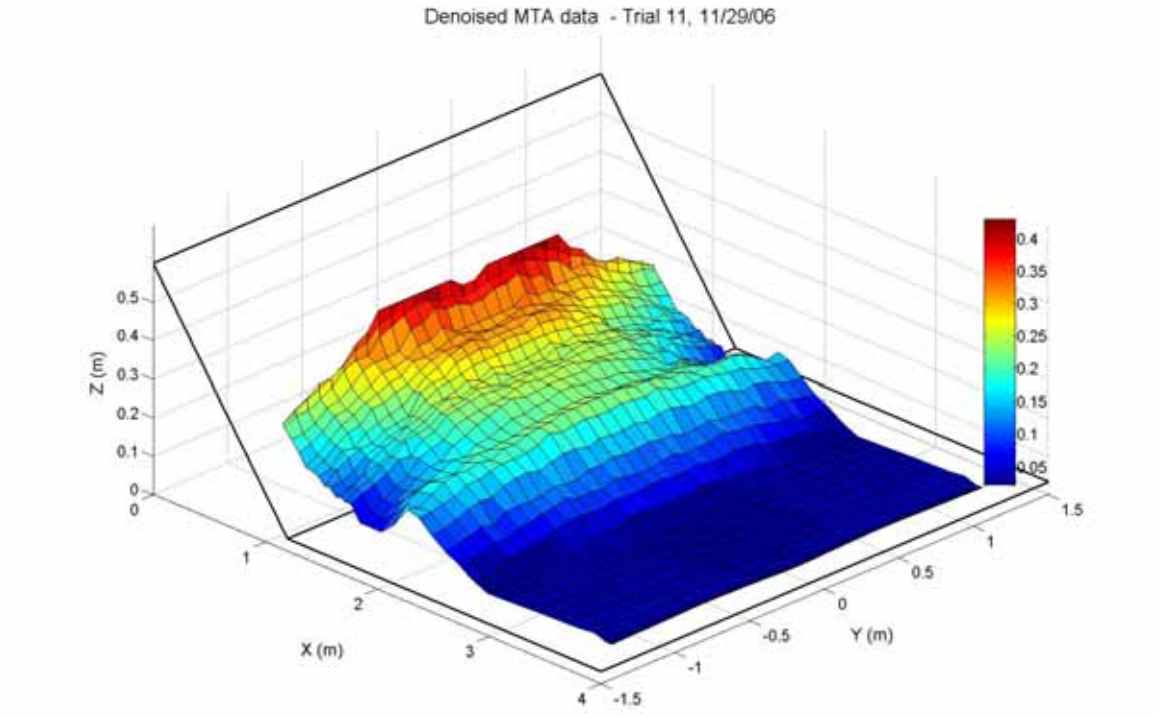

Figure 45. Denoised MTA data for trial 11, 11/29/06

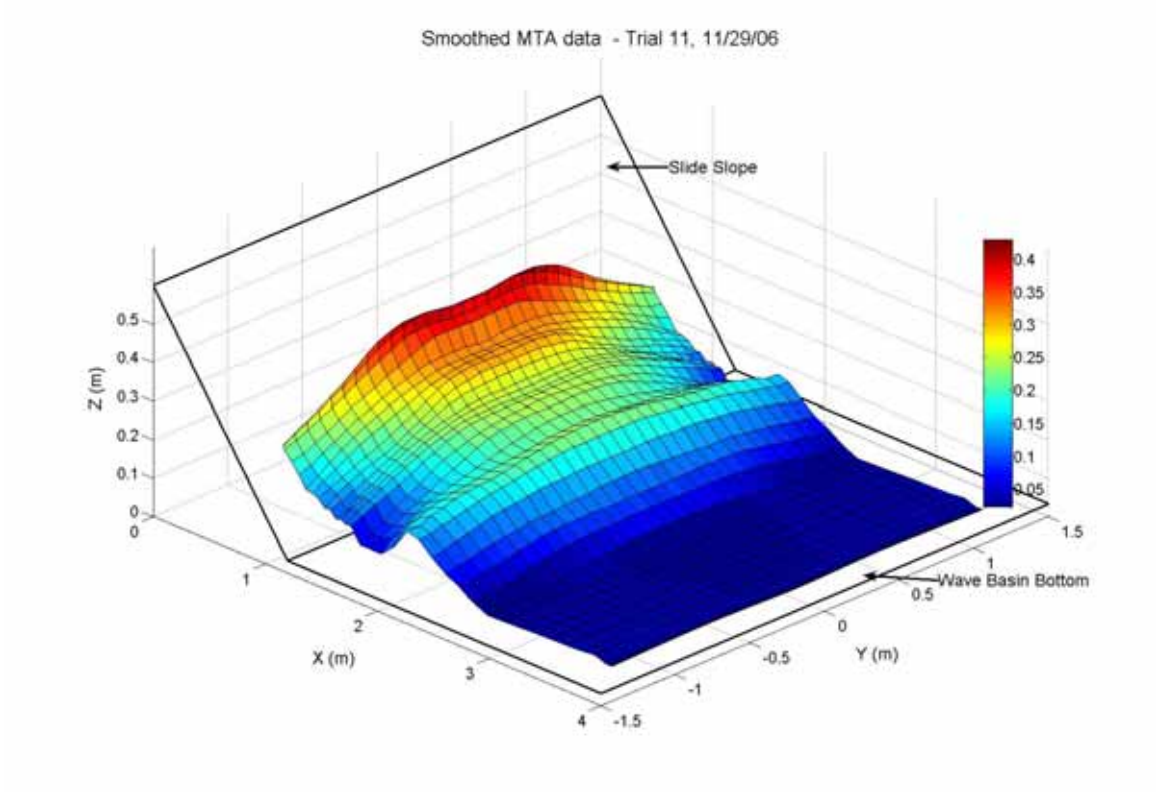

Figure 46. Smoothed MTA data for trial 11, 11/29/06

This MTA provides us information on the amount of the slide material that gets deposited on the basin bottom and thus the percentage of the original volume of the slide material that generates the tsunami wave. Since, the initial sled with the landslide material is fired with different pneumatic pressures, corresponding to different impact velocity of the slide at the water surface, these different conditions result in a difference in the shape of the deposited slide material. The denoised slide deposit shape for four different conditions is shown in figure 47. These cases correspond to the experimental trials conducted in a water depth of 60cm with full initial sled loading. The figures 47(a) and 47(b) demonstrate a repeatability of result for the same experimental trial conditions. As the firing pressure decreases, corresponding to a lower slide impact velocity, the deposited slide volume also decreases. Figure 48 shows the four different slide deposit shapes for different firing condition at the water depth of 60 cm, for an initial half mass sled load. The net volumes in these cases are considerably lower when compared to the full mass loading cases as expected. Apart from the volumes, the length to which the slide deposit extends is also shorter when compared to the full mass loading case.

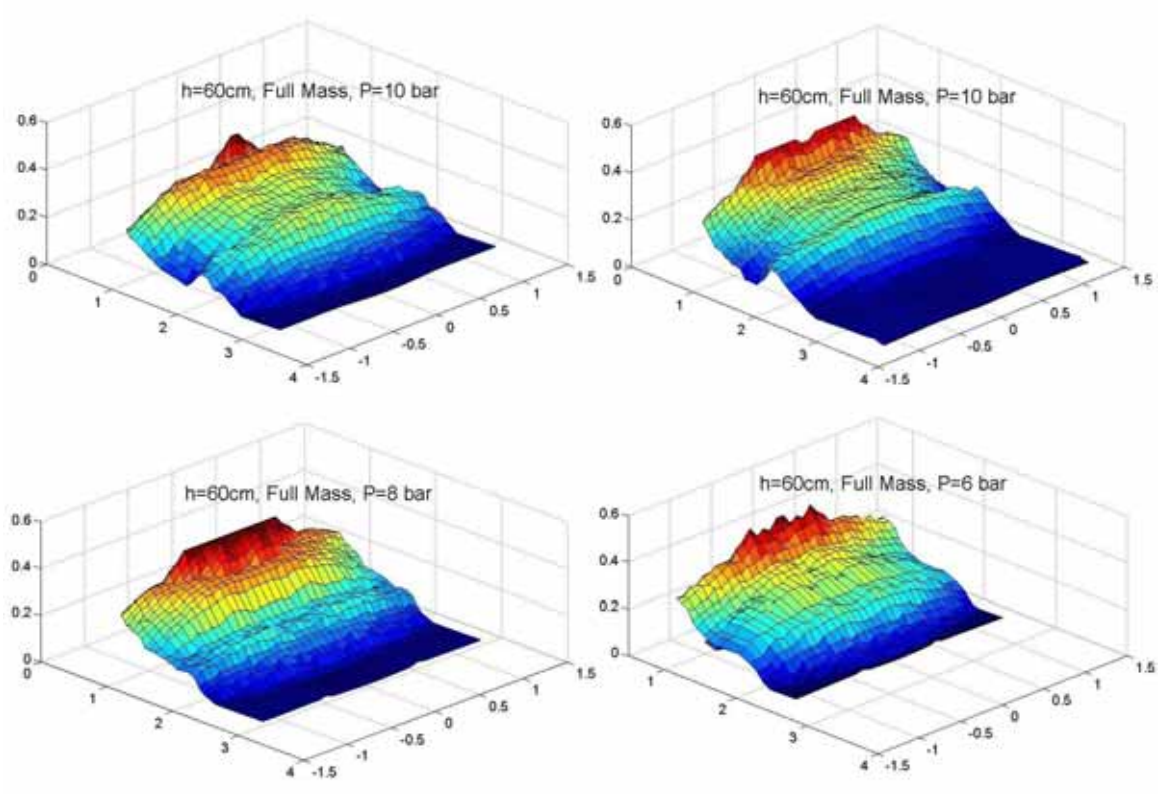

Figure 47. Slide deposit shapes for Full Mass, h = 60cm for different firing pressure

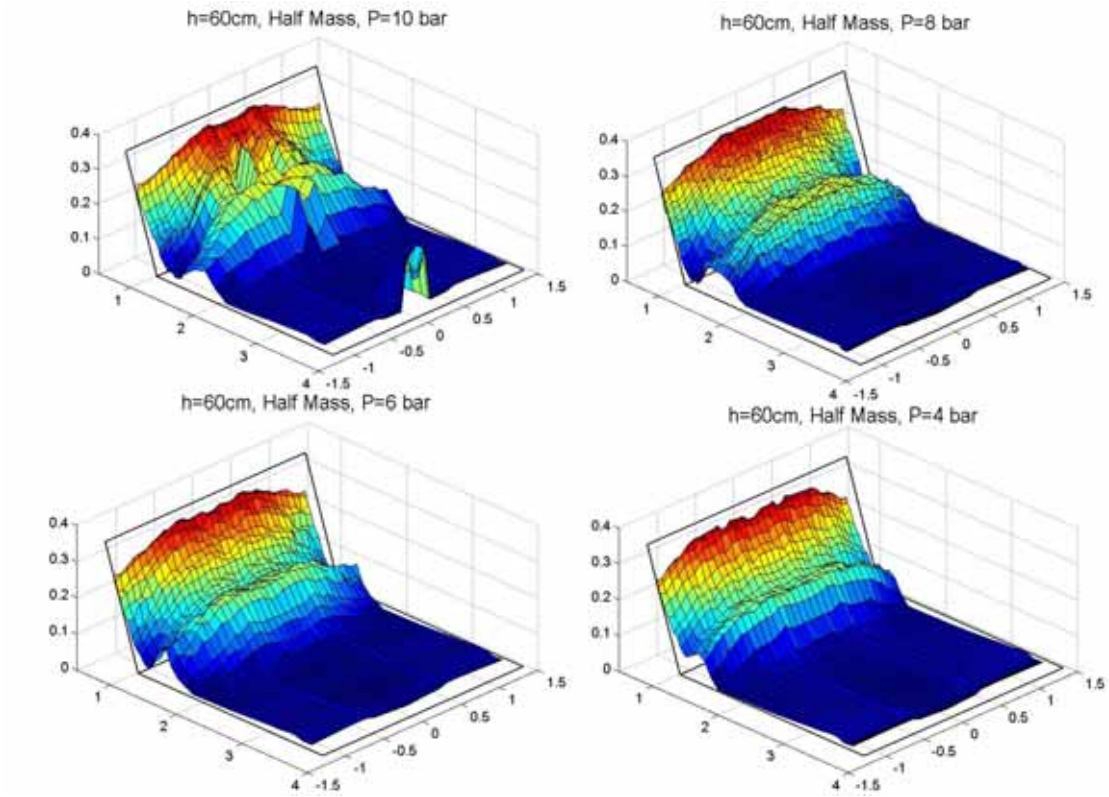

Figure 48. Slide deposit shapes for Half Mass, h = 60cm for different firing pressure

OUTREACH PROGRAMS

The NEES Tsunami Research Facility hosts over 500 people at each of three open houses every year. The summer open house is held in conjunction with a science and engineering celebration in Corvallis Oregon. Goals included increasing public awareness of tsunamis and tsunami research, and encouraging science and engineering literacy. National Science Foundation George E. Brown Network for Earthquake Engineering Researcher (NEESR) Dr. Hermann Fritz was a guest speaker at the summer 2006 open house. Dr. Fritz's field research experience includes conducting field surveys along coastlines from Indonesia to Somalia in the aftermath of the 2004 Indian Ocean Tsunami.

Hermann Fritz, NEESR PI, shows his Landslide Tsunami Generator to a tour group at the NEES Tsunami Research Facility.

He spoke to numerous groups of 25-40 people about tsunamis and tsunami research. This was a unique opportunity for visitors to interact with an active NEESR Principal Investigator. After the tours Fritz commented that "...it was important to explain how tsunamis are generated, how they propagate and what the Oregon coast could look like after a tsunami. Realistic scenarios were discussed without scaring people." Tsunami awareness was raised by introducing tsunami precursors such as shoreline drawback and groundshaking as well as evacuation strategies. Educating the general public about tsunamis is important because experience gained from the recent Indian Ocean tsunami

showed that educated and tsunami-aware coastal residents have a significantly higher chance of survival.

Television Documentary Movies:

1. The History Channel (USA): "Mega Disasters" series, *The 1883 Krakatau Volcanic Explosion and Tsunami*, (60'). The TV-documentary encompassed Dr. Fritz's scale experiments of the Krakatau volcanic island collapse generated tsunami as part of the NEES landslide tsunami experiments in the tsunami wave basin at OSU, as well as various interviews of Dr. Fritz, among other international experts. (Co-Production: 12/2006, aired on National TV in 2007 on September 11, 12, 15, 21 and 22).

The experiment was also covered by different TV stations and newspapers who participated in the media day on 21st of December 2006. Following is the list of the participants that covered the landslide tsunami generation experiment.

- KGW-TV from Portland, Oregon.
- KATU-TV from Portland, Oregon.
- KEZI-TV from Eugene, Oregon.
- KVAL-TV from Eugene, Oregon.
- KMTR-TV from Eugene, Oregon.
- NSF Television and
- Gazette Times newspaper from Corvallis, Oregon.

K12-seminar presentations:

1. "Civil Engineering and Coastal Hazards Research: Landslide generated tsunami experiments, the Indian Ocean Tsunami and Hurricane Katrina", Junior Achievement High School Students, Savannah, Georgia (02/02/2007)

Pure appl. geophys. 165 (2008) 1–23
DOI 10.1007/s00024-008-0435-4

Pure and Applied Geophysics

Lituya Bay Landslide Impact Generated Mega-Tsunami 50th Anniversary

HERMANN M. FRITZ, FAHAD MOHAMMED, and JESEON YOO

Abstract—On July 10, 1958, an earthquake M_w 8.3 along the Fairweather fault triggered a major subaerial landslide into Gilbert Inlet at the head of Lituya Bay on the southern coast of Alaska. The landslide impacted the water at high speed generating a giant tsunami and the highest wave runup in recorded history. The mega-tsunami runup to an elevation of 524 m caused total forest destruction and erosion down to bedrock on a spur ridge in direct prolongation of the slide axis. A cross section of Gilbert Inlet was rebuilt at 1:675 scale in a two-dimensional physical laboratory model based on the generalized Froude similarity. A pneumatic landslide tsunami generator was used to generate a high-speed granular slide with controlled impact characteristics. State-of-the-art laser measurement techniques such as particle image velocimetry (PIV) and laser distance sensors (LDS) were applied to the decisive initial phase with landslide impact and wave generation as well as the runup on the headland. PIV provided instantaneous velocity vector fields in a large area of interest and gave insight into kinematics of wave generation and runup. The entire process of a high-speed granular landslide impact may be subdivided into two main stages: (a) Landslide impact and penetration with flow separation, cavity formation and wave generation, and (b) air cavity collapse with landslide run-out and debris detrainment causing massive phase mixing. Formation of a large air cavity — similar to an asteroid impact — in the back of the landslide is highlighted. A three-dimenional pneumatic landslide tsunami generator was designed, constructed and successfully deployed in the tsunami wave basin at OSU. The Lituya Bay landslide was reproduced in a three-dimensional physical model at 1:400 scale. The landslide surface velocities distribution was measured with PIV. The measured tsunami amplitude and runup heights serve as benchmark for analytical and numerical models.

Key words: Tsunami, landslide, landslide generated tsunami, natural hazard, nonlinear gravity water waves, wave runup, near-field wave characteristics, slide energy conversion, three-phase flow, Alaska.

1. Introduction

Lituya Bay is a T-shaped tidal inlet that cuts through the coastal lowlands and the foothills flanking the Fairweather Range of the St. Elias Mountains on the southern coast of Alaska shown in Figure 1a. The stem corresponding to the main part of the T-shaped bay is 12 km long and extends northeastward from the bay entrance. The width of the stem ranges from 1.2 to 3.3 km except at the entrance, which is only 300 m wide. The bay fills and slightly overflows a depression carved by a valley glacier of which Lituya, North Crillon and Cascade glaciers are remnants. Submarine contours show a pronounced

School of Civil and Environmental Engineering, Georgia Institute of Technology, 210 Technology Circle, Savannah, GA 31407, U.S.A. E-mail: fritz@gatech.edu

Journal : 24 | Dispatch : 22-12-2008 | Pages : 23
Article No. : 0435 | ☐ LE | ☐ TYPESET
MS Code : 0435 | ☑ CP | ☑ DISK

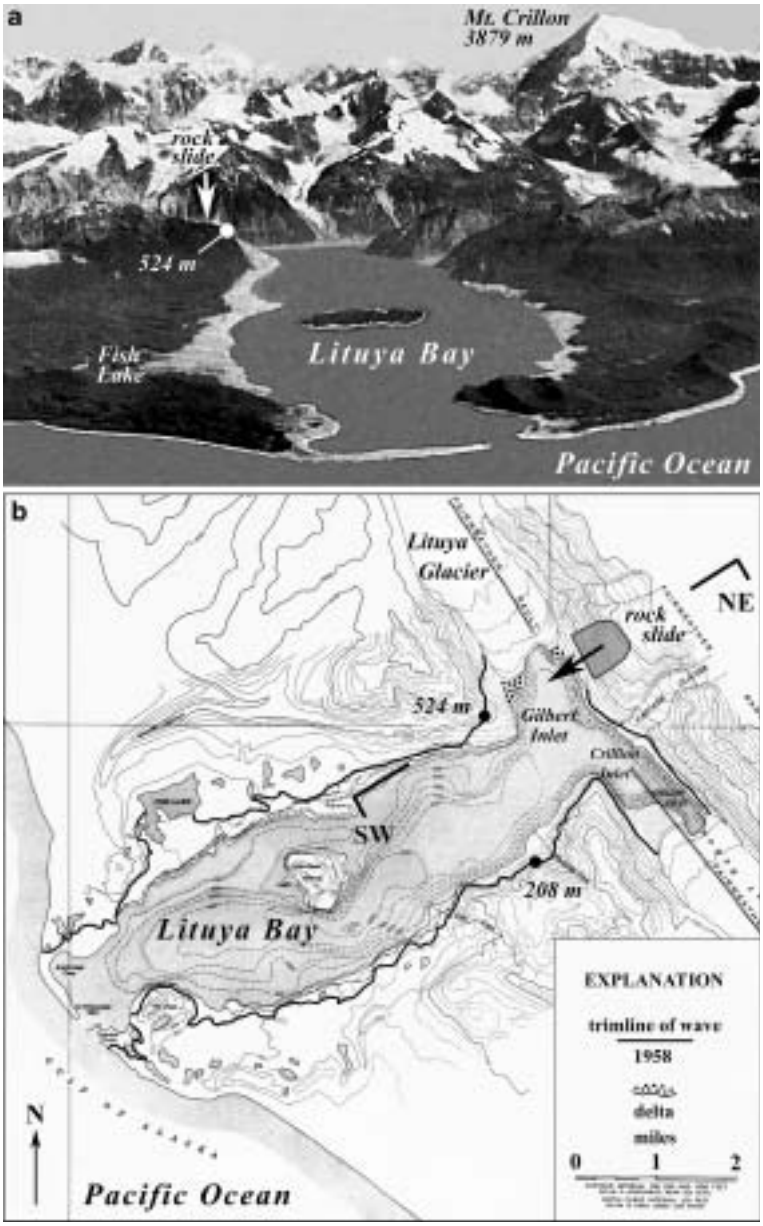

Figure 1

Lituya Bay, Alaska: (a) Overview in August 1958 (MILLER, 1960). Forest destroyed to a maximum elevation of 524 m and a maximum distance of 1100 m from high-tide shoreline at Fish Lake due to a giant tsunami generated on 10 July 1958 by a landslide at the head of the bay. (b) Map showing topographic and bathymetric contours, trace of Fairweather fault, 1958 landslide and trimline of tsunami runup (MILLER, 1960).

Journal : 24 Dispatch : 22-12-2008 Pages : 23
Article No. : 0435 ☐ LE ☐ TYPESET
MS Code : 0435 ☑ CP ☑ DISK

U-shaped trench with steep walls and a broad flat floor sloping gently downward from the head of the bay to a maximum depth of 220 m. Minimum depth at the entrance of the bay is 10 m. At the head of the bay the walls are fjord-like glacially over-steeped. The walls have been buttressed by glaciers until recently. Radiocarbon dates on high moraines suggest retreat of glaciers only in the last millennium (SLINGERLAND and VOIGHT, 1979). The two arms at the head of the bay are part of a great trench that extends tens of kilometers to the northwest and southeast as a topographic expression of the Fairweather transform fault shown in Figure 1b.

Giant waves have occurred in Lituya Bay probably five times during the last two centuries emphasizing the unique geologic and tectonic setting of the bay. Frequent occurrence of giant waves in Lituya Bay, as compared to other similar bays, is attributed to the combined effect of recently glaciated steep slopes, highly fractured rocks and deep water in an active fault zone, heavy rainfall, frequent freezing and thawing (MILLER, 1960). Three extreme wave runup heights in 1853 or 1854, 1936 and 1958 carved sharp trimlines of chopped trees to elevations beyond 100 m on to the slopes of Lituya Bay. Photographic evidence and eyewitness accounts suggest two additional giant waves occurred possibly in 1874 and 1899 (MILLER, 1960). In 1853 or 1854 a giant wave caused forest destruction on Lituya Bay shores to a maximum elevation of 120 m. A landslide from the steep wall on the south shore of Lituya Bay near Mudslide Creek is the likely source directly opposite to the maximum destruction on the north shore. The trimline of the 1936 waves reached a maximum height of 150 m above sea level on the northeast wall of Crillon Inlet and indicates a wave generation near the head of Crillon Inlet. MILLER (1960) suggests a landslide or rock avalanche from the southwest wall of Crillon Inlet, opposite the high point on the trimline. In 1958 the largest wave runup of 524 m in recorded history was observed on a spur ridge on the southwest wall of Gilbert Inlet. Only the 1958 event is further considered here as the exact sources of the earlier events remain to be confirmed by bathymetric and geologic surveys of the seafloor.

2. 1958 Landslide Impact and Tsunami Runup

Beginning at 06:16 UTC on July 10, 1958, the southwest sides and bottoms of Gilbert and Crillon Inlets moved northwestward and relative to the northeast shore at the head of the bay, on the opposite side of the Fairweather fault. Total movements of 6.4 m horizontally and 1 m vertically were estimated for the earthquake M_w 8.3 (TOCHER and MILLER, 1959). Intense shaking in Lituya Bay continued for 1 to 4 minutes according to two eyewitnesses that anchored in the bay. Between 1 and 2½ minutes after the earthquake was first felt a large mass of rock slid from the northeast wall of Gilbert Inlet (Fig. 2). The landslide was triggered impulsively by fault movement and intense earthquake vibrations. It is highly probable that the entire mass plunged into Gilbert Inlet as a unit at the time of the earthquake. PARARAS-CARAYANNIS (1999) classified the mass movement as subaerial rockfall to distinguish from gradual processes of ordinary

Journal : 24 Dispatch : 22-12-2008 Pages : 23
Article No. : 0435 ☐ LE ☐ TYPESET
MS Code : 0435 ☑ CP ☑ DISK

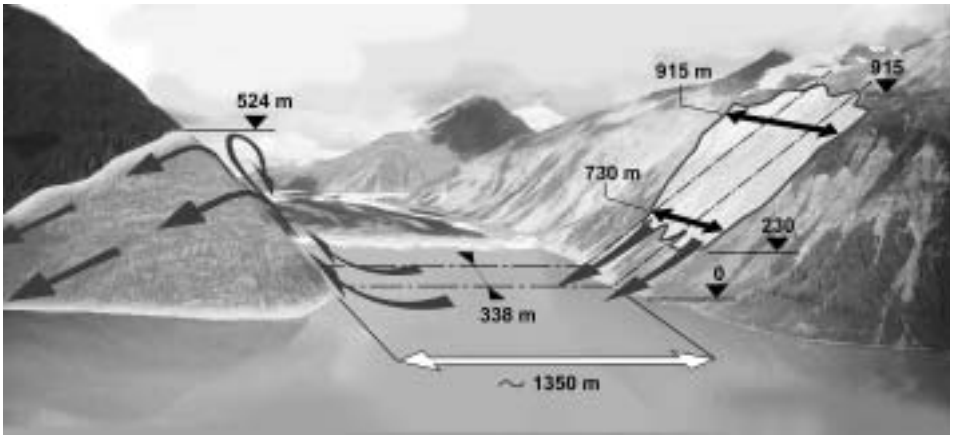

Figure 2
Gilbert Inlet illustration showing landslide dimensions, impact site and tsunami runup to 524 m on spur ridge directly opposite to landslide impact. Direction of view is north and the front of Lituya Glacier is set to 1958 post-slide position. Illustration background is synthesized from two aerial photos recorded in 1997 (Photos: courtesy of Charles L. Mader).

landslides whereas MILLER (1960) judged it to be near the borderline between landslide and rockfall as defined by SHARPE (1938) and VARNES (1958). The landslide occurred in an area of previously active sliding to an elevation of 915 m on a slope averaging 40°. The rocks are mainly amphibole and biotite schists with an estimated density of 2.7 t/m^3. The dimensions of the slide on the slope are accurate, but the thickness of the slide mass normal to the slope could be estimated only roughly (MILLER, 1960). The main mass of the slide presumably involved a prism of rock roughly triangular in cross section, with width dimensions from 730 m to 915 m (MILLER, 1960; SLINGERLAND and VOIGHT, 1979), a slope parallel length of 970 m (SLINGERLAND and VOIGHT, 1979), a maximum thickness of about 92 m normal to the slope, and a center of gravity at about 610 m elevation (MILLER, 1960). Dimensions are illustrated in Figure 2. Miller estimated the slide volume from these as 30.6×10^6 m^3.

Prior to the landslide low deltas of gravel had built out into Gilbert Inlet at the southeast and northwest margins of the Lituya Glacier front. Part of the slide must have hit the Lituya Glacier and glacial gravel deltas due to the pre-slide location of slide mass, deltas and glacier front (MILLER, 1960). The Lituya Glacier front was characterized by a vertical wall normal to the Gilbert Inlet axis after the event (Figs. 3a, b). During the event as much as 400 m of ice had been sheared off on parts of the glacier front and the gravel deltas were pushed or washed away. The landslide impact created a giant tsunami and a resulting maximum tsunami runup of 524 m in straight prolongation of the slide axis on a spur ridge on the southwest shore of Gilbert Inlet (Figs. 3a, b, c).

The maximum tsunami runup of the 1958 event was incomparable at the time to any other event outside of Lituya Bay. The 524 meter runup is seven times larger than

Journal : 24 Dispatch : 22-12-2008 Pages : 23
Article No. : 0435 ☐ LE ☐ TYPESET
MS Code : 0435 ☑ CP ☑ DISK

Figure 3
Trimlines carved by tsunami in 1958: (a) NE-view of Lituya Bay from Cenotaph Island to Gilbert Inlet with landslide scar at the head of the bay and trimlines of destructed forest with 524 m runup on spur ridge. (b) NW-view of Gilbert Inlet with landslide scar, post-event Lituya Glacier front, forest destruction and soil erosion down to bedrock. (c) N-view of spur ridge. (d) S-view of trimline in the Mudslide Creek area on the south shore of Lituya Bay with wiped out trees to an elevation of 208 m. (Photos: courtesy of USGS).

the highest tsunami runup of 75 m observed 1936 in Norwegian Lake Loen (JØRSTAD, 1968) and roughly doubles wave runup heights in the Vajont reservoir, Italy (MÜLLER, 1964) and Spirit Lake, U.S.A. (VOIGHT *et al*., 1983). A simplified 3-D physical model of Lituya Bay at a 1:1,000 scale was constructed at the University of California, Berkeley (R.L. WIEGEL in MILLER, 1960, pp. 65-66). Wiegel concluded from physical model observations, that a sheet of water washed up the slope opposite to the landslide to an elevation of at least three times the water depth for a slide impacting Gilbert Inlet as a unit and very rapidly. At the same time a large wave, several hundred feet high, moved in the southerly direction, causing a peak rise to occur in the vicinity of Mudslide Creek. Unfortunately no measured data are available from these three dimensional experiments. The highest mark of chopped trees at an elevation of 208 m on the south shore trimline is shown in Figure 3d. WIEGEL (1964) estimated the hydrodynamic forces exerted on the trees by the wave as roughly ten times greater than the force necessary to snap or uproot trees.

Journal : 24 Dispatch : 22-12-2008 Pages : 23
Article No. : 0435 ☐ LE ☐ TYPESET
MS Code : 0435 ☑ CP ☑ DISK

3. Physical Model of Gilbert Inlet

Based on the generalized Froude similarity a cross section of Gilbert Inlet was rebuilt at a 1:675 scale in a two-dimensional physical laboratory model (L × W × H: 11 m, 0.5 m and 1 m) by FRITZ *et al.*, 2001. The Froude similarity has been confirmed by a laboratory scale series (HELLER *et al.*, 2008). The modeled Gilbert Inlet cross section is shown in Figure 4a and its NE-SW orientation in Figure 1b. The prismatic Gilbert Inlet slice rebuilt in the model is shown in Figure 2. The width of 338 m represented in the 2-D model corresponds to 40% of the mean slide width of 823 m (SLINGERLAND and VOIGHT, 1979). The volume per unit width $V_s' = 37.2 \times 10^3$ m^3/m′ was estimated by equal distribution of the total slide volume $V_s = 30.6 \times 10^6$ m^3 over an averaged slide width of 823 m. This is a conservative assumption neglecting the volume concentration in the slide center due to roughly triangular slide cross sections along the slope. The indicated geometry corresponds to the physical model assumptions with a hill slope angle α and a headland angle β of both 45°. The simplified Gilbert Inlet bathymetry roughly corresponds to bedrock of the glacially carved U-shaped trench. Pre-slide gravel deltas

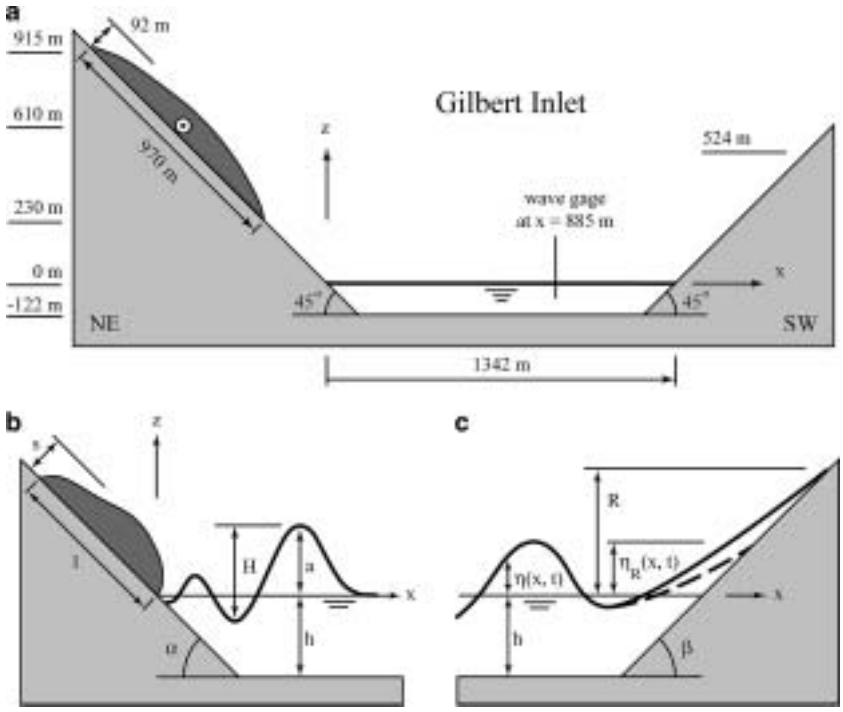

Figure 4
(a) Cross section of Gilbert Inlet along slide axis in NE to SW orientation shown in Figure 1b. Geometry corresponds to physical model assumptions and simplifications. (b) Notation for landslide impact and wave propagation; (c) notation for wave runup.

Journal : 24 Dispatch : 22-12-2008 Pages : 23
Article No. : 0435 ☐ LE ☐ TYPESET
MS Code : 0435 ☑ CP ☑ DISK

along parts of the glacier front shown in Figure 1b were neglected. The assumed stillwater depth $h = 122$ m matches the maximum water depth in Gilbert Inlet. The notation for landslide impact, wave propagation and wave runup are defined (Figs. 4b, c).

Radial or lateral wave spreading is neglected in the two-dimensional model. In northern direction the impact area is confined to the Lituya Glacier front. In this specific topographic situation wave height reduction due to 3-D effects is further limited by the small ratio of 1.6 between propagation distance and slide width. Therefore it is expected that the present 2-D model can give a good estimate of wave and runup heights in Gilbert Inlet.

The dynamic slide impact characteristics were controlled with a specifically designed pneumatic landslide generator shown in Figure 5 (FRITZ and MOSER, 2003). The pneumatic landslide generator models the transition from block slide motion to granular flow. The first stage with acceleration up to the granulate release velocity corresponds to block sliding whereas the second stage from granulate release to impact into the water body is purely gravity driven granular flow.

Three different measurement techniques were built into the physical model: Laser distance sensors (LDS), particle image velocimetry (PIV) and capacitance wave gauges

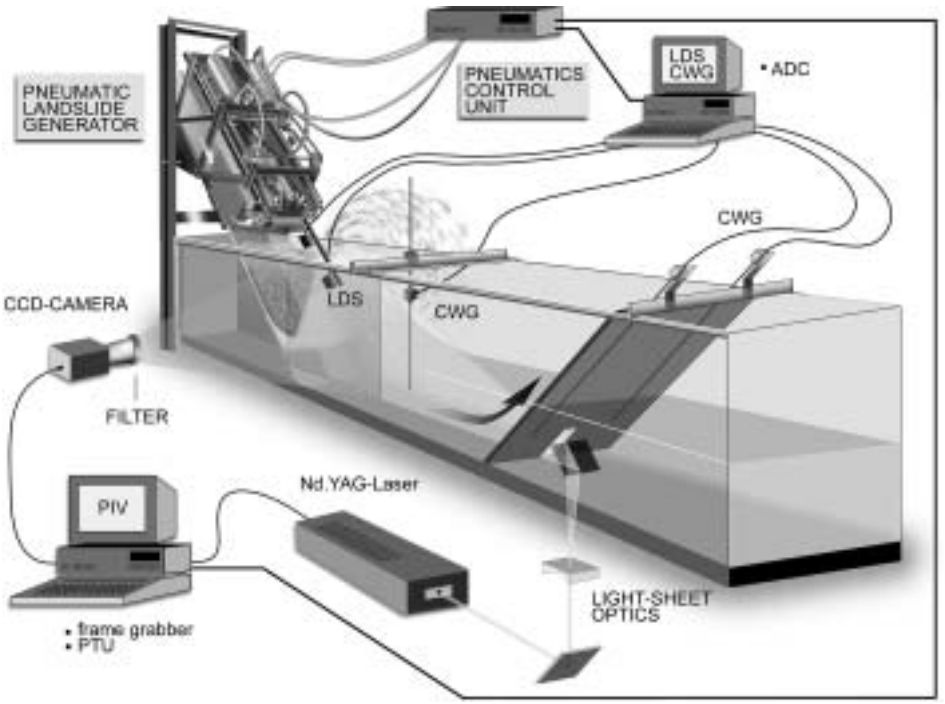

Figure 5
Experimental setup with pneumatic installation and measurement systems: Laser distance sensors (LDS), capacitance wave gages (CWG) and particle image velocimetry (PIV).

Journal : 24 Dispatch : 22-12-2008 Pages : 23
Article No. : 0435 ☐ LE ☐ TYPESET
MS Code : 0435 ☑ CP ☑ DISK

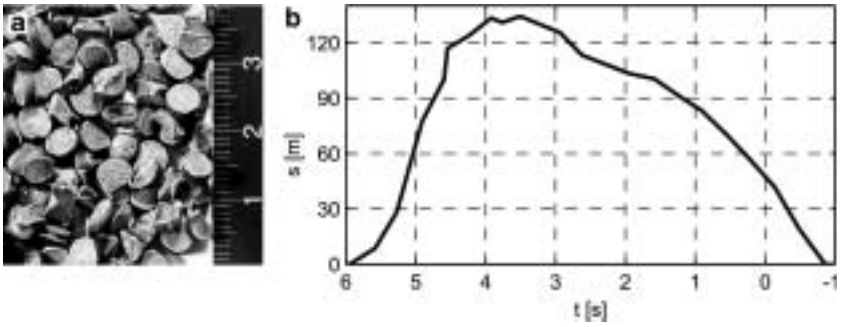

Figure 6
(a) Granulate: PP-$BaSO_4$, $d_g = 4$ mm, $\rho_g = 2.64$ g/cm^3; (b) granular slide profile scanned with a laser distance sensor orthogonal to ramp at location $x = -67$ m and $z = 67$ m.

(CWG). The laser-based digital PIV-system was introduced in FRITZ (2002a). The planar PIV provided instantaneous velocity vector fields in the slide impact area and gave insight into the kinematics of wave generation (FRITZ *et al.*, 2003a). Water displacement volumes and rates were extracted from the PIV recordings (FRITZ *et al.*, 2003b). Instantaneous image areas as large as 529(H) × 516(V) m in prototype scale were acquired. By means of cross-correlation analysis instantaneous 2D-2C velocity vector fields were computed using an adaptive multi-pass algorithm (SCARANO and RIETHMULLER, 1999) and second-order correlation (HART, 2000). Spatial resolution is determined by the window size of 8.4 × 8.4 m used in cross-correlation analysis. Time resolution of the PIV-system for 2D-2C velocity vector field estimation was 0.6 Hz in prototype time scale.

The landslides were modeled with an artificial granular material (PP-$BaSO_4$) shown in Figure 6a. The granulate properties were: grain density $\rho_g = 2.64$ t/m^3, grain diameter $d_g = 4$ mm, bulk slide density $\rho_s = 1.62$ t/m^3, bulk slide porosity $n_{\text{por}} = 39\%$, effective internal friction angle $\phi' = 43°$, and dynamic bed friction angle $\delta = 24°$ (FRITZ, 2002b). The slip between the bed and the granular mass was dominant, resulting in slug-type flow (SAVAGE, 1979). Its grain density perfectly matches the estimated schist density of $\rho_s = 2.7$ t/m^3 and resulted in a slide mass per unit width of $m' = 98.5 \times 10^3$ t/m$'$. The assumed porosity corresponds to data from Alpine debris flows (TOGNACCA, 1999). Slide profiles before impact are scanned with two laser distance sensors. A landslide profile recorded orthogonal to the ramp and 67 m above the stillwater level is shown in Figure 6b. The maximum slide thickness of 134 m equals 1.4 times the pre-motion slide thickness of 92 m (MILLER, 1960). This increase of 40% in slide thickness is necessary in the model to compensate for the void fraction present in granular flow in order to match the slide mass-flux per unit width. The prototype landslide porosity likely also increased due to fragmentation of the schist slide mass prior to impact. The generated slide length before impact was conservatively estimated to 748 m with the mean slide velocity of 110 m/s and the slide profile duration of 6.8 s. The mean landslide impact velocity v_s of

110 m/s is estimated assuming free fall equations for a slide centroid at 610 m elevation (LAW and BREBNER, 1968; NODA, 1970). The kinetic impact energy of the landslide is at the upper limit neglecting frictional losses. This gives an impact slide Froude number of 3.18 based on the definition $F = v_s/(gh)^{1/2}$. The slide Froude number relates the mean impact velocity v_s of the centroid to the shallow water wave propagation velocity (NODA, 1970). Scale effects regarding viscosity and surface tension may be assumed smaller than 5% (STIVE, 1985; MÜLLER, 1995).

Wave features during propagation and runup are determined with capacitance wave gages (CWG). One CWG records the wave profile at $x = 885$ m and two CWGs record wave runup profiles on the headland ramp. Laser distance sensors and capacitance wave gauges are sampled at 20 Hz in prototype time scale (FRITZ *et al.*, 2001).

4. 2-Dimensional Experimental Results

A series of experiments was conducted with the assumptions for Lituya Bay topography, bathymetry, landslide impact velocity, mass and shape described in the physical model section. The waves generated by the granulate inflow (Fig. 6b) and recorded with a capacitance wave gauge at location $x = 885$ m are shown in Figure 7a. The wave propagating away from the impact area in positive x-direction creates a single initial peak at $t = 16$ s with a maximum positive amplitude $a = 152$ m. In the two-dimensional model of Gilbert Inlet the single outward travelling wave is reflected back and forth from both headland and landslide ramps. The main trailing peaks recorded on the wave gauge have altering propagation directions from positive to negative x-direction, respectively. The second peak ($a = 85$ m, $t = 48$ s) on the wave record corresponds to the wave reflection from the headland propagating in the negative x-direction. An experiment without the headland ramp showed that the first wave trough ($\eta = 37$ m, $t = 30$ s) is truncated by the reflection from the headland and not fully developed. In the experiment without headland ramp a flat trough with a negative amplitude $a = -10$ m was recorded behind the single outward travelling wave crest. Therefore the total wave height is estimated to $H = 162$ m. The measured wave height to stillwater depth ratio $H/h = 1.33$ is well beyond any breaking criterion (DEAN and DALRYMPLE, 1991). The experimental run without headland ramp showed that breaking and transformation to a nonlinear bore initiated roughly at $x = 1500$ m — after the beginning of the headland ramp at location $x = 1342$ m. The third main peak ($a = 111$ m, $t = 93$ s) and the fifth peak ($a = 57$ m, $t = 180$ s) correspond to the wave reflected back from the landslide slope. The fourth peak ($a = 73$ m, $t = 129$ s) and the sixth peak ($a = 57$ m, $t = 214$ s) are wave reflections from the headland ramp. This partial back and forth wave reflection in Gilbert Inlet could account for the "jumping and shaking" reported by one eyewitness (MILLER, 1960).

The corresponding wave runup recorded by a capacitance wave gage on the headland ramp is shown in Figure 7b. The runup gauge record acquired parallel to the 45° inclined

Journal : 24 Dispatch : 22-12-2008 Pages : 23
Article No. : 0435 ☐ LE ☐ TYPESET
MS Code : 0435 ☑ CP ☑ DISK

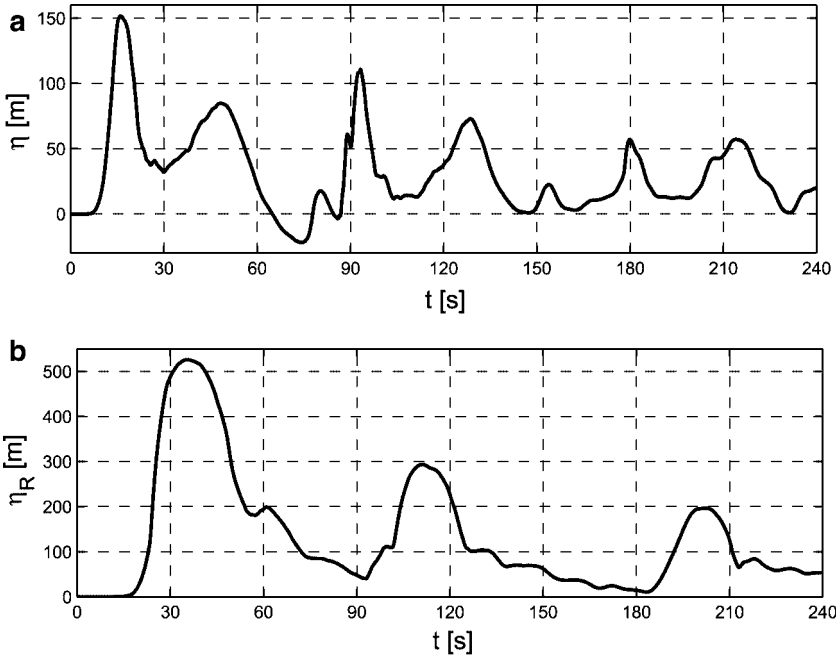

Figure 7
(a) Tsunami record at location $x = 885$ m; (b) tsunami runup record on headland ramp at locations $x = 1342$ m $+ \eta_R$ measured with capacitance wave gauges.

headland ramp is transformed into an elevation record. On the headland ramp a maximum runup height of $R = 526$ m is measured at $t = 35$ s. The measured runup of 526 m perfectly matches the highest elevation of 524 m on the trimline of forest destruction in Gilbert Inlet. The two trailing peaks on the runup record correspond to the first and second reflection of the single initial wave runup. The peak-to-peak period increases from 76 s to 91 s. This decay in propagation velocity with diminishing wave amplitude is due to the characteristic amplitude dispersion of nonlinear waves.

A sequence of twelve instantaneous velocity vector plots computed with PIV is shown in Figure 8. The sequence starts at t = 0.76 s after landslide impact and continues with a time step of 1.73 s covering roughly a time span of 20 s. Instantaneous velocity vector plots provide insight into kinematics during landslide impact and tsunami generation. The entire process may be subdivided into two main stages: (a) Slide impact and penetration (Fig. 8a), flow separation (Fig. 8b), cavity formation (Figs. 8c, d, e, f) while slide penetration velocity exceeds wave propagation velocity, and (b) cavity collapse (Figs. 8g, h), slide run-out along channel bottom, slide detrainment and deposition (Figs. 8i, j, k, l) as the wave overtakes the landslide and propagates out of the impact area. At the beginning of the cavity collapse (Fig. 8g) the splash amplitude exceeds 200 m in elevation at $x = 600$ m and $t = 11.14$ s before decaying synchro-

Journal : 24 Dispatch : 22-12-2008 Pages : 23
Article No. : 0435 ☐ LE ☐ TYPESET
MS Code : 0435 ☑ CP ☑ DISK

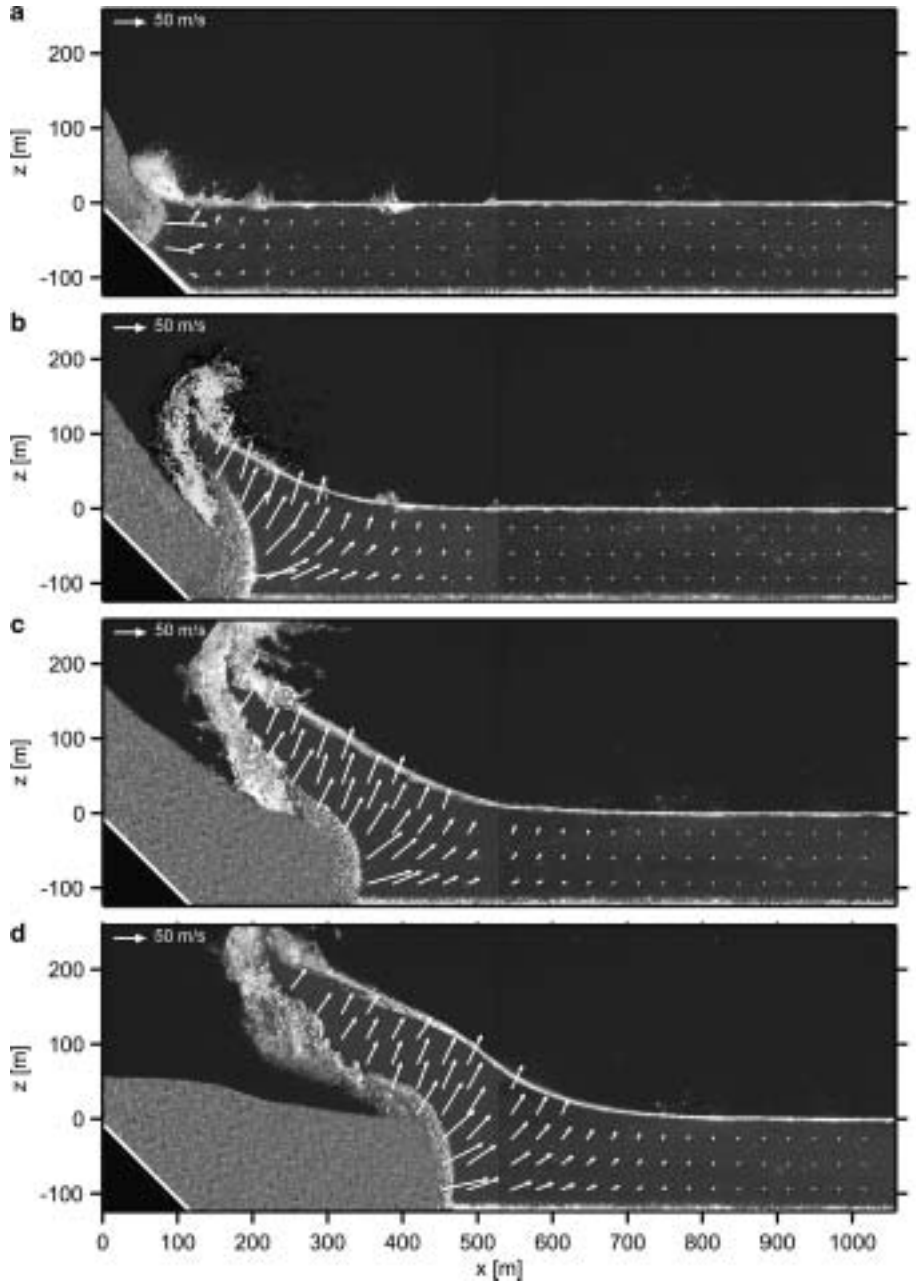

Figure 8
PIV velocity vector plot sequence of two synchronized granular slide impact experiments with juxtaposed areas of view and upscaled parameters: F = 3.18, $v_s = 110$ m/s, $m' = 98.5 \times 10^3$ t/m′, $h = 122$ m, $\alpha = \beta = 45°$, time increment 1.73 s with first image at $t = 0.76$ s after impact.

Journal : 24 Dispatch : 22-12-2008 Pages : 23
Article No. : 0435 ☐ LE ☐ TYPESET
MS Code : 0435 ☑ CP ☑ DISK

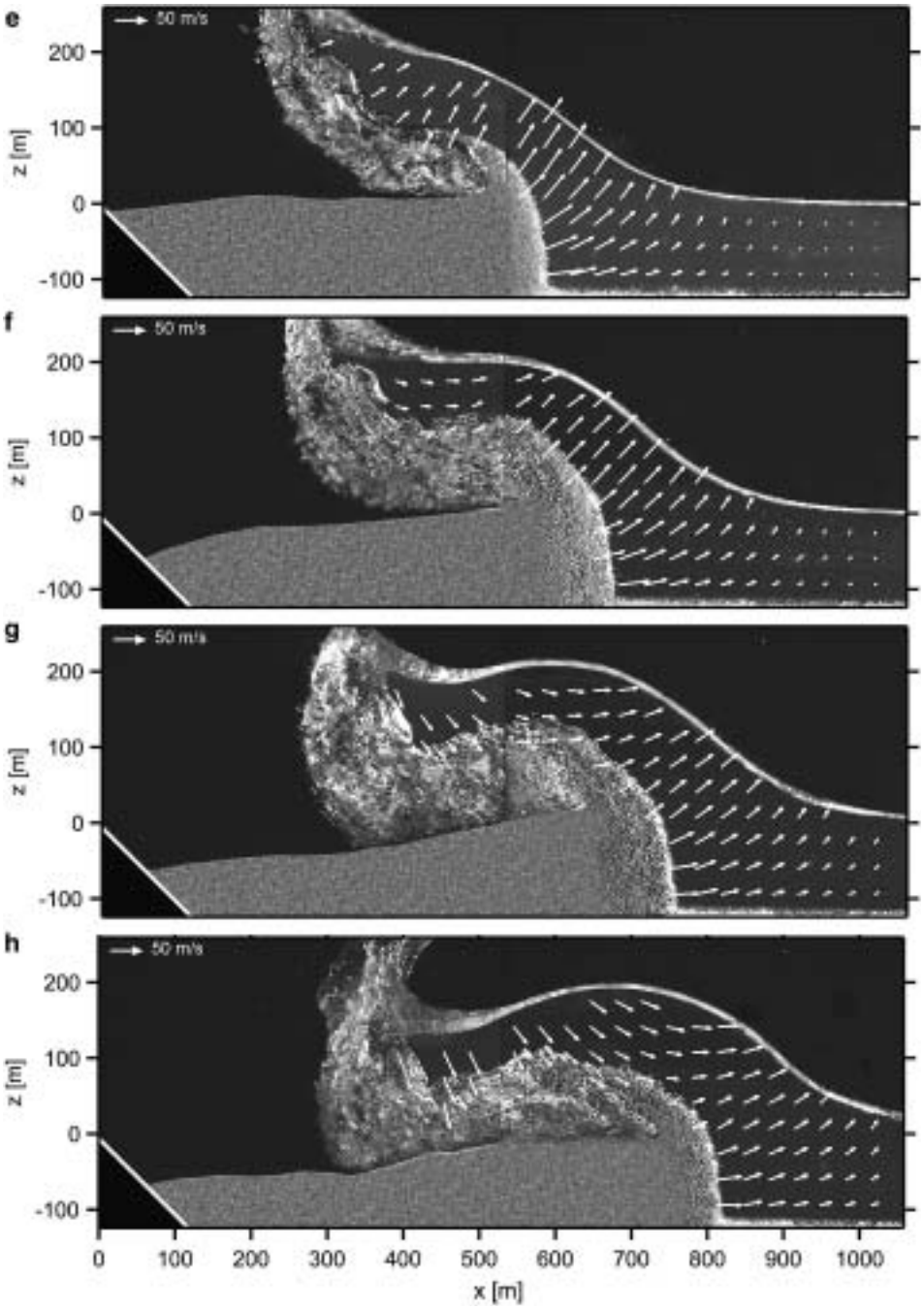

Figure 8
contd.

Journal : **24** Dispatch : **22-12-2008** Pages : **23**
Article No. : **0435** ☐ LE ☐ TYPESET
MS Code : **0435** ☑ CP ☑ DISK

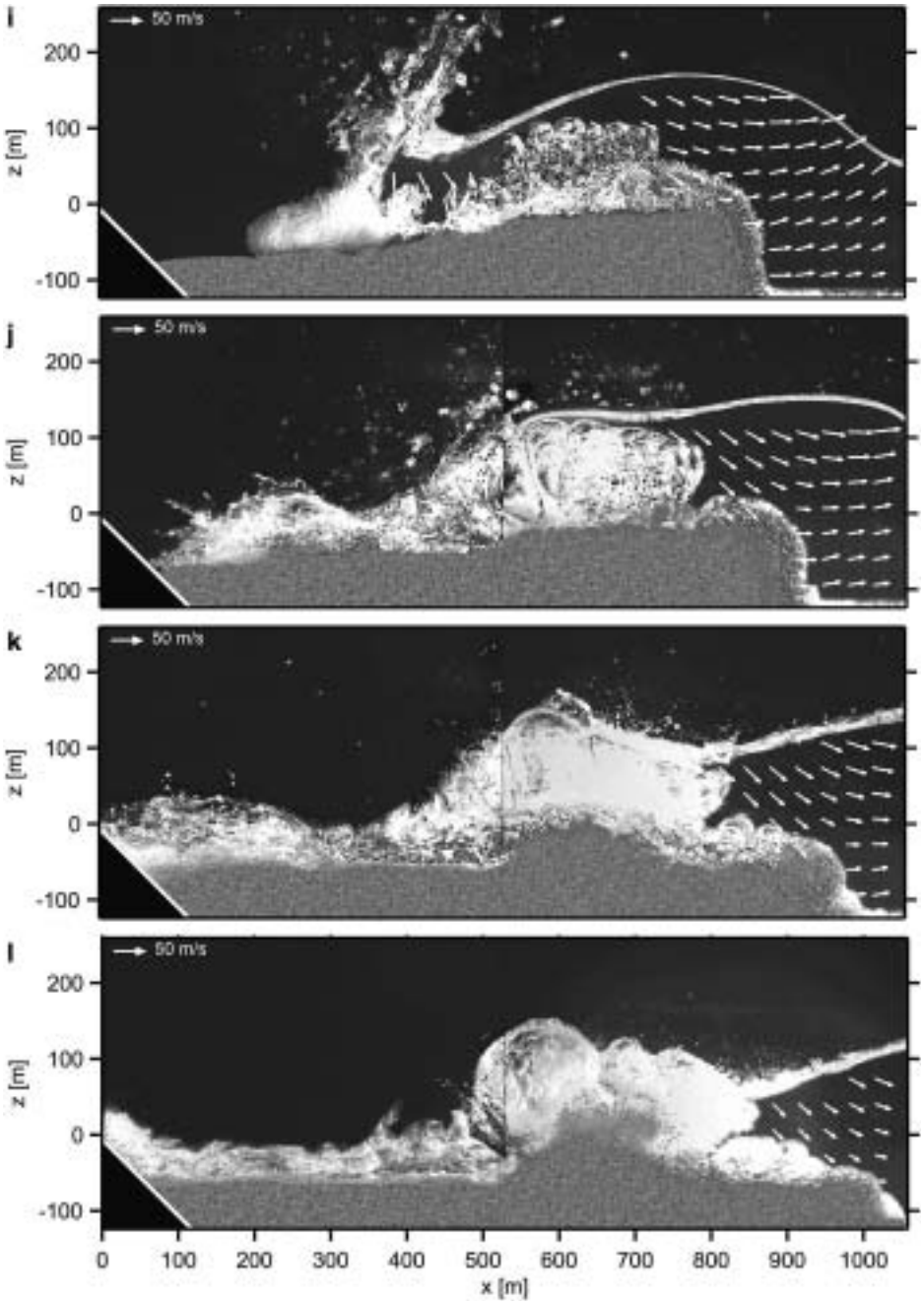

Figure 8
contd.

Journal : **24** Dispatch : **22-12-2008** Pages : **23**
Article No. : **0435** ☐ LE ☐ TYPESET
MS Code : **0435** ☑ CP ☑ DISK

nously with the cavity collapse to a tsunami wave with $a = 152$ m at $t = 16$ s and $x = 885$ m (Fig. 7a). A high velocity gradient at the slide-water interface during impact and penetration causes sediment transport on the slide front leading to a sheet flow effect (Fig. 8b). The three phases — granular material, water and air — are clearly separated along distinct borderlines before flow reattachment occurs (Fig. 8h). Flow reattachment traps a large volume of air in the back of the landslide (Fig. 8i), which leads to large cavity formation (Fig. 8j), bubble break-up and massive phase mixing (Figs. 8k, l). Slide detrainment further increases phase mixing. The granular slide is deformed due to impact and deflection at the channel bottom reaching a maximum thickness and minimum length (Fig. 8d). The slide front forms an almost vertical wall with culminating height at the beginning of the cavity collapse (Figs. 8f, g). Thereafter the slide front thickness decays with slide run-out (Figs. 8j, k, l).

A sequence of eight PIV velocity vector plots acquired during tsunami runup on the headland is shown in Figure 9. The view area begins above the stillwater level. The sequence starts at $t = 23.28$ s after landslide impact and continues with a time step of

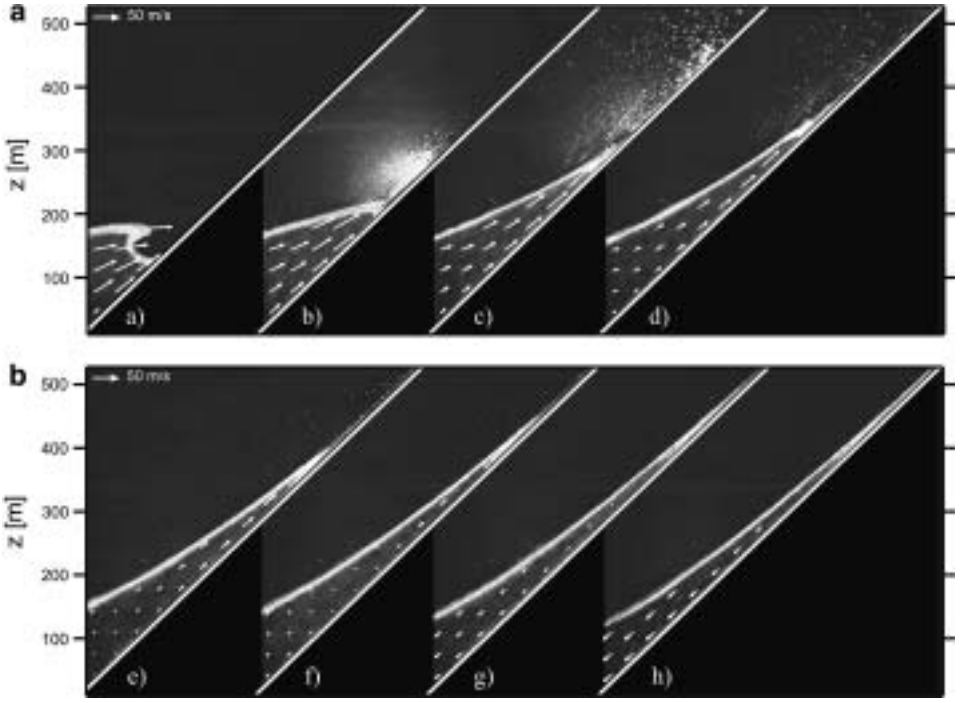

Figure 9
PIV velocity vector plot sequence of tsunami runup on headland slope created by a landslide impact with upscaled parameters: F = 3.18, $v_s = 110$ m/s, $m' = 98.5 \times 10^3$ t/m′, $h = 122$ m, $\alpha = \beta = 45°$, time increment 1.73 s, first image at $t = 23.28$ s after impact, lower left image corner at location $x = 1353$ m and $z = 11$ m.

Journal : **24** Dispatch : **22-12-2008** Pages : **23**
Article No. : **0435** ☐ LE ☐ TYPESET
MS Code : **0435** ☑ CP ☑ DISK

1.73 s covering roughly a time span of 12 s. At $t = 23.28$ s the wave is shown prior to plunging onto the headland ramp. The wave amplitude has increased beyond 180 m. Wave-breaking during runup is initiated but does not fully develop due to the steep slope. The runup process is more surging than breaking and therefore with little air-entrainment (SYNOLAKIS, 1987; JENSEN *et al*., 2003). In the following images the wave surges up the headland slope with high velocity. At $t = 30.2$ s (Fig. 9e) an instantaneous stagnation point appears in the lower left corner of the velocity vector field. The stagnation point propagates up the headland ramp phase which shifted to the runup wave front. In the area below the stagnation point water rushes down the headland ramp, whereas above the stagnation point water still surges upward. Therefore the sheet of water located on the headland ramp thinned significantly at the lower end by $t = 35$ s when the time of maximum runup height is reached (Fig. 9h). Sufficient water rushed up the headland slope to cause the flooding observed in Lituya Bay as estimated by MADER (1999) with numerical simulations of Lituya Bay outside the immediate impact area.

5. Comparison with two-dimensional Predictive Models

Various predictive relationships for the landslide-generated tsunami amplitude are compared with the Lituya Bay benchmark experiment as no field data are available on the tsunami height itself. Characteristic for highly non-linear waves is the large difference between the wave crest and the wave trough amplitudes. Predicting solely the total wave height H is insufficient and misleading (FRITZ *et al*., 2006). The comparison between the measured and predicted wave amplitudes and heights using the various equations is shown in Table 1.

The equation by FRITZ *et al*. (2004) for the maximum leading crest amplitude matched the measured crest amplitude $a = 155$ m. The relationship presented by KAMPHUIS and BOWERING (1970) from tray impact experiments matched the measured wave height $H = 162$ m. NODA (1970) used linear wave theory to predict the form of the wave motion produced by a body falling vertically into a tank. The theoretical solution underestimates the maximum wave amplitude with $a = 122$ m by 20%. The linear solution does not distinguish between the wave crest and trough amplitudes. Hence the trailing wave trough is massively overestimated. NODA (1970) obtained a theoretical solution for the case of a horizontally penetrating wall, which overestimates the measured wave crest amplitude by a factor of three. Similar overestimations may be produced by depth averaging shallow water equations in the wave generation area (MADER, 1999). SLINGERLAND and VOIGHT (1982) derived an empirical regression from two case studies, which overestimate the measured wave height by a factor of two. The empirical formula of HUBER and HAGER (1997) for 2-D-impulse wave characteristics predicts a wave height of $H = 94$ m, which underestimates the wave height by a factor of 1.8. Rough estimations of slide thickness from photos (HUBER, 1980) indicate that Huber's slides at comparable impact Froude

Journal : 24 Dispatch : 22-12-2008 Pages : 23
Article No. : 0435 ☐ LE ☐ TYPESET
MS Code : 0435 ☑ CP ☑ DISK

Table 1

Lituya Bay 1958 benchmark comparison of wave amplitude and runup predictions

R eference	Equations and remarks	a_C [m]	a_T [m]	H [m]	R [m]
Fritz *et al*. (2001) (scale model case study)	measured	152	10	162	530
Fritz (2002); Fritz *et al*. (2004) (granular slide model)	$\frac{a_C}{h} = 0.25\left(\frac{v_s}{\sqrt{gh}}\right)^{1.4}\left(\frac{s}{h}\right)^{0.8}$	155			
Huber and Hager (1997) (granular slide model)	$H = 0.88\sin\alpha\left(\frac{\rho_s}{\rho_w}\right)^{1/4}\left(\frac{V_s}{b}\right)^{1/2}\left(\frac{h}{x}\right)^{1/4}$			94	
Kamphuis and Bowering (1970) (block/weighted tray model)	$\frac{H}{h} = \left(\frac{v_s}{\sqrt{gh}}\right)^{0.7}\left(0.31 + 0.2\log\left(\frac{l_s s}{h^2}\right)\right) + 0.35e^{-0.08(x/h)}$			159	
Noda (1970) (theoretical solution)	$\frac{\eta(x,t)}{s} = f\left(\frac{v_s}{\sqrt{gh}}, \frac{x}{h}\right)$	122			
Noda (1970) (piston model)	$\frac{a_C}{h} = 1.32\left(\frac{v_s}{\sqrt{gh}}\right)$	515			
Slingerland and Voight (1982) (granular bag model)	$\log\left(\frac{a_C}{h}\right) = -1.25 + 0.71\log\left(\frac{1}{2}\frac{\rho_s}{\rho_w}\frac{V_s}{h^3}\frac{v_s^2}{gh}\right)$	329			
Mader and Gittings (2002)	full Navier-Stokes numerical simulation	170			580
Hall and Watts (1953) (R only based on measured H by Fritz *et al*., 2001)	$\frac{R}{h} = 3.1\left(\frac{H}{h}\right)^{1.15}$				526
Synolakis (1987) (R only based on measured H by Fritz *et al*. 2001)	$\frac{R}{h} = 2.831\sqrt{\cot\beta}\left(\frac{H}{h}\right)^{5/4}$				493

numbers were thinner $s < h$. The present study and the sliding block experiments conducted by Noda (1970) and Kamphuis and Bowering (1970) showed a strong dependency of the generated wave heights on the slide impact thickness and the slide Froude number $\mathbf{F} = v_s/.(gh)^{0.5}$. The relationship given by Fritz *et al*. (2004) is recommended to predict the maximum leading crest amplitude a, because the relationship presented by Kamphuis and Bowering (1970) allows only the prediction of the total wave height H. The Lituya bay cross section was modeled numerically by Mader and Gittings (2002), Quecedeo *et al*. (2004) and Weiss and Wuennemann (2007) with full Navier-Stokes hydrodynamic codes in two dimensions. Both the Hall and Watts (1953) and Synolakis (1987) solutions for solitary wave runup on an impermeable slope match the experimentally measured wave runup and the observed elevation of forest destruction in Lituya Bay with predictions of $R = 526$ m and $R = 493$ m based on the experimentally measured incident wave parameters $H = 162$ m and $h = 122$ m (Fritz *et al*., 2001). This confirms the conclusion drawn by Slingerland and Voight (1979) using back-calculation of wave height from runup that a wave height of about 160 m was necessary to produce the wave runup in Gilbert Inlet.

6. Three-dimensional Landslide Tsunami Experiments

The coupling between landslide motion and three-dimensioinal tsunami wave propagation and runup is of critical importance given the local, strongly-directional source mechanism. A unique pneumatic landslide generator was designed by the authors at Georgia Tech and installed at the NEES Tsunami Wave Basin (TWB) at OSU as shown in Figure 10. The apparatus simulated the impact of landslides that occur both above and below the water's surface. The landslide tsunami generator was constructed as an open aluminum box that is mounted on a steel slide and filled with up to 1,350 kg of gravel. The box accelerates down the slide by means of four pneumatic pistons. The granular mass is accelerated inside the box and released by opening the front tarp while the sled is slowed down pneumatically. The box measures 2.1 m by 1.2 m by 0.3 m with subdivisions to adjust initial slide length and thickness, and is placed on a slide that can vary in length. The box itself is able to travel approximately 2 m before the gravel is released down the 2H:1 V slope at initial velocities up to 5 m/sec. Using cameras placed above and within the water, the researchers measured the shape, length, and thickness of the gravel masses while they were in motion.

The measured front velocity of the granular landslide and the corresponding acceleration are shown in Figure 11. The landslide velocity prior to release from the box is measured using the string pot data from the slide box. The landslide velocity after release from the box is measured from the image sequences recorded by a 2-megapixel PIV camera. The impact velocity of the landslide is compared to the velocity evolution of a dry granular landslide run. The PIV camera is setup at a distance of 6.8 m perpendicular to the hill slope providing an approximate 15 m^2 (4.5 m by 3.38 m) view area. A characteristic image sequence is shown in Figure 11b. This image sequence highlights the lateral spreading of the granular landslide after exiting the slide box prior to impact on

Figure 10
Granular landslide tsunami generator deployed in the three-dimensional NEES Tsunami Wave Basin at OSU in 2006/2007.

Journal : 24 Dispatch : 22-12-2008 Pages : 23
Article No. : 0435 ☐ LE ☐ TYPESET
MS Code : 0435 ☑ CP ☑ DISK

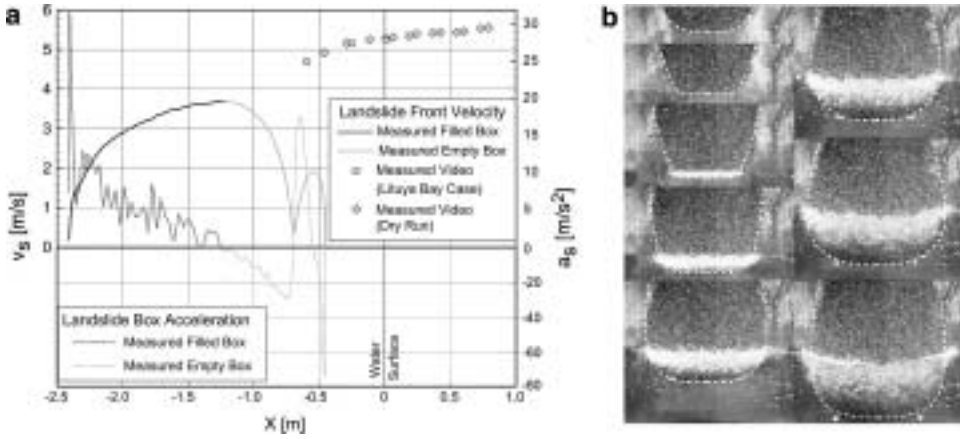

Figure 11
Granular Landslide kinematics at F = 3.2: (a) granular landslide front kinematics with transition from pneumatic acceleration inside the landslide generator to subaerial gravity slide; (b) lateral spreading and deformation of the granular landslide on the hill slope in a video image sequence.

the water body. The landslide shape is geometrically similar to the Lituya Bay landslide shown in Figure 2 at a 1:400 scale. The granular landslide front velocity prior to impact on the water surface was calculated from recorded subaerial landslide shown in Figure 11a. At the impact, a landslide velocity of 5.26 m/s was measured, which corresponds to an impact slide Froude number of 3.07 based on a still water depth 0.3 m and the definition $F = v_s/(gh)^{1/2}$. This corresponds to a full three- dimensional physical model of the Lituya Bay landslide at a 1:400 scale. Hence the pneumatic landslide generator can reproduce landslide velocities scaled to real world physical events.

The recorded high-resolution image sequences were processed with PIV to analyze the landslide characteristics at the impact location and the wave generation process by measuring the surface velocity field. The speckle patterns generated by the landslide granulate surface were used for iterative multi-pass cross-correlation analysis with decreasing window sizes 32 by 32 pixels. A PIV velocity vector plot of the landslide surface shortly after impact corresponding to a 1:400 scale landslide model of the three-dimensional Lituya Bay landslide is shown in Figure 12a. The landslide front penetrated below the water surface enabling the PIV based analysis of the water surface in the impact zone, which was seeded with 5 mm diameter naturally buoyant tracer particles prior to each experiment. The granular landslide deposits were scanned with an acoustic multi-transducer array (Fig. 12b). Unfortunately the Lituya Bay landslide deposit has not been surveyed to date, which would be necessary to compare physical model results with the landslide deposits in the field. The proposed landslide deposit mapping was conducted, for example, in Lake Lucerne, Switzerland (SCHNELLMANN *et al.*, 2002).

Wave gauges were placed to measure the size and shape of the tsunami waves that were generated, including the lateral onshore runup. The locations of wave and runup

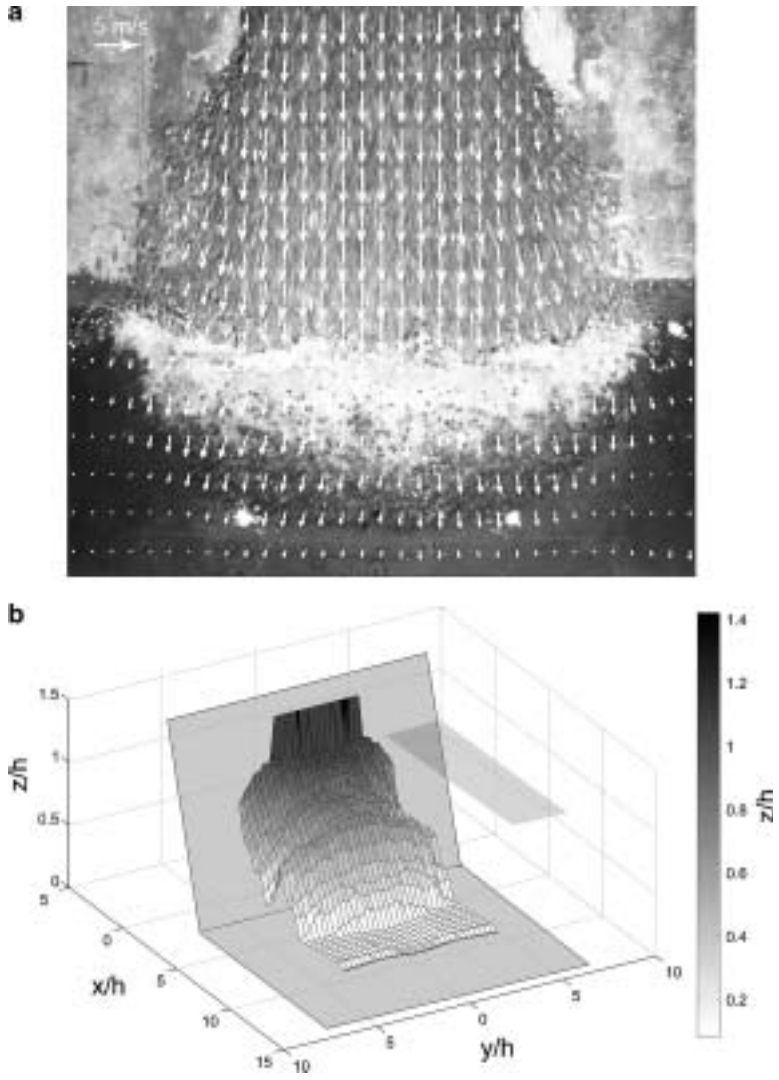

Figure 12
Landslide tsunami generation in 3-D: (a) PIV velocity vector plot of the landslide surface shortly after impact with the landslide front penetrating below the water surface and tsunami wave generation (note: the displayed number of vectors is reduced for visibility); (b) granular landslide deposit scanned with an acoustic multi-transducer array.

gauges in the tsunami wave basin measuring 48.8 m by 26.5 m by 2.1 m (L × W × H) at OSU are shown in Figure 13a. The scaled gauge locations are based on a 0.3 m water depth, which corresponds to a 1:400 scale model given the 122 m water depth at the impact site in Lituya Bay. The scaled Lituya Bay coastline is superimposed to highlight the complicated setting. The detailed fully three-dimensional bathymetry and topography

Journal : 24 Dispatch : 22-12-2008 Pages : 23
Article No. : 0435 ☐ LE ☐ TYPESET
MS Code : 0435 ☑ CP ☑ DISK

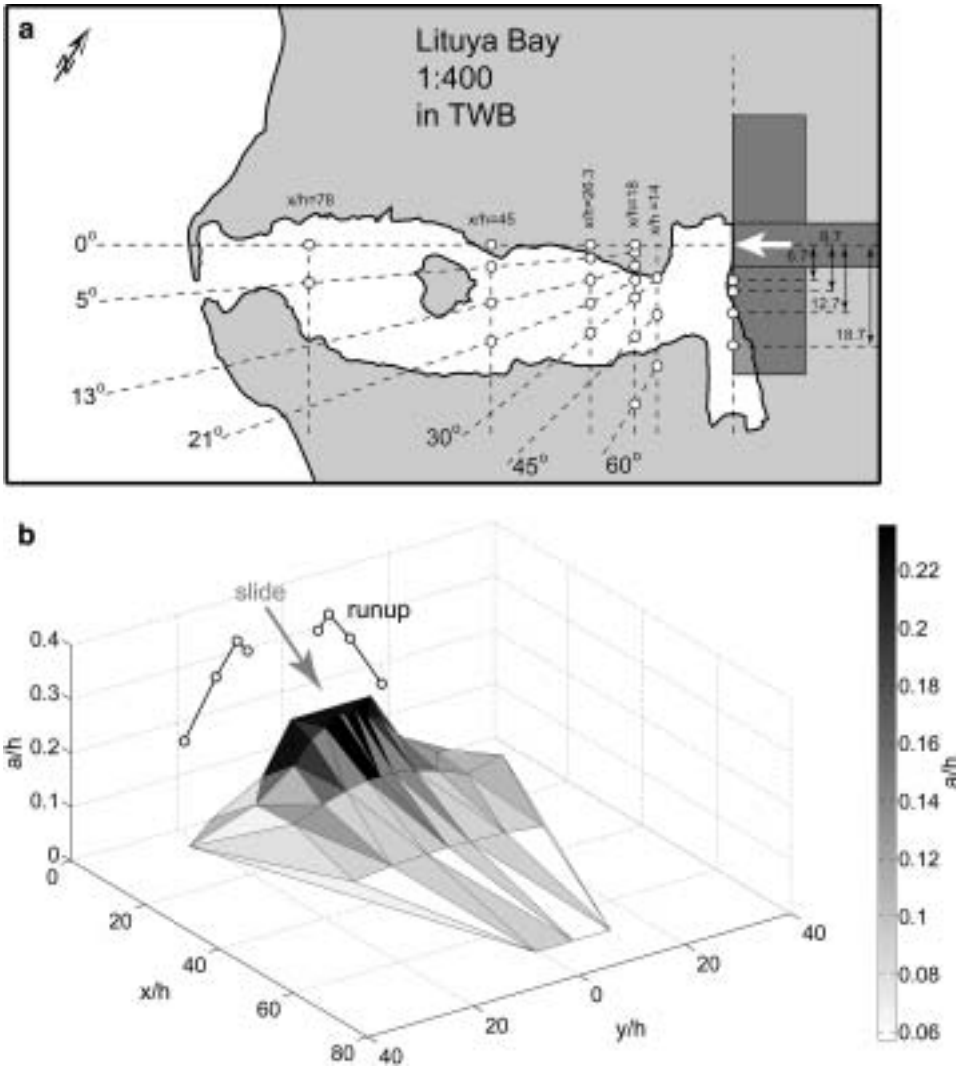

Figure 13
Landslide tsunami propagation in 3-D: (a) Locations of wave and runup gauges in tsunami wave basin at OSU based on a 1:400 scale Lituya Bay water depth with superimposed Lituya Bay coastline for reference; (b) tsunami amplitude attenuation with strong directional component and the high wave runup as edge waves along the hill slope.

of Lituya Bay would have to be reconstructed in the physical model to enable a direct comparison between the measurements and the observations in the field. The tsunami amplitude attenuation and the wave runup along the hill slope are shown in Figure 13b. The recorded wave profiles were extremely directional, unsteady, nonlinear, and located mostly in the intermediate water depth wave regime. Among the principal differences

Journal : 24 Dispatch : 22-12-2008 Pages : 23
Article No. : 0435 ☐ LE ☐ TYPESET
MS Code : 0435 ☑ CP ☑ DISK

between a tectonic-generated tsunami and a landslide-generated tsunami is that the latter has a strong directional component that can be devastating to the immediate area. Because it has a shorter wavelength, however, it dissipates quickly over a short distance. Landslide tsunamis exhibit a more dispersive and strongly directional propagation than tectonic tsunamis. Currently more than 60 successful runs have been completed and the main tsunamigenic parameters identified that will serve as key benchmarks for numerical models. However a fully three-dimensional benchmark of the Lituya Bay with the detailed bathymetry remains to be conducted to validate numerical simulations of the entire Lituya Bay with three-dimensional tsunami generation, propagation and runup.

7. Conclusions

The two-dimensional physical model at 1:675 scale of the Lituya Bay 1958 event includes landslide impact, tsunami generation, propagation and runup on headland. A unique pneumatic landslide generator was used to generate a high-speed granular slide with controlled impact velocity and shape. State-of-the-art laser measurement techniques such as particle image velocimetry (PIV) and laser distance sensors (LDS) were applied to cope with an extremely unsteady three phase flow due to high speed granular slide impact, high velocity gradients, flow separation, cavity formation, wave generation and runup. A granular slide with density and volume given by MILLER (1960) impacting at a mean velocity of 110 m/s generates a large air cavity and an extremely nonlinear wave beyond breaking criterion, which remains nonbreaking due to the short propagation distance to the headland runup. The formation of a large air cavity is highlighted (FRITZ *et al*., 2001). The predictive tsunami amplitude equation by FRITZ *et al*. (2004) matches the experimentally measured tsunami amplitude in Gilbert Inlet. The experimentally measured wave runup matches the trimline of forest destruction on the spur ridge in Gilbert Inlet. Back-calculations of wave height from observed trimline of forest destruction using HALL and WATTS (1953) and SYNOLAKIS (1987) runup formulas equal the measured wave height in Gilbert Inlet. Further research on slide impact characteristics, wave generation and energy conversion using three-dimensional models is necessary. MADER and GITTINGS (2002), QUECEDO *et al*. (2004) as well as WEISS and WUENNEMANN (2007) reproduced the physical model results of the Lituya Bay landslide tsunami with full Navier-Stokes models in two dimensions. A three-dimenional pneumatic landslide tsunami generator was designed, constructed and successfully deployed in the tsunami wave basin at OSU. The Lituya Bay landslide was reproduced in a three-dimensional physical model at 1:400 scale. The landslide surface velocities distribution was measured with PIV. The landslide deposits in Lituya Bay should be mapped to validate the experiments and establish a baseline bathymetry prior to a possible future landslide tsunami in Lituya Bay. A detailed three-dimensional benchmark experiment of the Lituya Bay remains to be conducted with the exact bathymetry to validate numerical simulations of the entire Bay with three-dimensional tsunami generation, propagation and runup.

Journal : 24 Dispatch : 22-12-2008 Pages : 23
Article No. : 0435 ☐ LE ☐ TYPESET
MS Code : 0435 ☑ CP ☑ DISK

Acknowledgments

This research work is supported by the National Science Foundation under Grant No. CMS-0421090. Any opinions, findings, and conclusions or recommendations expressed herein are those of the author(s) and do not necessarily reflect the views of the National Science Foundation. The two-dimensional experiments conducted at VAW (ETH Zürich) were supported by the Swiss National Science Foundation, grant number 2100-050586.97.

References

Dean, R.G. and Dalrymple, R.A., *Water wave mechanics for engineers and scientists*. *Advanced Series on Ocean Engineering* 2 (World Scientific, Singapore 1991).

Fritz, H.M., Hager, W.H. and Minor, H.-E. (2001), *Lituya Bay case: rockslide impact and wave runup*, Science of Tsunami Hazards *19*(1), 3–22.

Fritz, H.M., *PIV applied to landslide generated impulse waves*, In (Adrian, R.J. *et al*., eds) *Laser Techniques for Fluid Mechanics*, pp. 305–320 (Springer, New York, Berlin, Heidelberg 2002a).

Fritz, H.M., *Initial phase of landslide generated impulse waves*, In (Minor, H.-E., ed.) *VAW Mitteilung 178* (Versuchsanstalt für Wasserbau, Hydrologie und Glaziologie, ETH Zürich 2002b).

Fritz, H.M. and Moser, P. (2003), *Pneumatic landslide generator*. Int. J. Fluid Power *4*(1), 49–57.

Fritz, H.M., Hager, W.H. and Minor, H.-E. (2003a), *Landslide generated impulse waves, Part 1: Instantaneous flow fields*, Exp. Fluids *35*, 505–519.

Fritz, H.M., Hager, W.H., and Minor, H.-E. (2003b), *Landslide generated impulse waves, Part 2: Hydrodynamic impact craters*, Exp. Fluids *35*, 520–532.

Fritz, H.M., Hager, W.H., and Minor, H.-E. (2004), *Near field characteristics of landslide generated impulse waves*, J. Waterway, Port, Coastal, and Ocean Engrg., ASCE *130*, 287–302.

Fritz, H.M., Physical modeling of landslide generated tsunami. In (A. Mercado-Irizarry and P.L.-F. Liu, eds) *Caribbean Tsunami Hazard* (World Scientific, Singapore 2006), pp. 308–324.

Hall, J.V., Jr. and Watts, G.M. (1953), *Laboratory investigation of the vertical rise of solitary waves on impermeable slopes*, Tech. Memo *33*, U.S. Army Corps of Engineers, Beach Erosion Board.

Hart, D., *PIV error correction*. In *Laser Techniques Applied to Fluid Mechanics*, selected papers from the 9th Internat. Symp., Lisbon 1998, Portugal. (Eds. Adrian, R.J. *et al*.) (Springer, New York 2000).

Heller, V., Hager, W.H., and Minor, H.-E. (2008), *Scale effects in subaerial landslide generated impulse waves*, Exp. Fluids *44*(5), 691–703, doi:10.1007/s00348-007-0427-7.

Huber, A., *Schwallwellen in Seen als Folge von Bergstürzen* (in German), *VAW-Mitteilung 47*, (Ed. Vischer, D.) (Versuchsanstalt für Wasserbau, Hydrologie und Glaziologie, ETH Zürich 1980).

Huber, A. and Hager, W.H. (1997), *Forecasting impulse waves in reservoirs*. *Dix-neuvième Congrès des Grands Barrages* C**31**:993–1005. Florence, Italy. Commission International des Grands Barrages, Paris.

Jensen, A., Pedersen, G.K., and Wood, D.J. (2003), *An experimental study of wave runup at a steep beach*, J. Fluid Mech. *486*, 161-188, doi:10.1017/S0022112003004543.

Jørstad, F. (1968), *Waves generated by landslides in Norwegian fjords and lakes*. Norwegian Geotechnical Institute Publication *79*:13–32, Norwegian Geotechnical Institute, Oslo.

Kamphuis, J.W. and Bowering, R.J. (1970), *Impulse waves generated by landslides*. In *Proc. 12th Coastal Engin. Conf.* ASCE *1*, 575–588.

Law, L. and Brebner, A. (1968), *On water waves generated by landslides*, *3rd Australas. Conf. on Hydraulics and Fluid Mechanics*, Sydney, Paper *2561*, 155–159.

Mader, C.L. (1999), *Modelling the 1958 Lituya Bay mega-tsunami*. Science of Tsunami Hazards *17*(2), 57–67.

Mader, C.L. and Gittings, M.L. (2002), *Modeling the 1958 Lituya Bay mega-tsunami, II*. Science of Tsunami Hazards *20*(5), 241–250.

MILLER, D.J. (1960), *Giant waves in Lituya Bay, Alaska*, Geological Survey Professional Paper *354*-C, U.S. Government Printing Office, Washington D.C.

MÜLLER, D., *Auflaufen und Überschwappen von Impulswellen an Talsperren* (in German). *VAW-Mitteilung* 137 (Ed. Vischer, D.) (Versuchsanstalt für Wasserbau, Hydrologie und Glaziologie, ETH Zürich 1995).

MÜLLER, L. (1964), *The rock slide in the Vajont Valley*. Rock Mech. Eng. Geol. *2*(3–4), 148–212.

Noda, E. (1970), *Water waves generated by landslides*, J. Waterw. Harbors Coastal Eng. Div. ASCE *96*(WW4), 835–855.

PARARAS-CARAYANNIS, G. (1999), *Analysis of mechanism of tsunami generation in Lituya Bay*, Science of Tsunami Hazards *17*(3), 193–206.

QUECEDO, M., PASTOR, M., and HERREROS, M.I. (2004), *Numerical modelling of impulse wave generated by fast landslides*, Int. J. Numer. Meth. Engin. *59*, 1633–1656. doi: 10.1002/nme.934.

SAVAGE, S.B. (1979), *Gravity flow of cohesionless granular materials in chutes and channels*, J. Fluid Mech. *92*, 53–96.

SCARANO, F. and RIETHMULLER, M. (1999), *Iterative multigrid approach in PIV image processing with discrete window offset*, Experiments in Fluids *26*, 513–523.

SCHNELLMANN, M., ANSELMETTI, F.S., GIARDINI, D., MCKENZIE, J.A., and WARD, S.N. (2002), *Prehistoric earthquake history revealed by lacustrine slump deposits*, Geology *30*(12), 1131–1134.

SHARPE, C.F.S., *Landslides and Related Phenomena* (Columbia Univ. Press, New York 1938).

SLINGERLAND, R.L. and VOIGHT, B., *Occurrences, properties and predictive models of landslide-generated impulse waves*, Rockslides and Avalanches *2*, 317–397 (Ed. Voight, B) *Developments in Geotechnical Engin.* **14B** (Elsevier, Amsterdam 1979).

STIVE, M.J.F. (1985), *A scale comparison of waves breaking on a beach*, Coastal Engin. *9*, 151–158.

Synolakis, C.E. (1987), *The runup of solitary waves*, J. Fluid Mech. *185*, 523–545.

TOCHER, D. and MILLER, D.J. (1959), *Field observations on effects of Alaskan earthquake of 10 July, 1958*, Science *129*, 394–395.

TOGNACCA, C., *Beitrag zur Untersuchung der Entstehungsmechanismen von Murgängen (in German)*, *VAW-Mitteilung* 164 (Ed. Minor, H.-E.) (Versuchsanstalt für Wasserbau, Hydrologie und Glaziologie, ETH Zürich 1999).

VARNES, D.J. (1958), *Landslide types and processes*, Highw. Res. Board Spec. Rep. *29*, Natl. Acad. Sci.-Natl. Res. Counc. Publ. *544*, 22–47.

VOIGHT, B., JANDA, R.J., GLICKEN, H., and DOUGLASS, P.M. (1983), *Nature and mechanics of the Mount St. Helens rockslide-avalanche of 18 May 1980*, Géotechnique *33*, 243–273.

WEISS, R. and WUENNEMANN, K. (2007), *Understanding tsunami by landslides as the next challenge for hazard, risk and mitigation: Insight from multi-material hydrocode modeling*, EOS Trans. AGU *88*(52), Fall Meet. Suppl., Abstract S51C-06.

WIEGEL, R.L., *Oceanographical Engineering* (Prentice-Hall, Englewood Cliffs, N.J. 1964).

(Received December 31, 2007, revised September 2, 2008)

Journal : **24** Dispatch : **22-12-2008** Pages : **23**
Article No. : **0435** ☐ LE ☐ TYPESET
MS Code : **0435** ☑ CP ☑ DISK